LATERAL TORSIONAL BUCKLING OF STEEL BEAMS STRENGTHENED WITH GFRP PLATE

Phe Van Pham [a, 1], Magdi Mohareb [a], Amir Fam [b]

[a] Department of Civil Engineering, University of Ottawa, Ottawa, ON, Canada K1N 6N5

[b] Department of Civil Engineering, Queen's University, Kingston, ON, Canada K7L 3N6

Abstract

The present study investigates the lateral-torsional buckling of wide flange steel members strengthened by a Glass Fiber Reinforced Polymer (GFRP) plate bonded to one of the flanges through an adhesive layer. A variational formulation and two finite elements are developed for the problem. The formulation captures global and local warping effects, shear deformation due to bending and twist, and partial interaction between the steel and GFRP provided by the flexible layer of adhesive. The destabilizing effects due to strong axis bending, axial force and load height effect are incorporated into the formulation. The first element involves two nodes and 16 buckling degrees of freedom (DOFs) while the second element involves three nodes and 14 DOFs. Comparisons of present model results against those based on 3D finite element analysis based on solid elements demonstrate the ability of the present models to accurately predict the buckling loads and mode shapes at a fraction of the modelling and computational efforts. Practical examples quantify the gain in elastic buckling strength achieved by GFRP strengthening, and characterize the moment gradient factors and load height effects. Elastic buckling interaction diagrams are developed for beam-columns and comparisons are provided to interaction diagrams of un-strengthened beams.

Keywords: Lateral torsional buckling, flexural torsional buckling, GFRP strengthening, wide flange beam, three node element, finite element analysis, shear deformation

This article is to be cited as

Pham PV, Mohareb M, Fam A, (2018) Lateral torsional buckling of Steel beams strengthened with GFRP plate, Thin-Walled Structures, 131: 55-75.

The copy-edited version of this article is available at https://doi.org/10.1016/j.tws.2018.06.025

[1] Corresponding author. Tel: (+1) 613 562 5800 ext. 6066;
Email: ppham040@uottawa.ca (P. Pham).

1. Introduction

GFRP is a lightweight, durable, and economic material that can be formed into thick plates capable of resisting tensile, shear and compression stresses [1]. Strengthening existing steel structures using adhesively bonded GFRP plates has become a viable option in recent years given the advantages it offers; when compared to traditional strengthening methods using either welded- or bolted-steel plates [2], GFRP installation is relatively easier and faster. When compared to bonded carbon-FRP (CFRP) plates with relatively high elasticity modulus [3,4], GFRP plates possess a lower stiffness. However, this drawback can be compensated for by using thicker plates [1]. This provides the added advantage of achieving a higher flexural stiffness compared to stiffer but thinner CFRP plates and thus can be advantageous when strengthening thin compression flanges to increase their local and global buckling strengths [5, 6]. Additionally, when in contact with steel, GFRP do not induce galvanic corrosion.

Strengthening applications involving GFRP plates were investigated in a number of studies. El Damatty et al. [1] conducted an experimental study for W-shaped steel beams strengthened with GFRP plate bonded to the tensile flange to increase the ultimate load capacity of the system. Youssef [7] experimentally investigated the ultimate load capacity of W-steel beams strengthened with two GFRP plates bonded to the compressive and tensile steel flanges. Accord and Earls [5] numerically investigated the enhancement of local buckling capacity and ductility of W-section cantilever steel beams with four GFRP plates bonded to the compression flange. Harries et al. [8] conducted experiments on WT steel columns strengthened with GFRP plates bonded to the web to delay local buckling. Other GFRP strengthening arrangements were investigated on members with cruciform cross-sections [9]. Aguilera and Fam [6] reported an experimental study on T-joints made of hollow steel sections strengthened with GFRP plates. Siddique and El Damatty [10] developed a finite element technique to characterize the enhancement in local buckling capacity for steel beams strengthened with GFRP plate bonded to the compression flange. The model was based on a 13-node consistent degenerated triangular sub-parametric shear-locking free shell elements. Each layer (GFRP, steel) was modelled by a shell element while the adhesive layer joining them was idealized as 2D distributed springs with zero thickness to represent the shear stiffness and a distributed transverse spring to represent its compressibility. Zaghian [11] developed a non-conforming four-node finite shell element for the buckling analysis of steel plates strengthened with GFRP plates. While the above studies focused on developing models for

predicting the local buckling strength or ultimate load capacity of steel-adhesive-GFRP systems, none of them tackled their lateral torsional buckling strength.

Buckling solutions for composite systems in general include the work of Girhammar and Pan [12] who developed a Euler-Bernoulli buckling theory for two-layer members with deformable shear connectors. Xu and Wu [13] developed a shear deformable buckling theory for two-layer members with partial interaction. Challamel and Girhammar [14] formulated a non-shear deformable theory for the lateral torsional buckling analysis of layered composite beams that captures the effect of partial interaction between the layers. Zaghian [11] developed a non-conforming four-node finite shell element for the buckling analysis of steel plates symmetrically strengthened with GFRP plates. The previous models are limited to members with rectangular sections, and thus do not incorporate warping effects which are significant in beams of wide flange cross-sections of interest in the present study. Also, most studies neglected shear deformations in their formulations. Shear deformation effects were shown to influence lateral torsional buckling predictions in short span beams with homogeneous materials [15, 16, 17, 18, 19].

Pham and Mohareb [20] developed a non-shear deformable theory for the static analysis of steel beams strengthened with GFRP plates and formulated a closed solution. A shear deformable theory was developed in [21] and the field equations were solved using the finite difference technique. Finite element formulations based on shear and non-shear deformable theories were developed in [22]. Pham et al. [23] developed a model that captures the effect of pre-existing stresses induced in steel beams prior to GFRP strengthening. A common theme in the studies in [20-23] is that they are limited to linear static analysis and has not tackled buckling problems. In this respect, the present study complements past work by developing a lateral torsional buckling solution. The work of static analyses in Pham and Mohareb [20, 21] has shown that shear deformation effects are more important than in homogeneous beams. As such, the present study benefits from past knowledge by incorporating the effect of shear deformation due to bending and warping into the lateral torsional buckling analysis formulation sought.

Additionally, because the modulus of elasticity of adhesives is orders of magnitude lower than those of steel or GFRP, it may provide only partial interaction between both materials. As a result, throughout pre-buckling bending, a plane cross-section for the system before deformation may not remain plane after deformation [14, 24]. Traditional analysis methods based on the plane section assumption (e.g., the transformed section method) are thus expected to under-predict the displacement response [25]. Hence, the present formulation incorporates the effect of partial

interaction by relaxing the plane section assumption, both throughout pre-buckling and buckling. Also, global and local warping effects are included in the present formulation owing to their importance in buckling analysis of beams with open sections.

In summary, the present study develops finite element formulations for the lateral-torsional buckling analysis of beams with wide flange steel sections strengthened with a single GFRP plate adhesively bonded to one of the flanges. Distinctive features of the theory include: (1) it is based on a 1D beam solution, (2) it captures partial interaction between steel beam and GFRP plate, (3) it includes the contribution of shear strains within the adhesive layer, and (4) it includes the effect of shear deformations due to bending and warping.

2. Statement of the problem

A wide flange steel beam with a doubly symmetric cross-section is strengthened with a GFRP plate bonded to one of the flanges through a thin adhesive layer (Figure 1). The beam is subjected to general transversely distributed load $q_y(z,y)$ acting along the curve $y_{qy}(z)$ within the web middle surface and/or a longitudinally distributed load $q_z(z,y)$ acting along $y_{qz}(z)$. The loads are increased to $\lambda q_y(z,y)$ and/or $\lambda q_z(z,y)$ at which the member is assumed to buckle in a lateral torsional mode. It is required to determine the buckling load level λ and the corresponding buckling mode by developing one-dimensional finite element formulation.

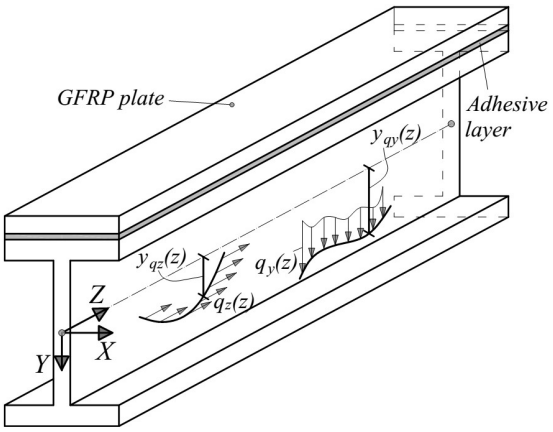

Figure 1. A GFRP-reinforced steel beam under the application of distributed loads

3. Assumptions

The assumptions of the present theory are an extension of those adopted under Vlasov [26] and Gjelsvik [27] beams to the composite beam, i.e.,

(i) In line with Vlasov theory, the section contours for the beam and the GFRP plate are assumed to remain un-deformed in their own plane,

(ii) The displacement fields are expressed according to the Gjelsvik beam theory [27] which captures global and local warping effects,

(iii) The steel beam and the GFRP plate are assumed to act as Timoshenko beams, i.e., their rotations about the x, y axes are considered distinct from the derivatives of the transverse and lateral displacements. The assumption is further extended to warping which is assumed to be distinct from the derivative of the angle of twist.

The following additional kinematic assumptions are also made:

(iv) Perfect bond is assumed at interfaces between the adhesive-GFRP and adhesive-steel interfaces,

(v) The adhesive is assumed to act as a flexible elastic material with a small modulus of elasticity relative to those of the beam or GFRP. As a result, the adhesive internal strain energy due to longitudinal normal stresses is considered negligible compared to that of the GFRP and steel,

(vi) The compressibility of the adhesive layer in the transverse direction is assumed negligible compared to the transverse displacements of the GFRP and the steel section, i.e., the transverse displacement of the steel beam and the GFRP can be assumed to be nearly equal,

(vii) The displacement fields within the adhesive are assumed to have a linear variation across the thickness,

(viii) Within the steel and GFRP, only the longitudinal normal stresses and the shear stresses in the tangential plane are assumed to contribute to the internal strain energy while contributions of all other stress components are assumed to be comparatively negligible.

Finally, the following assumptions are made regarding the materials and buckling configurations

(ix) The steel, GFRP and adhesive are assumed to be characterized by two material constants; the Young modulus and the shear modulus in a manner akin to linearly elastic isotropic materials. The time-dependent properties of the adhesive are omitted in the present pre-buckling analysis. If such properties are known, proper modifications can be made to the pre-buckling analysis while the present buckling analysis remains applicable to assess the stability of the system at any point on the equilibrium path.

The two-constant constitutive model adopted for the GFRP is applicable for isotropic GFRP plates made of chopped random fibers, and for orthotropic GFRP plates with fibers oriented in the longitudinal direction. Past 3D FEA analyses [28] have shown that the critical loads are sensitive only to the Young modulus E_z in longitudinal direction z (Fig. 1) and the shear

moduli G_{yz}, G_{xz} for stresses acting on the transverse plane and insensitive to remaining properties. In such cases, it was possible to accurately predict the buckling loads for orthotropic beams using an isotropic-like two-constant models (e.g., [29,30]). Other GFRP constitutive representations such as anisotropic or orthotropic materials where the fibers are not oriented longitudinally, are outside the scope of the present model.

(x) The member buckles in an inextensional mode. This means that during buckling, the centroidal strain and the curvature in the principal *yz*-plane remain unchanged, so that the member buckles under constant axial force and bending moments [16,17,31], and

(xi) Pre-buckling deformation, distortion and P-delta effects are neglected.

4. Kinematics

Figures 2a and 2b present four configurations which describe the strengthened beam starting from an un-deformed state (Configuration 1) to a lateral-torsional buckling state (configuration 4). Under the application of transversely distributed load $q_y(z)$ and longitudinally distributed load $q_z(z)$, the beam is displaced from Configuration 1 to 2. The displacement fields throughout this step are shown in Fig. 2b, in which $w_{1p}(z)$ is the longitudinal displacement at the wide flange beam centroid, $w_{3p}(z)$ is that of the GFRP plate centroid, $v_p(z)$ is the transverse deflection for the entire system (the beam, the GFRP plate and the adhesive), and $\theta_{xp}(z)$ is the rotation angle about the strong bending axis (X) for the GFRP plate and the steel section. Subscript p is used to imply that displacements take place in the pre-buckling state.

The applied reference loads are increased to $\lambda q_y(z)$, $\lambda q_z(z)$ until the system attains the point of onset of buckling (Configuration 3), in which the unknown load multiplier λ is to be determined from the buckling analysis. As a result, the associated pre-buckling displacements are assumed to linearly increase with the reference loads (Assumption x) and the corresponding displacements become $\lambda w_{1p}(z), \lambda w_{3p}(z)$, $\lambda v_p(z)$ and $\lambda\theta_{xp}(z)$.

Throughout buckling (from Configuration 3 to 4), the applied loads $\lambda q_y(z)$, $\lambda q_z(z)$ are assumed to remain constant in direction and magnitude while the steel beam and the GFRP plate centroids undergo lateral displacements $u_{1b}(z)$ and $u_{3b}(z)$, respectively. In Configuration 4, the steel beam and GFRP plate undergo weak axis rotation $\theta_{y1b}(z)$ and $\theta_{y3b}(z)$, respectively, while the entire

strengthened cross-section is assumed to undergo a twisting angle $\theta_{zb}(z)$. The global warping deformation of the steel beam is $\psi_{1b}(z)$ while that of the GFRP plate is denoted as $\psi_{3b}(z)$. Global warping deformation of the GFRP plate vanishes. The local warping deformations for both the GFRP plate and the steel beam are assumed to be linearly proportional to $\theta_{zb}'(z)$ in a manner that is consistent with the Gjelsvik theory.

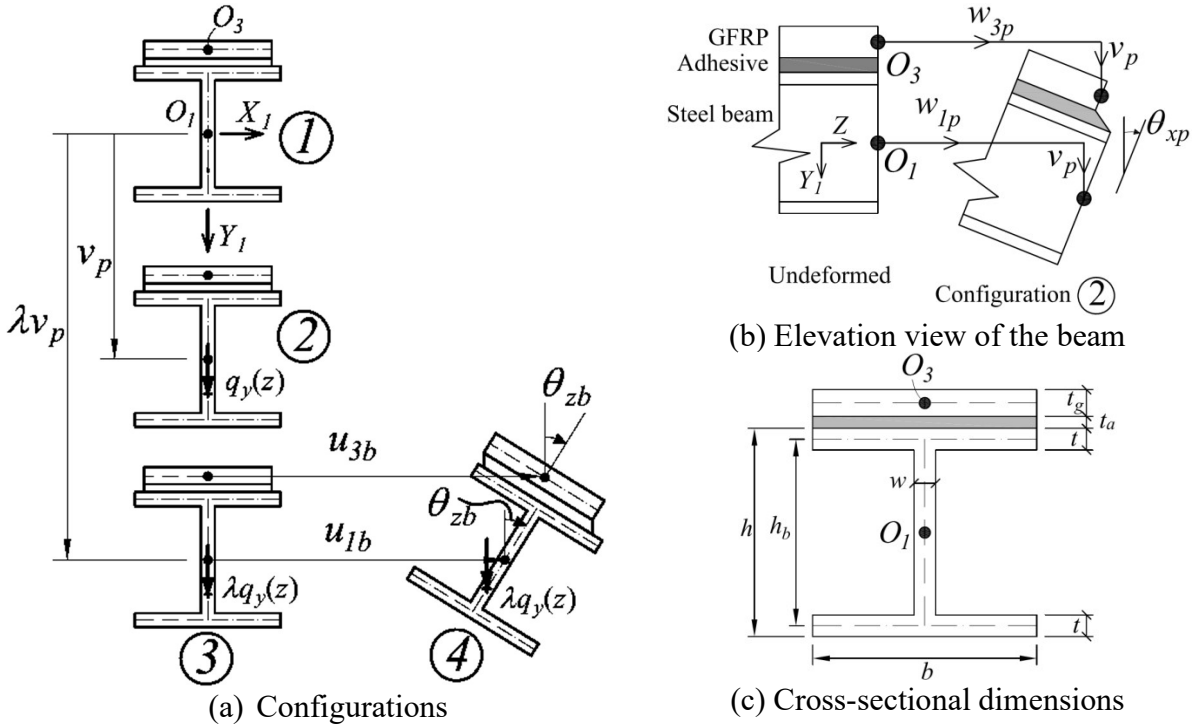

Figure 2. Beam configurations (a, b) and cross-sectional dimensions (c)

As a matter of convention, rotations θ_{xp}, $\theta_{y1b}(z)$ and $\theta_{y3b}(z)$ are assumed positive when rotating in the same direction as $v_p'(z)$, $u_{1b}'(z)$ and $u_{3b}'(z)$, respectively, while twisting angle $\theta_{zb}(z)$ is assumed positive when rotating clockwise [29]. The sign convention for other displacement fields are shown in Figs. 2a,b. Also, all field variables with a subscript p denote fields (displacements, strains, stresses, or stress resultants) arising during the pre-buckling stage (from Configuration 1 to 2) and variables with a subscript b denote fields arising during buckling (from Configuration 3 to 4). Total fields arising in going from Configuration 1 to 4 are denoted by the superscript *, while fields with no subscripts p,b nor a superscript * are generic and are considered valid for pre-buckling, buckling, or total responses.

Figure 2c shows the geometric parameters for the cross-section. The steel beam has a total depth h, an centerline depth h_b, web thickness w, flange thickness t, and flange width b, while the thickness of the adhesive layer is t_a and that of GFRP plate is t_g. Material elasticity and shear moduli of steel are denoted as E_s and G_s, respectively while those of GFRP are E_g and G_g. The shear modulus of adhesive is assumed as G_a.

5. Coordinate systems and displacements at an arbitrary point lying on sections

Three global coordinate systems $O_iX_iY_iZ$ ($i=1,2,3$) are defined for the wide flange steel beam, adhesive layer and GFRP plate, respectively, in which O_i are centroids of each material (Fig. 3a) and subscripts $i=1,2,3$ respectively denote the steel section, the adhesive, and the GFRP plate.

In a manner consistent with the Gjelsvik thin walled beam theory, the local coordinates of a point A_i offset from the section contour (Fig. 3b) are determined by three local coordinates (s_i, n_i, z) in which s_i is a curvilinear contour coordinate measured from Origin O_i while n_i is normal distance measured from contour line. As a matter of sign convention, positive signs of n_i, z and the contour tangent follows a right-handed coordinate system. Angle $\alpha(s_i)$ between the positive directions of the tangent to the contour at the point of interest and global $X-$direction is taken positive in the clockwise direction from the $X-$axis. When the beam deforms under the application of loads, a Point A_i undergoes displacements (ξ_i, η_i, ζ_i) along the tangent, normal, and longitudinal directions, respectively.

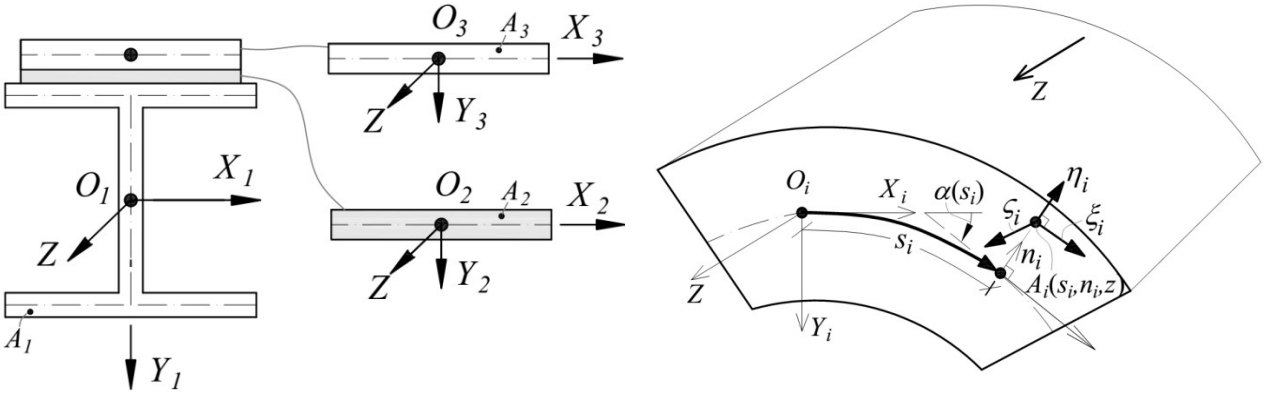

(a) Global coordinate systems for steel beam, adhesive layer, and GFRP plate

(b) Displacement fields of a Point A_i offset from the section contour

Figure 3. Coordinate systems and local displacement fields

6. Pre-buckling displacement fields

Based on Gjelsvik [27], the expression of the pre-bucking displacements $\left(\xi_{ip},\eta_{ip},\zeta_{ip}\right)$ of Point $A_i\left(s_i,n_i,z\right)$ along the local directions (Figs.3a,b) can be related to the global displacement fields $w_{1p}\left(z\right)$, $w_{3p}\left(z\right)$, $v_p\left(z\right)$ and $\theta_{xp}\left(z\right)$. For the steel beam ($i=1$), the displacements of $A_1\left(s_1,n_1,z\right)$ are given by

$$\begin{Bmatrix}\xi_{1p}\left(s_1,n_1,z\right)\\ \eta_{1p}\left(s_1,n_1,z\right)\\ \zeta_{1p}\left(s_1,n_1,z\right)\end{Bmatrix}=\begin{bmatrix}0 & \sin\alpha\left(s_1\right) & 0\\ 0 & -\cos\alpha\left(s_1\right) & 0\\ 1 & n_1\cos\alpha\left(s_1\right)D & -y_1\left(s_1\right)\end{bmatrix}\begin{Bmatrix}w_{1p}\left(z\right)\\ v_p\left(z\right)\\ \theta_{xp}\left(z\right)\end{Bmatrix} \tag{1}$$

where $\alpha_1\left(s\right)=0^o$ for the flanges, $\alpha_1\left(s\right)=90^o$ for the web and D denotes the derivative operator $\partial\,/\partial z$. Also, for the pre-buckling displacement fields of Point A_3 within the GFRP plate and noting that $\alpha\left(s_3\right)=0$, one obtains $\xi_{3p}=0$ and

$$\begin{Bmatrix}\eta_{3p}\left(s_3,n_3,z\right)\\ \zeta_{3p}\left(s_3,n_3,z\right)\end{Bmatrix}=\begin{Bmatrix}0 & -1 & 0\\ 1 & n_3D & y_3\left(s_3\right)\end{Bmatrix}\begin{Bmatrix}w_{3p}\left(z\right)\\ v_p\left(z\right)\\ \theta_{xp}\left(z\right)\end{Bmatrix} \tag{2}$$

For the adhesive layer, the displacement fields of a point A_2 are linearly interpolated from the displacements at the top surface of steel flange and the bottom surface of the GFRP plate (Assumption vii), i.e.,

$$\begin{Bmatrix}\xi_{2p}\left(s_2,n_2,z\right)\\ \eta_{2p}\left(s_2,n_2,z\right)\\ \zeta_{2p}\left(s_2,n_2,z\right)\end{Bmatrix}=\left(\frac{1}{2}+\frac{n_2}{t_a}\right)\begin{Bmatrix}\xi_{3p}\left(s_3,-t_g/2,z\right)\\ \eta_{3p}\left(s_3,-t_g/2,z\right)\\ \zeta_{3p}\left(s_3,-t_g/2,z\right)\end{Bmatrix}+\left(\frac{1}{2}-\frac{n_2}{t_a}\right)\begin{Bmatrix}\xi_{1p}\left(s_1,t/2,z\right)\\ \eta_{1p}\left(s_1,t/2,z\right)\\ \zeta_{1p}\left(s_1,t/2,z\right)\end{Bmatrix} \tag{3}$$

By noting that $\alpha\left(s_1\right)=0$ for the top flange, Eq. (3) simplifies to $\xi_{2p}=0$ and

$$\begin{Bmatrix}\eta_{2p}\left(s_2,n_2,z\right)\\ \zeta_{2p}\left(s_2,n_2,z\right)\end{Bmatrix}=\begin{Bmatrix}0 & 0 & -1 & 0\\ \left(\frac{1}{2}-\frac{n_2}{t_a}\right) & \left(\frac{1}{2}+\frac{n_2}{t_a}\right) & \left[\left(\frac{1}{2}-\frac{n_2}{t_a}\right)\frac{t}{2}-\left(\frac{1}{2}+\frac{n_2}{t_a}\right)\frac{t_g}{2}\right]D & \left(\frac{1}{2}-\frac{n_2}{t_a}\right)\frac{h_b}{2}\end{Bmatrix}\begin{Bmatrix}w_{1p}\\ w_{3p}\\ v_p\\ \theta_{xp}\end{Bmatrix} \tag{4}$$

7. Total displacement fields

Under the application of loads $\lambda q_y\left(z\right)$ and $\lambda q_z\left(z\right)$, the strengthened beam deforms from Configuration 1 to 4. The associated total displacement fields $\left(\xi_i^*,\eta_i^*,\zeta_i^*\right)$ of Point $A_i\left(s_i,n_i,z\right)$

(Figs. 3a,b), where $i=1,2,3$ respectively, denotes steel, adhesive, and GFRP, can be expressed in terms of displacements $\lambda w_{1p}(z), \lambda w_{3p}(z), \lambda v_p(z)$, $\lambda\theta_{xp}(z)$ and $u_{1b}(z)$, $u_{3b}(z)$, $\theta_{y1b}(z)$, $\theta_{y3b}(z)$, $\theta_{zb}(z)$, $\psi_{1b}(z)$. For the steel beam, one can express the displacements of point A_1 as:

$$\begin{aligned}
\xi_1^*(s_1,n_1,z) &= \sin\alpha(s_1)\lambda v_p(z) + \cos\alpha(s_1)u_{1b}(z) + \left[r(s_1)+n_1 q'(s_1)\right]\theta_{zb}(z)\\
\eta_1^*(s_1,n_1,z) &= -\cos\alpha(s_1)\lambda v_p(z) + \sin\alpha(s_1)u_{1b}(z) - q(s_1)\theta_{zb}(z)\\
\zeta_1^*(s_1,n_1,z) &= \left[\lambda w_{1p}(z) + n_1\cos\alpha(s_1)\lambda v_p'(z) - y_1(s_1)\lambda\theta_{xp}(z)\right] - n_1\sin\alpha(s_1)u_{1b}'(z)\\
&\quad -x(s_1)\theta_{y1b}(z) + n_1 q(s_1)\theta_{zb}'(z) - \omega(s_1)\psi_{1b}(z)
\end{aligned} \tag{5}$$

in which $q(s_1)=x_1(s_1)\cos\alpha(s_1)+y_1(s)\sin\alpha(s_1)$, $r(s_1)=x(s_1)\sin\alpha(s_1)-y_1(s)\cos\alpha(s_1)$, and $\omega(s_1)=\int_0^{s_1} r(s_1)\,ds_1$ are defined. Also, the displacement components of Point A_3 within the GFRP plate ($\alpha(s_3)=0$) can be expressed as:

$$\begin{aligned}
\xi_3^*(s_3,n_3,z) &= u_3(z) + n_3\theta_{zb}(z)\\
\eta_3^*(s_3,n_3,z) &= -\lambda v_p(z) - x_3(s_3)\theta_{zb}(z)\\
\zeta_3^*(s_3,n_3,z) &= \lambda w_{3p}(z) + n_3\lambda v_p'(z) + n_3 x_3(s_3)\theta_{zb}'(z) - x_3(s_3)\theta_{y3b}(z)
\end{aligned} \tag{6}$$

For the adhesive layer, the displacement fields of point A_2 within this layer are linearly interpolated between the displacements at the top surface of steel flange and the bottom surface of the GFRP plate (Assumption vii), i.e.,

$$\begin{Bmatrix} \xi_2^*(s_2,n_2,z)\\ \eta_2^*(s_2,n_2,z)\\ \zeta_2^*(s_2,n_2,z)\end{Bmatrix} = \left(\frac{1}{2}+\frac{n_2}{t_a}\right)\begin{Bmatrix} \xi_{3b}(s_3,-t_g/2,z)\\ \eta_{3b}(s_3,-t_g/2,z)\\ \zeta_{3b}(s_3,-t_g/2,z)\end{Bmatrix} + \left(\frac{1}{2}-\frac{n_2}{t_a}\right)\begin{Bmatrix} \xi_{1b}(s_1,t/2,z)\\ \eta_{1b}(s_1,t/2,z)\\ \zeta_{1b}(s_1,t/2,z)\end{Bmatrix} \tag{7}$$

It is noted that in Eq. (7), one has $\alpha(s_1)=0$ and $y(s)=-h_b/2$ for the top flange and $x_1(s_1)=x_2(s_2)=x_3(s_3)=x(s)$. From Eqs. (5) and (6), by substituting into Eq.(7), one obtains:

$$\xi_2^* = \left(\frac{1}{2}-\frac{n_2}{t_a}\right)u_{1b}(z)+\left(\frac{1}{2}+\frac{n_2}{t_a}\right)u_{3b}(z)+\left(\frac{h-t_g}{4}-\frac{h+t_g}{2t_a}n_2\right)\theta_{zb}(z)$$

$$\eta_2^* = -\lambda v_p(z)-x(s)\theta_{zb}(z)$$

$$\zeta_2^* = \left(\frac{1}{2}-\frac{n_2}{t_a}\right)\lambda w_{1p}(z)+\left(\frac{1}{2}+\frac{n_2}{t_a}\right)\lambda w_{3p}(z)+\left(\frac{t-t_g}{4}-\frac{t+t_g}{2t_a}n_2\right)\lambda v_p'(z)+\frac{h_b}{2}\left(\frac{1}{2}-\frac{n_2}{t_a}\right)\lambda\theta_{xp}(z)$$
$$-\left(\frac{1}{2}-\frac{n_2}{t_a}\right)x(s)\theta_{y1b}(z)-\left(\frac{1}{2}+\frac{n_2}{t_a}\right)x(s)\theta_{y3b}(z)+\left(\frac{t-t_g}{4}-\frac{t+t_g}{2t_a}n_2\right)x(s)\theta_{zb}'(z)$$
$$-\frac{h_b}{2}\left(\frac{1}{2}-\frac{n_2}{t_a}\right)x(s)\psi_{1b}(z) \qquad \text{(8)a-c}$$

8. Strain-Displacement Relations

8.1. Total strains

The nonlinear strain-displacement terms are retained throughout lateral torsional buckling. For the steel beam ($i=1$) and the GFRP ($i=3$), the non-vanishing strains take the form:

$$\varepsilon_i^* = \varepsilon_i^{*L}+\varepsilon_i^{*N} = \frac{\partial\zeta_i^{*\prime}}{\partial z}+\frac{1}{2}\left[\left(\frac{\partial\eta_i^{*\prime}}{\partial z}\right)^2+\left(\frac{\partial\xi_i^{*\prime}}{\partial z}\right)^2\right]$$
$$\gamma_i^* = \gamma_i^{*L}+\gamma_i^{*N} = \frac{\partial\xi_i^*}{\partial z}+\frac{\partial\zeta_i^*}{\partial s_i}+\frac{\partial\xi_i^*}{\partial z}\frac{\partial\xi_i^*}{\partial s_i}+\frac{\partial\zeta_i^*}{\partial s_i}\frac{\partial\zeta_i^*}{\partial z}+\frac{\partial\eta_i^*}{\partial s_i}\frac{\partial\eta_i^*}{\partial z} \qquad \text{(9)a-b}$$

in which ε_i^{*L} and ε_i^{*N} are the linear and the non-linear strain components of ε_i^*, and $\gamma_i^{*L}, \gamma_i^{*N}$ are the linear and the non-linear strain components of γ_i^*. From Eqs.(5)-(6) by substituting into Eqs. (9)a-b, and introducing symbols ' and " to respectively denote for derivative operators $\partial/\partial z$ and $\partial^2/\partial z^2$, the linear and non-linear strain components are expressed as

$$\varepsilon_1^{*L} = \lambda w_{1p}{}'(z)+n_1\cos\alpha(s_1)\lambda v_p''(z)-y_1(s_1)\lambda\theta_{xp}'(z)+\frac{1}{2}\left[\lambda v_p'(z)\right]^2-n_1\sin\alpha(s_1)u_{1b}''(z)$$
$$-x_1(s_1)\theta_{y1b}'(z)+\lambda v_p'(z)\left\{x_1(s_1)+n_1q'(s_1)\sin\alpha(s_1)\right\}\theta_{zb}'(z)+n_1q(s_1)\theta_{zb}''(z)-\omega(s_1)\psi_{1b}'(z)$$
$$\varepsilon_1^{*N} = \frac{1}{2}u_{1b}'{}^2(z)+\left[n_1q'(s_1)\cos\alpha(s_1)-y_1(s_1)\right]u_{1b}'(z)\theta_{zb}'(z)+\frac{1}{2}q^2(s_1)\theta_{zb}'{}^2(z) \qquad \text{(10)a,b}$$
$$+\frac{1}{2}\left[r(s_1)+n_bq'(s_1)\right]^2\theta_{zb}'{}^2(z)$$

$$\gamma_1^{*L} = \lambda \sin\alpha(s_1)\left\{v_p'(z) - \theta_{xp}(z) - \left[w_{1p}{}'(z) - y_1(s_1)\lambda\theta_{xp}'(z)\right]\theta_{xp}(z)\right\} + \cos\alpha(s_1)u_{sb}'(z)$$
$$+\lambda\theta_{xp}(z)n_1\sin^2\alpha(s_1)u_{1b}''(z) - \cos\alpha(s_1)\left[1 + \lambda w_{1p}{}'(z) + n_1\cos\alpha(s_1)\lambda v_p''(z) - y_1(s_1)\lambda\theta_{xp}'(z)\right]\theta_{y1b}(z)$$
$$+\lambda\theta_{xp}(z)x\sin\alpha(s_1)\theta_{y1b}'(z) + \lambda v_p'(z)q'(s_1)\cos\alpha(s_1)\theta_{zb}(z) - \lambda\theta_{xp}(z)n_1q(s_1)\sin\alpha(s_1)\theta_{zb}''(z)$$
$$+\left\{r(s_1) + 2n_1q'(s_1) + \lambda\left[w_{1p}{}'(z) + n_b\cos\alpha(s_1)v_p''(z) - y_1(s_1)\theta_{xp}'(z)\right]n_1q'(s_1)\right\}\theta_{zb}'(z)$$
$$-\omega'(s_1)\left\{1 + \lambda\left[w_{1p}{}'(z) + n_1\cos\alpha(s_1)v_p''(z) - y_1(s_1)\theta_{xp}'(z)\right]\right\}\psi_{1b}(z) + \lambda\theta_{xp}(z)\omega(s_1)\sin\alpha(s_1)\psi_{1b}'(z)$$
$$\gamma_1^{*N} = -q'(s_1)\sin\alpha(s_1)u_{1b}'(z)\theta_{zb}(z) - n_1^2q'(s_1)\sin\alpha(s_1)u_{1b}''(z)\theta_{zb}'(z) + n_1\omega'(s_1)\sin\alpha(s_1)u_{1b}''(z)\psi_{1b}(z)$$
$$+x(s_1)\cos\alpha(s_1)\theta_{y1b}(z)\theta_{y1b}'(z) - n_1q(s_1)\cos\alpha(s_1)\theta_{y1b}(z)\theta_{zb}''(z) + \omega(s_1)\cos\alpha(s_1)\theta_{y1b}(z)\psi_{1b}'(z)$$
$$+q(s_1)q'(s_1)\theta_{zb}(z)\theta_{zb}'(z) - x(s_1)n_1q'(s_1)\theta_{y1b}'(z)\theta_{zb}'(z) + x(s_1)\omega'(s_1)\theta_{y1b}'(z)\psi_{1b}(z)$$
$$+n_1^2q(s_1)q'(s_1)\theta_{zb}'(z)\theta_{zb}''(z) - \omega(s_1)n_1q'(s_1)\theta_{zb}'(z)\psi_{1b}'(z) - \omega'(s_1)n_1q(s_1)\theta_{zb}''(z)\psi_{1b}(z)$$
$$+\omega(s_1)\omega'(s_1)\psi_{1b}'(z)\psi_{1b}(z)$$

(11)a,b

$$\varepsilon_3^{*L} = \lambda w_{3p}'(z) + n_3\lambda v_p''(z) + \frac{1}{2}\left(\lambda v_p'(z)\right)^2 - x_3(s_3)\theta_{y3b}'(z) + n_3x_3(s_3)\theta_{zb}''(z) + \lambda x_3(s_3)v_p'(z)\theta_{zb}'(z)$$
$$\varepsilon_3^{*N} = \frac{1}{2}u_{3b}'{}^2(z) + n_3u_{3b}'(z)\theta_{zb}'(z) + \frac{1}{2}n_3^2\theta_{zb}'{}^2(z) + \frac{1}{2}x_3^2(s_3)\theta_{zb}'{}^2(z)$$

(12)a,b

and

$$\gamma_3^{*L} = u_{3b}'(z) - \left[1 + \lambda w_{3p}'(z) + n_3\lambda v_p''(z)\right]\theta_{y3b}(z) + n_3\left[2 + \lambda w_{3p}'(z) + n_3\lambda v_p''(z)\right]\theta_{zb}'(z) + \lambda v_p'(z)\theta_{zb}(z)$$
$$\gamma_3^{*N} = x_2(s_2)\left[\theta_{y3b}'(z)\theta_{y3b}(z) - n_3\theta_{y3b}'(z)\theta_{zb}'(z) - n_3\theta_{y3b}(z)\theta_{zb}''(z) + \theta_{zb}(z)\theta_{zb}'(z) + n_3^2\theta_{zb}'(z)\theta_{zb}''(z)\right]$$

(13)a,b

For the adhesive layer, normal strains are neglected (Assumption v) while all three shear strains are retained. The total shear strains are

$$\gamma_{2zn}^* = \gamma_{2zn}^{*L} + \gamma_{2zn}^{*N} = \frac{\partial\eta_2^*}{\partial z} + \frac{\partial\zeta_2^*}{\partial n_2} + \frac{\partial\eta_2^*}{\partial z}\frac{\partial\eta_2^*}{\partial n_2} + \frac{\partial\zeta_2^*}{\partial z}\frac{\partial\zeta_2^*}{\partial n_2} + \frac{\partial\xi_2^*}{\partial z}\frac{\partial\xi_2^*}{\partial n_2};$$
$$\gamma_{2sn}^* = \gamma_{2sn}^{*L} + \gamma_{2sn}^{*N} = \frac{\partial\eta_2^*}{\partial s_2} + \frac{\partial\xi_2^*}{\partial n_2} + \frac{\partial\eta_2^*}{\partial s_2}\frac{\partial\eta_2^*}{\partial n_2} + \frac{\partial\xi_2^*}{\partial s_2}\frac{\partial\xi_2^*}{\partial n_2} + \frac{\partial\zeta_2^*}{\partial s_2}\frac{\partial\zeta_2^*}{\partial n_2};$$
$$\gamma_{2sz}^* = \gamma_{2sz}^{*L} + \gamma_{2sz}^{*N} = \frac{\partial\xi_2^*}{\partial z} + \frac{\partial\zeta_2^*}{\partial s_2} + \frac{\partial\xi_2^*}{\partial z}\frac{\partial\xi_2^*}{\partial s_2} + \frac{\partial\zeta_2^*}{\partial z}\frac{\partial\zeta_2^*}{\partial s_2} + \frac{\partial\eta_2^*}{\partial z}\frac{\partial\eta_2^*}{\partial s_2};$$

(14)a-c

in which γ_{2zn}^{*L} and γ_{2zn}^{*N} are the linear and non-linear shear strain components of γ_{2zn}^{*}. Also, γ_{2sn}^{*L} and γ_{2sn}^{*N} are those of γ_{2sn}^{*} while γ_{2sz}^{*L} and γ_{2sz}^{*N} are those of γ_{2sz}^{*}. From Eqs. (8)a-c, by substituting into Eqs. (14)a-c, components for shearing strains are obtained as

$$\begin{aligned}\gamma_{2zn}^{*L} &= -\lambda\left(1+c_6\right)v_p'\left(z\right)-\lambda c_5 w_{1p}\left(z\right)+\lambda c_5 w_{3p}\left(z\right)-\lambda c_5 c_7\theta_{xp}\left(z\right)+\lambda^2 B_{1p}\left(z,n_2\right)B_{2p}\left(z\right)\\ &+\lambda c_5 x\left(s\right)B_{1p}\left(z,n_2\right)\theta_{y1b}\left(z\right)-\lambda c_1\left(n_2\right)x\left(s\right)B_{2p}\left(z\right)\theta_{y1b}'\left(z\right)-\lambda c_5 x\left(s\right)B_{1p}\left(z,n_2\right)\theta_{y3b}\left(z\right)\\ &-\lambda c_2\left(n_2\right)x\left(s\right)B_{2p}\left(z\right)\theta_{y3b}'\left(z\right)-\lambda c_6 x\left(s\right)B_{1p}\left(z,n_2\right)\theta_{zb}'\left(z\right)+\lambda c_3\left(n_2\right)x\left(s\right)B_{2p}\left(z\right)\theta_{zb}''\left(z\right)\\ &+\lambda c_5 c_7 x\left(s\right)B_{1p}\left(z,n_2\right)\psi_{1b}\left(z\right)-\lambda c_7 c_1\left(n_2\right)x\left(s\right)B_{2p}\left(z\right)\psi_{1b}'\left(z\right)\\ &-x\left(s\right)\theta_{zb}'\left(z\right)+c_5 x\left(s\right)\theta_{y1b}\left(z\right)-c_5 x\left(s\right)\theta_{y3b}\left(z\right)-c_6 x\left(s\right)\theta_{zb}'\left(z\right)+c_5 c_7 x\left(s\right)\psi_{1b}\left(z\right)\end{aligned} \tag{15}$$

in which

$$B_{1p}\left(z,n_2\right)=\left(\frac{1}{2}-\frac{n_2}{t_a}\right)w_{1p}'\left(z\right)+\left(\frac{1}{2}+\frac{n_2}{t_a}\right)w_{3p}'\left(z\right)+\left(\frac{t-t_g}{4}-\frac{t+t_g}{2t_a}n_2\right)v_p''\left(z\right)+\frac{h_b}{2}\left(\frac{1}{2}-\frac{n_2}{t_a}\right)\theta_{xp}'\left(z\right)$$

$$B_{2p}\left(z\right)=\left(-\frac{1}{t_a}\right)w_{1p}\left(z\right)+\left(\frac{1}{t_a}\right)w_{3p}\left(z\right)+\left(-\frac{t+t_g}{2t_a}\right)v_p'\left(z\right)+\frac{h_b}{2}\left(-\frac{1}{t_a}\right)\theta_{xp}\left(z\right)$$

and

$$\begin{aligned}\gamma_{2zn}^{*N} &= -c_5 c_1\left(n_2\right)x^2\left(s\right)\theta_{y1b}'\theta_{y1b}-c_5 c_2\left(n_2\right)x^2\left(s\right)\theta_{y1b}\theta_{y3b}'+c_5 c_3\left(n_2\right)x^2\left(s\right)\theta_{zb}''\theta_{y1b}\\ &-c_5 c_7 c_1\left(n_2\right)x^2\left(s\right)\psi_{1b}'\theta_{y1b}+c_5 c_1\left(n_2\right)x^2\left(s\right)\theta_{y1b}'\theta_{y3b}+c_5 c_2\left(n_2\right)x^2\left(s\right)\theta_{y3b}'\theta_{y3b}\\ &-c_5 c_3\left(n_2\right)x^2\left(s\right)\theta_{zb}''\theta_{y3b}+c_5 c_7 c_1\left(n_2\right)x^2\left(s\right)\psi_{1b}'\theta_{y3b}+c_6 c_1\left(n_2\right)x^2\left(s\right)\theta_{y1b}'\theta_{zb}'\\ &+c_6 c_2\left(n_2\right)x^2\left(s\right)\theta_{y3b}'\theta_{zb}'-c_6 c_3\left(n_2\right)x^2\left(s\right)\theta_{zb}''\theta_{zb}'+c_6 c_7 c_1\left(n_2\right)x^2\psi_{1b}'\theta_{zb}'\\ &-c_5 c_7 c_1\left(n_2\right)x^2\left(s\right)\theta_{y1b}'\psi_{1b}-c_5 c_7 c_2\left(n_2\right)x^2\left(s\right)\theta_{y3b}'\psi_{1b}+c_5 c_7 c_3\left(n_2\right)x^2\left(s\right)\theta_{zb}''\psi_{1b}\\ &-c_5 c_7^2 c_1\left(n_2\right)x^2\left(s\right)\psi_{1b}'\psi_{1b}-c_5 c_1\left(n_2\right)u_{1b}u_{1b}'-c_5 c_2\left(n_2\right)u_{1b}u_{3b}'-c_5 c_4\left(n_2\right)u_{1b}\theta_{zb}'\\ &+c_5 c_1\left(n_2\right)u_{1b}'u_{3b}+c_5 c_2\left(n_2\right)u_{3b}u_{3b}'+c_5 c_4\left(n_2\right)u_{3b}\theta_{zb}'-\left(c_6+c_5 c_7\right)c_1\left(n_2\right)u_{1b}'\theta_{zb}\\ &-\left(c_6+c_5 c_7\right)c_2\left(n_2\right)u_{3b}'\theta_{zb}-\left(c_6+c_5 c_7\right)c_4\left(n_2\right)\theta_{zb}\theta_{zb}'\end{aligned} \tag{16}$$

in which

$$c_1\left(n_2\right)=\frac{1}{2}-\frac{n_2}{t_a};\qquad c_2\left(n_2\right)=\frac{1}{2}+\frac{n_2}{t_a};\qquad c_3\left(n_2\right)=\frac{t-t_g}{4}-\frac{t+t_g}{2t_a}n_2;\qquad c_4\left(n_2\right)=\frac{h-t_g}{4}-\frac{h+t_g}{2t_a}n_2$$

$$c_5=\frac{1}{t_a};\qquad c_6=\frac{t+t_g}{2t_a};\qquad c_7=\frac{h_b}{2};\qquad c_5 c_7=\frac{h_b}{2t_a};\qquad \left(c_6+c_5 c_7\right)=\frac{h+t_g}{2t_a}$$

Also, one has

$$\gamma_{2sn}^{*L} = -\theta_{zb} - c_5 u_{1b} + c_5 u_{3b} - \left(c_6 + c_5 c_7\right)\theta_{zb} + \lambda B_{2p}(z)\Big[-c_1(n_2)\theta_{y1b} - c_2(n_2)\theta_{y3b} + c_3(n_2)\theta'_{zb} - c_7 c_1(n_2)\psi_{1b}\Big] \tag{17}$$

$$\begin{aligned}\gamma_{2sn}^{*N} = {} & -c_5 c_1(n_2)x(s)\theta_{y1b}{}^2 - c_5 c_2(n_2)x(s)\theta_{y1b}\theta_{y3b} + c_5 c_3(n_2)x(s)\theta_{y1b}\theta'_{zb} - c_5 c_7 c_1(n_2)x(s)\theta_{y1b}\psi_{1b} \\ & + c_5 c_1(n_2)x(s)\theta_{y1b}\theta_{y3b} + c_5 c_2(n_2)x(s)\theta_{y3b}{}^2 - c_5 c_3(n_2)x(s)\theta_{y3b}\theta'_{zb} + c_5 c_7 c_1(n_2)x(s)\theta_{y3b}\psi_{1b} \\ & + c_6 c_1(n_2)x(s)\theta_{y1b}\theta'_{zb} + c_6 c_2(n_2)x(s)\theta_{y3b}\theta'_{zb} - c_6 c_3(n_2)x(s)\theta'_{zb}{}^2 + c_7 c_6 c_1(n_2)x(s)\theta'_{zb}\psi_{1b} \\ & - c_5 c_7 c_1(n_2)x(s)\theta_{y1b}\psi_{1b} - c_5 c_7 c_2(n_2)x(s)\theta_{y3b}\psi_{1b} + c_5 c_7 c_3(n_2)x(s)\theta'_{zb}\psi_{1b} - c_5 c_7^2 c_1(n_2)x(s)\psi_{1b}{}^2\end{aligned} \tag{18}$$

$$\begin{aligned}\gamma_{2sz}^{*L} = {} & c_1(n_2)u_{1b}{}' + c_2(n_2)u_{3b}{}' + c_4(n_2)\theta_{zb}{}' - c_1(n_2)\theta_{y1b} - c_2(n_2)\theta_{y3b} + c_3(n_2)\theta'_{zb} + \\ & - c_7 c_1(n_2)\psi_{1b} + \lambda B_{1p}(z,n_2)\Big[-c_1(n_2)\theta_{y1b} - c_2(n_2)\theta_{y3b} + c_3(n_2)\theta'_{zb} - c_7 c_1(n_2)\psi_{1b}\Big] + \lambda v_p{}'(z)\theta_{zb}\end{aligned} \tag{19}$$

and

$$\begin{aligned}\gamma_{2sz}^{*N} = {} & c_1^2(n_2)x(s)\theta_{y1b}{}'\theta_{y1b} + c_1(n_2)c_2(n_2)x(s)\theta_{y1b}{}'\theta_{y3b} - c_3(n_2)c_1(n_2)x(s)\theta_{y1b}{}'\theta'_{zb} \\ & + c_7 c_1^2(n_2)x(s)\theta_{y1b}{}'\psi_{1b} + c_1(n_2)c_2(n_2)x(s)\theta_{y1b}\theta_{y3b}{}' + c_2^2(n_2)x(s)\theta_{y3b}{}'\theta_{y3b} \\ & - c_3(n_2)c_2(n_2)x(s)\theta_{y3b}{}'\theta'_{zb} + c_7 c_1(n_2)c_2(n_2)x(s)\theta_{y3b}{}'\psi_{1b} - c_3(n_2)c_1(n_2)x(s)\theta_{y1b}\theta''_{zb} \\ & - c_3(n_2)c_2(n_2)x(s)\theta_{y3b}\theta''_{zb} + c_3^2(n_2)x(s)\theta''_{zb}\theta'_{zb} - c_7 c_3(n_2)c_1(n_2)x(s)\theta''_{zb}\psi_{1b} \\ & + c_7 c_1^2(n_2)x(s)\theta_{y1b}\psi'_{1b} + c_7 c_1(n_2)c_2(n_2)x(s)\theta_{y3b}\psi'_{1b} - c_7 c_3(n_2)c_1(n_2)x(s)\theta'_{zb}\psi'_{1b} \\ & + c_7^2 c_1^2(n_2)x(s)\psi'_{1b}\psi_{1b} + x(s)\theta_{zb}{}'\theta_{zb}\end{aligned} \tag{20}$$

8.2. Strain fields throughout Pre-buckling

When the beam is displaced from Configuration 1 to 2, the strains are assumed small and thus only the linear terms are retained. From Eqs. (10) through (20), by omitting the nonlinear terms and the buckling displacements, and setting $\lambda = 1$, the pre-buckling strains are obtained as

$$\varepsilon_{1p} = w'_{1p}(z) + n_1 \cos\alpha(s_1)v''_p(z) - y_1(s_1)\theta'_{xp}(z); \qquad \gamma_{1p} = \sin\alpha(s_1)\left[v'_p(z) - \theta_{xb}(z)\right] \tag{21a-b}$$

$$\varepsilon_{3p} = w'_{3p}(z) + n_3 v''_p(z); \qquad \gamma_{3p} = 0 \tag{22a-b}$$

$$\gamma_{2szp} = 0; \quad \gamma_{2nsp} = 0; \quad \gamma_{2nzp} = -\frac{1}{t_a}w_{1p}(z) + \frac{1}{t_a}w_{3p}(z) - \left(1 + \frac{t+t_g}{2t_a}\right)v'_p(z) - \frac{h_b}{2t_a}\theta_{xp}(z) \tag{23a-c}$$

Equations (21-23) are similar to those reported in [22].

9. Stress-Strain Relations

All materials are assumed linearly elastic and isotropic (Assumption ix) throughout the pre-buckling and buckling analyses. As a result, the pre-buckling stress-strains at Configuration 2 are $\sigma_{1p} = E_1\varepsilon_{1p}$, $\tau_{1p} = G_1\gamma_{1p}$, $\sigma_{3p} = E_3\varepsilon_{3p}$, $\tau_{3p} = G_3\gamma_{3p}$ and $\tau_{zn2p} = G_2\gamma_{zn2p}$ while those at the end of the buckled state at Configuration 4 are $\sigma_1^* = E_1\varepsilon_1^*$, $\tau_1^* = G_1\gamma_1^*$, $\sigma_3^* = E_3\varepsilon_3^*$, $\tau_3^* = G_3\gamma_3^*$, $\tau_{zn2}^* = G_2\gamma_{zn2}^*$, $\tau_{sn2}^* = G_2\gamma_{sn2}^*$ and $\tau_{sz2}^* = G_2\gamma_{sz2}^*$.

10. Pre-buckling Stress Resultants

From Eq. (21), the stress fields within the steel beam can be expressed as

$$\sigma_{1p} = E_1\varepsilon_{1p} = E_1\left\langle 1 \;\vdots\; n_1\cos\alpha(s_1) \quad -y_1(s_1)\right\rangle\begin{Bmatrix} w'_{1p}(z) \\ v''_p(z) \\ \theta'_{xp}(z)\end{Bmatrix} \qquad \text{(24)a-b}$$

$$\tau_{1p} = G_1\gamma_{1p} = G_1\left[v'_p(z) - \theta_{xb}(z)\right]\sin\alpha(s_1)$$

The stress resultant-displacement relations [32] are $N_{1p}(z) = E_1A_sw'_{1p}(z)$; $M_{sp}(z) = E_1I_{ss}v''_p(z)$; and $M_{xp}(z) = E_1I_{xx}\theta'_{xp}(z)$. From Eqs. (24)a, by substituting from the stress resultant-displacement relations for the steel beam, one obtains

$$\sigma_{1p} = \frac{1}{A_s}N_{1p}(z) + \frac{n_1\cos\alpha(s_1)}{I_{ss}}M_{sp}(z) - \frac{y_1(s_1)}{I_{xx}}M_{xp}(z) \qquad (25)$$

in which $I_{ss} = 2bt^3/12 + bt_g^3/12$; $I_{xx} = t_wh_w^3/12 + 2h_b^2bt/4$ are defined. The shear stress component in Eq. (24)b can be related to the shear force also by integrating over the cross-section area to yield

$$\tau_{1p} = \frac{Q_{1p}}{A_w}\sin\alpha(s_1) \qquad (26)$$

in which the shear force $Q_{1p} = \int_A \tau_{1p}dA = G_1\left[v'_p(z) - \theta_{xb}(z)\right]A_w$ has been defined. Also from Eq. (22), the stress functions within the GFRP plate can be obtained as:

$$\sigma_{3p} = E_3\varepsilon_{3p} = E_3\left\langle 1 \quad n_3 \quad -y_3(s_3)\right\rangle\begin{Bmatrix} w'_{3p}(z) \\ v''_p(z) \\ \theta'_{xp}(z)\end{Bmatrix}; \qquad \tau_{3p} = G_3\gamma_{3p} = 0 \qquad \text{(27)a-b}$$

From Eq. (27)a, by substituting from stress-resultant displacement relations $N_{3p}(z) = E_3A_gw'_{3p}(z)$; $M_{sp}(z) = E_3I_{xxp}\theta'_{xp}(z)$ [32], one obtains

$$\sigma_{3p} = \frac{1}{A_g}N_{3p}(z) + \frac{n_3}{I_{xxp}}M_{sp}(z) \qquad (28)$$

The pre-buckling shear strain γ_{2znp} can be related to the shear force resultant $Q_{2p}(z)$ for the adhesive by integrating the shear stresses over the adhesive area. From Eq. (23)c, by integrating the shear stress $\tau_{2znp} = G\gamma_{2znp}$ within the adhesive over the adhesive cross-section yielding

$$Q_{2p}(z) = \int_{A_a} G_2\gamma_{2znp}(z)dA_a = A_a\tau_{2znp}(z) \qquad (29)$$

11. Second Variation of Total Buckling Potential Energy

The total potential energy π of the system is the summation of the internal strain energy U and total load potential loss V. The buckling load can be mathematically obtained when the variation of the second variation of the total potential energy vanishes, i.e.,

$$\delta\left(\frac{1}{2}\overline{\overline{\pi}}\right)=\delta\left[\frac{1}{2}\left(\overline{\overline{U}}+\overline{\overline{V}}\right)\right]=0 \tag{30}$$

in which $\overline{(\ )}$ and $\overline{\overline{(\ )}}$ respectively denote the first and second variations with respect to the argument function (e.g., $\overline{U}=\delta U$ and $\overline{\overline{U}}=\delta^2 U$). The total internal strain energy is obtained by summing the contributions of the steel beam, the GFRP plate, the adhesive, i.e.,

$$U=\frac{1}{2}\int_0^L\int_{A_1}\left(\sigma_1^*\varepsilon_1^*+\tau_1^*\gamma_1^*\right)dA_1dz+\frac{1}{2}\int_0^L\int_{A_3}\left(\sigma_3^*\varepsilon_3^*+\tau_3^*\gamma_3^*\right)dA_3dz+\frac{1}{2}\int_0^L\int_{A_2}\left(\tau_{zn2}^*\gamma_{zn2}^*+\tau_{sn2}^*\gamma_{sn2}^*+\tau_{sz2}^*\gamma_{sz2}^*\right)dA_2dz \tag{31}$$

The total internal strain energy U contributed by the normal strains and transverse shear strains within the steel beam and GFRP plate, and the shear stresses within the adhesive layer. At buckled configuration (Configuration 4), Eq. (31) takes the form:

$$\begin{aligned}U=&\frac{1}{2}\int_0^L\int_{A_1}\left[\left(\sigma_{1b}+\lambda\sigma_{1p}\right)\left(\varepsilon_{1b}+\lambda\varepsilon_{1p}\right)+\left(\tau_{1b}+\lambda\tau_{1p}\right)\left(\gamma_{1b}+\lambda\gamma_{1p}\right)\right]dA_1dz+\\&+\frac{1}{2}\int_0^L\int_{A_3}\left[\left(\sigma_{3b}+\lambda\sigma_{3p}\right)\left(\varepsilon_{3b}+\lambda\varepsilon_{3p}\right)+\left(\tau_{3b}+\lambda\tau_{3p}\right)\left(\gamma_{3b}+\lambda\gamma_{3p}\right)\right]dA_3dz+\\&+\frac{1}{2}\int_0^L\int_{A_2}\left[\left(\tau_{2znb}+\lambda\tau_{2znp}\right)\left(\gamma_{2znb}+\lambda\gamma_{2znp}\right)+\left(\tau_{2snb}+\lambda\tau_{2snp}\right)\left(\gamma_{2snb}+\lambda\gamma_{2snp}\right)+\right.\\&\left.+\left(\tau_{2znb}+\lambda\tau_{2znp}\right)\left(\gamma_{2znb}+\lambda\gamma_{2znp}\right)\right]dA_2dz\end{aligned} \tag{32}$$

From Eqs. (32), by neglecting all zero pre-buckling strains as indicated in Eqs. (22)b and (23)a-b, (i.e., $\gamma_{3p}=\gamma_{2snp}=\gamma_{2szp}=0$), and noting that all materials are linearly elastic isotropic (Assumption ix), the second variation of the total strain energy can be expressed as

$$\begin{aligned}\frac{1}{2}\overline{\overline{U}}=&\frac{1}{2}\int_0^L\int_{A_1}E_1\left[\overline{\varepsilon}_{1b}^{2}+\lambda\varepsilon_{1p}\overline{\overline{\varepsilon}}_{1b}\right]dA_1dz+\frac{1}{2}\int_0^L\int_{A_1}G_1\left[\overline{\gamma}_{1b}^{2}+\lambda\gamma_{1p}\overline{\overline{\gamma}}_{1b}\right]dA_1dz+\\&+\frac{1}{2}\int_0^L\int_{A_3}E_3\left[\overline{\varepsilon}_{3b}^{2}+\lambda\varepsilon_{3p}\overline{\overline{\varepsilon}}_{3b}\right]dA_3dz+\frac{1}{2}\int_0^L\int_{A_3}G_3\overline{\gamma}_{3b}^{2}dA_3dz+\\&+\frac{1}{2}\int_0^L\int_{A_2}G_2\left[\overline{\gamma}_{2znb}^{2}+\lambda\gamma_{2znp}\overline{\overline{\gamma}}_{2znb}\right]dA_2dz+\frac{1}{2}\int_0^L\int_{A_2}G_2\overline{\gamma}_{2snb}^{2}dA_2dz+\frac{1}{2}\int_0^L\int_{A_2}G_2\overline{\gamma}_{2szb}^{2}dA_2dz\end{aligned} \tag{33}$$

The load potential energy is contributed by transverse and longitudinal distributed loads $\lambda q_y(z)$, $\lambda q_z(z)$ and concentrated loads P_{yi}, P_{zi} applied at both member ends i.e.,

$$\frac{1}{2}\overline{\overline{V}} = -\frac{1}{2}\int_0^L q_y(z)\, y_{q_y}(z)\left(\overline{\theta}_{zb}\right)^2 dz - \frac{1}{2}\sum_{i=0,L} P_{yi} y_i(z)\left[\overline{\theta}_{zb}(z_i)\right]^2 + \\ -\frac{1}{2}\int_0^L q_z(z)\, y_{q_z}(z)\,\overline{\theta}_{zb}\,\overline{\theta}_{y1b} dz - \frac{1}{2}\sum_{z_i=0,L} P_{zi} y_i(z)\,\overline{\theta}_{zb}(z_i)\,\overline{\theta}_{y1b}(z_i) \tag{34}$$

11.1. Expression of the first variation of buckling strains

By omitting pre-buckling deformation effects in line with the classical buckling treatment and omitting the non-linear terms, the first variation of the total strains expressions [Eqs. (10)-(20)] take the form

$$\overline{\varepsilon}_{1b} \approx -n_1 \sin\alpha(s_1)\,\overline{u}''_{1b} - x_1(s_1)\,\overline{\theta}'_{y1b} + n_1 q(s_1)\,\overline{\theta}''_{zb} - \omega(s_1)\,\overline{\psi}'_{1b};$$
$$\overline{\gamma}_{1b} \approx \cos\alpha(s_1)\,\overline{u}'_{1b} - \cos\alpha(s_1)\,\overline{\theta}_{y1b} + \left\{r(s_1) + 2n_1\right\}\overline{\theta}'_{zb} - r(s_1)\,\overline{\psi}_{1b};$$
$$\overline{\varepsilon}_{3b} \approx -x_3(s_3)\,\overline{\theta}'_{y3b} + n_3 x_3(s_3)\,\overline{\theta}''_{zb};$$
$$\overline{\gamma}_{3b} \approx \overline{u}'_{3b} - \overline{\theta}_{y3b} + 2n_3\overline{\theta}'_{zb}; \tag{35a-g}$$
$$\overline{\gamma}_{2znb} \approx c_5 x(s)\,\overline{\theta}_{y1b} - c_5 x(s)\,\overline{\theta}_{y3b} - (1+c_6)\,x(s)\,\overline{\theta}'_{zb} + c_5 c_7 x(s)\,\overline{\psi}_{1b};$$
$$\overline{\gamma}_{2snb} \approx -c_5\overline{u}_{1b} + c_5\overline{u}_{3b} - (1+c_6+c_5c_7)\,\overline{\theta}_{zb};$$
$$\overline{\gamma}_{2szb} \approx c_1(n_2)\,\overline{u}'_{1b} - c_1(n_2)\,\overline{\theta}_{y1b} + c_2(n_2)\,\overline{u}'_{3b} - c_2(n_2)\,\overline{\theta}_{y3b} + \left[c_3(n_2) + c_4(n_2)\right]\overline{\theta}'_{zb} - c_7 c_1(n_2)\,\overline{\psi}_{1b}$$

11.2. Second variation of buckling strains

Again, by neglecting pre-buckling terms, the second variation of the buckling strains in Eqs. (10) through (20) take the form

$$\bar{\bar{\varepsilon}}_{1b} \approx \left(\bar{u}'_{1b}\right)^2 + 2\left[n_1\cos\alpha\left(s_1\right) - y_1\left(s_1\right)\right]\bar{u}'_{1b}\bar{\theta}'_{zb} + \left\{q^2 + r^2 + 2rn_1 + n_1^2\right\}\left(\bar{\theta}'_{zb}\right)^2;$$

$$\begin{aligned}\bar{\bar{\gamma}}_{1b} \approx\ & -2\sin\alpha\left(s_1\right)\bar{u}'_{1b}\bar{\theta}_{zb} - 2n_1^2\sin\alpha\left(s_1\right)\bar{\bar{u}}''_{1b}\bar{\theta}'_{zb} + 2n_1 r\left(s_1\right)\sin\alpha\left(s_1\right)\bar{\bar{u}}''_{1b}\bar{\psi}_{1b} \\ & + 2x\left(s_1\right)\cos\alpha\left(s_1\right)\bar{\theta}_{y1b}\bar{\theta}'_{y1b} - 2n_1 q\left(s_1\right)\cos\alpha\left(s_1\right)\bar{\theta}_{y1b}\bar{\theta}''_{zb} + 2\omega\left(s_1\right)\cos\alpha\left(s_1\right)\bar{\theta}_{y1b}\bar{\psi}'_{1b} \\ & + 2q\left(s_1\right)\bar{\theta}_{zb}\bar{\theta}'_{zb} - 2x\left(s_1\right)n_1\bar{\theta}'_{y1b}\bar{\theta}'_{zb} + 2x\left(s_1\right)r\left(s_1\right)\bar{\theta}'_{y1b}\bar{\psi}_{1b} + 2n_1^2 q\left(s_1\right)\bar{\theta}'_{zb}\bar{\theta}''_{zb} \\ & - 2\omega\left(s_1\right)n_1\bar{\theta}'_{zb}\bar{\psi}'_{1b} - 2r\left(s_1\right)n_1 q\left(s_1\right)\bar{\theta}''_{zb}\bar{\psi}_{1b} + 2\omega\left(s_1\right)r\left(s_1\right)\bar{\psi}'_{1b}\bar{\psi}_{1b};\end{aligned}$$

$$\bar{\bar{\varepsilon}}_{3b} \approx \left(\bar{u}'_{3b}\right)^2 + 2n_3\bar{u}'_{3b}\bar{\theta}'_{zb} + \left[n_3^2 + x_3^2\left(s_3\right)\right]\left(\bar{\theta}'_{zb}\right)^2;$$

$$\begin{aligned}\bar{\bar{\gamma}}_{2znb} \approx\ & -2c_5c_1\left(n_2\right)x^2\left(s\right)\bar{\theta}'_{y1b}\bar{\theta}_{y1b} - 2c_5c_2\left(n_2\right)x^2\left(s\right)\bar{\theta}_{y1b}\bar{\theta}'_{y3b} + 2c_5c_3\left(n_2\right)x^2\left(s\right)\bar{\theta}''_{zb}\bar{\theta}_{y1b} \\ & - 2c_5c_7c_1\left(n_2\right)x^2\left(s\right)\bar{\psi}'_{1b}\bar{\theta}_{y1b} + 2c_5c_1\left(n_2\right)x^2\left(s\right)\bar{\theta}'_{y1b}\bar{\theta}_{y3b} + 2c_5c_2\left(n_2\right)x^2\left(s\right)\bar{\theta}'_{y3b}\bar{\theta}_{y3b} \\ & - 2c_5c_3\left(n_2\right)x^2\left(s\right)\bar{\theta}''_{zb}\bar{\theta}_{y3b} + 2c_5c_7c_1\left(n_2\right)x^2\left(s\right)\bar{\psi}'_{1b}\bar{\theta}_{y3b} + 2c_6c_1\left(n_2\right)x^2\left(s\right)\bar{\theta}'_{y1b}\bar{\theta}'_{zb} \\ & + 2c_6c_2\left(n_2\right)x^2\left(s\right)\bar{\theta}'_{y3b}\bar{\theta}'_{zb} - 2c_6c_3\left(n_2\right)x^2\left(s\right)\bar{\theta}''_{zb}\bar{\theta}'_{zb} + 2c_6c_7c_1\left(n_2\right)x^2\bar{\psi}'_{1b}\bar{\theta}'_{zb} \\ & - 2c_5c_7c_1\left(n_2\right)x^2\left(s\right)\bar{\theta}'_{y1b}\bar{\psi}_{1b} - 2c_5c_7c_2\left(n_2\right)x^2\left(s\right)\bar{\theta}'_{y3b}\bar{\psi}_{1b} + 2c_5c_7c_3\left(n_2\right)x^2\left(s\right)\bar{\theta}''_{zb}\bar{\psi}_{1b} \\ & - 2c_5c_7^2c_1\left(n_2\right)x^2\left(s\right)\bar{\psi}'_{1b}\bar{\psi}_{1b} - 2c_5c_1\left(n_2\right)\bar{u}_{1b}\bar{u}'_{1b} - 2c_5c_2\left(n_2\right)\bar{u}_{1b}\bar{u}'_{3b} - 2c_5c_4\left(n_2\right)\bar{u}_{1b}\bar{\theta}'_{zb} \\ & + 2c_5c_1\left(n_2\right)\bar{u}'_{1b}\bar{u}_{3b} + 2c_5c_2\left(n_2\right)\bar{u}_{3b}\bar{u}'_{3b} + 2c_5c_4\left(n_2\right)\bar{u}_{3b}\bar{\theta}'_{zb} - 2\left(c_6 + c_5c_7\right)c_1\left(n_2\right)\bar{u}'_{1b}\bar{\theta}_{zb} \\ & - 2\left(c_6 + c_5c_7\right)c_2\left(n_2\right)\bar{u}'_{3b}\bar{\theta}_{zb} - 2\left(c_6 + c_5c_7\right)c_4\left(n_2\right)\bar{\theta}_{zb}\bar{\theta}'_{zb}\end{aligned} \qquad (36)\text{a-d}$$

11.3. Second variation of internal strain energy

From Eqs. (25), (26), (28),(29), (35)a-g and (36)a-d, by substituting into Eq. (33), the second variation of the total strain energy can be expressed as

$$\frac{1}{2}\overline{\overline{U}}=\frac{1}{2}\int_0^L\int_{A_1}E_1\left[-n_1\sin\alpha(s_1)\overline{u}''_{1b}-x_1(s_1)\overline{\theta}'_{y1b}+n_1q(s_1)\overline{\theta}''_{zb}-\omega(s_1)\overline{\psi}'_{1b}\right]^2dA_1dz$$

$$+\frac{\lambda}{2}\int_0^L\int_{A_1}\left[\frac{N_{1p}(z)}{A_s}+\frac{n_1\cos\alpha(s_1)}{I_{ss}}M_{sp}(z)-\frac{y_1(s_1)}{I_{xx}}M_{xp}(z)\right]\left\{\left(\overline{u}'_{1b}\right)^2+2\left[n_1\cos\alpha(s_1)-y_1(s_1)\right]\overline{u}'_{1b}\overline{\theta}'_{zb}\right.$$

$$\left.+\left[q^2(s_1)+r^2(s_1)+2r(s_1)n_1+n_1^2\right]\left(\overline{\theta}'_{zb}\right)^2\right\}dA_1dz$$

$$+\frac{1}{2}\int_0^L\int_{A_1}G_1\left\{\cos\alpha(s_1)\overline{u}'_{1b}-\cos\alpha(s_1)\overline{\theta}_{y1b}+\left[r(s_1)+2n_1\right]\overline{\theta}'_{zb}-r(s_1)\overline{\psi}_{1b}\right\}^2dA_1dz$$

$$+\frac{\lambda}{2}\int_0^L\int_{A_1}\frac{Q_{1p}}{A_1}\sin\alpha(s_1)\left\{-2\sin\alpha(s_1)\overline{u}'_{1b}\overline{\theta}_{zb}-2n_1^2\sin\alpha(s_1)\overline{u}''_{1b}\overline{\theta}'_{zb}+2n_1r(s_1)\sin\alpha(s_1)\overline{u}''_{1b}\overline{\psi}_{1b}\right.$$

$$+2x(s_1)\cos\alpha(s_1)\overline{\theta}_{y1b}\overline{\theta}'_{y1b}-2n_1q(s_1)\cos\alpha(s_1)\overline{\theta}_{y1b}\overline{\theta}''_{zb}+2\omega(s_1)\cos\alpha(s_1)\overline{\theta}_{y1b}\overline{\psi}'_{1b}+2q(s_1)\overline{\theta}_{zb}\overline{\theta}'_{zb}$$

$$-2x(s_1)n_1\overline{\theta}'_{y1b}\overline{\theta}'_{zb}+2x(s_1)r(s_1)\overline{\theta}'_{y1b}\overline{\psi}_{1b}+2n_1^2q(s_1)\overline{\theta}'_{zb}\overline{\theta}''_{zb}-2\omega(s_1)n_1\overline{\theta}'_{zb}\overline{\psi}'_{1b}-2r(s_1)n_1q(s_1)\overline{\theta}''_{zb}\overline{\psi}_{1b}$$

$$\left.+2\omega(s_1)r(s_1)\overline{\psi}'_{1b}\overline{\psi}_{1b}\right\}dA_1dz+\frac{1}{2}\int_0^L\int_{A_3}E_3\left[-x_3(s_3)\overline{\theta}'_{y3b}+n_3x_3(s_3)\overline{\theta}''_{zb}\right]^2dA_3dz$$

$$+\frac{\lambda}{2}\int_0^L\int_{A_3}\left[\frac{N_{3p}(z)}{A_g}+\frac{n_3}{I_{xxg}}M_{sp}(z)\right]\left[\left(\overline{u}'_{3b}\right)^2+2n_3\overline{u}'_{3b}\overline{\theta}'_{zb}+\left[n_3^2+x_3^2(s_3)\right]\left(\overline{\theta}'_{zb}\right)^2\right]dA_3dz+\frac{1}{2}\int_0^L\int_{A_3}G_3\left(\overline{u}'_{3b}-\overline{\theta}_{y3b}+2n_3\overline{\theta}'_{zb}\right)^2dA_3dz$$

$$+\frac{1}{2}\int_0^L\int_{A_2}G_2\left[c_5x(s)\overline{\theta}_{y1b}-c_5x(s)\overline{\theta}_{y3b}-(1+c_6)x(s)\overline{\theta}'_{zb}+c_5c_7x(s)\overline{\psi}_{1b}\right]^2dA_2dz$$

$$+\frac{\lambda}{2}\int_0^L\int_{A_2}\frac{Q_{2p}(z)}{A_a}\left\{-2c_5c_1(n_2)x^2(s)\overline{\theta}'_{y1b}\overline{\theta}_{y1b}-2c_5c_2(n_2)x^2(s)\overline{\theta}_{y1b}\overline{\theta}'_{y3b}\right.$$

$$+2c_5c_3(n_2)x^2(s)\overline{\theta}''_{zb}\overline{\theta}_{y1b}-2c_5c_7c_1(n_2)x^2(s)\overline{\psi}'_{1b}\overline{\theta}_{y1b}+2c_5c_1(n_2)x^2(s)\overline{\theta}'_{y1b}\overline{\theta}_{y3b}+2c_5c_2(n_2)x^2(s)\overline{\theta}'_{y3b}\overline{\theta}_{y3b}$$

$$-2c_5c_3(n_2)x^2(s)\overline{\theta}''_{zb}\overline{\theta}_{y3b}+2c_5c_7c_1(n_2)x^2(s)\overline{\psi}'_{1b}\overline{\theta}_{y3b}+2c_6c_1(n_2)x^2(s)\overline{\theta}'_{y1b}\overline{\theta}'_{zb}$$

$$+2c_6c_2(n_2)x^2(s)\overline{\theta}'_{y3b}\overline{\theta}'_{zb}-2c_6c_3(n_2)x^2(s)\overline{\theta}''_{zb}\overline{\theta}'_{zb}+2c_6c_7c_1(n_2)x^2\overline{\psi}'_{1b}\overline{\theta}'_{zb}$$

$$-2c_5c_7c_1(n_2)x^2(s)\overline{\theta}'_{y1b}\overline{\psi}_{1b}-2c_5c_7c_2(n_2)x^2(s)\overline{\theta}'_{y3b}\overline{\psi}_{1b}+2c_5c_7c_3(n_2)x^2(s)\overline{\theta}''_{zb}\overline{\psi}_{1b}$$

$$-2c_5c_7^2c_1(n_2)x^2(s)\overline{\psi}'_{1b}\overline{\psi}_{1b}-2c_5c_1(n_2)\overline{u}_{1b}\overline{u}'_{1b}-2c_5c_2(n_2)\overline{u}_{1b}\overline{u}'_{3b}-2c_5c_4(n_2)\overline{u}_{1b}\overline{\theta}'_{zb}$$

$$+2c_5c_1(n_2)\overline{u}'_{1b}\overline{u}_{3b}+2c_5c_2(n_2)\overline{u}_{3b}\overline{u}'_{3b}+2c_5c_4(n_2)\overline{u}_{3b}\overline{\theta}'_{zb}-2(c_6+c_5c_7)c_1(n_2)\overline{u}'_{1b}\overline{\theta}_{zb}$$

$$\left.-2(c_6+c_5c_7)c_2(n_2)\overline{u}'_{3b}\overline{\theta}_{zb}-2(c_6+c_5c_7)c_4(n_2)\overline{\theta}_{zb}\overline{\theta}'_{zb}\right\}dA_2dz$$

$$+\frac{1}{2}\int_0^L\int_{A_2}G_2\left[-c_5\overline{u}_{1b}+c_5\overline{u}_{3b}-(1+c_6+c_5c_7)\overline{\theta}_{zb}\right]^2dA_2dz$$

$$+\frac{1}{2}\int_0^L\int_{A_2}G_2\left[c_1(n_2)\overline{u}'_{1b}-c_1(n_2)\overline{\theta}_{y1b}+c_2(n_2)\overline{u}'_{3b}-c_2(n_2)\overline{\theta}_{y3b}+\left[c_3(n_2)+c_4(n_2)\right]\overline{\theta}'_{zb}-c_7c_1(n_2)\overline{\psi}_{1b}\right]^2dA_2dz$$

(37)

11.4. Second variation of total potential energy

From Eqs. (34) and (37), by substituting into Eq. (30), the second variation of the total potential energy of the system can be expressed as

$$\delta\frac{1}{2}\bar{\bar{\pi}}=\delta\frac{1}{2}\left(\bar{\bar{U}}+\bar{\bar{V}}\right)=\delta\frac{1}{2}\Big(\bar{\bar{U}}_{en1}+\bar{\bar{U}}_{es1}+\bar{\bar{U}}_{en3}+\bar{\bar{U}}_{es3}+\bar{\bar{U}}_{ezn2}+\bar{\bar{U}}_{esn2}+\bar{\bar{U}}_{esz2}+\bar{\bar{V}}_{gN_1}+\bar{\bar{V}}_{g\bar{M}_x}+\bar{\bar{V}}_{g\bar{\bar{M}}_s}+\bar{\bar{V}}_{gQ_1}+\bar{\bar{V}}_{gQ2}+\bar{\bar{V}}_{gqy}+\bar{\bar{V}}_{gP_{yi}}+\bar{\bar{V}}_{gqz}+\bar{\bar{V}}_{gP_{zi}}\Big)=0 \tag{38}$$

in which $\bar{\bar{U}}_{en1}$ is the second variation of elastic strain energy contributed by the longitudinal normal strain within the wide flange beam (Appendix A) and can be evaluated over the steel section as

$$\bar{\bar{U}}_{en1}=E_1\int_0^L\left\langle \bar{u}''_{1b}\quad \bar{\theta}'_{y1b}\quad \bar{\theta}''_{zb}\quad \bar{\psi}'_{1b}\right\rangle\begin{bmatrix} I_{yyw} & 0 & 0 & 0\\ 0 & 2I_{yyf} & 0 & 0\\ 0 & 0 & I_{\omega\omega l} & 0\\ 0 & 0 & 0 & I_{\omega\omega g}\end{bmatrix}\begin{Bmatrix}\bar{u}''_{1b}\\ \bar{\theta}'_{y1b}\\ \bar{\theta}''_{zb}\\ \bar{\psi}'_{1b}\end{Bmatrix}dz \tag{39}$$

in which $I_{yyw}=h_w t_w^3/12;\ I_{yyf}=tb^3/12;\ I_{\omega\omega l}=2b^3t^3/144+h_w^3t_w^3/144;\ I_{\omega\omega gs}=h_b^2b^3t/24$ are defined. Also, $\bar{\bar{U}}_{es1}$ is the second variation of the elastic strain energy contributed by the transverse shear strain within the steel beam (Appendix A) and can be is evaluated over the steel section as

$$\bar{\bar{U}}_{es1}=G_1\int_0^L\left\langle \bar{u}'_{1b}\quad \bar{\theta}_{y1b}\quad \bar{\theta}'_{zb}\quad \bar{\psi}_{1b}\right\rangle\begin{bmatrix} 2A_f & -2A_f & 0 & 0\\ -2A_f & 2A_f & 0 & 0\\ 0 & 0 & J_1 & -h_b^2A_f/2\\ 0 & 0 & -h_b^2A_f/2 & h_b^2A_f/2\end{bmatrix}\begin{Bmatrix}\bar{u}'_{1b}\\ \bar{\theta}_{y1b}\\ \bar{\theta}'_{zb}\\ \bar{\psi}_{1b}\end{Bmatrix}dz \tag{40}$$

in which $A_f=bt;\ J_1=h_b^2A_f/2+2bt^3/3+h_wt_w^3/3$ are defined and $\bar{\bar{U}}_{en3}$ and $\bar{\bar{U}}_{es3}$ are the second variation of the elastic strain energies contributed by the longitudinal normal strain and shear strain within the GFRP plate (Appendix A) and are expressed as

$$\bar{\bar{U}}_{en3}=E_3\int_0^L\left\langle \bar{\theta}'_{y3b}\quad \bar{\theta}''_{zb}\right\rangle\begin{bmatrix} I_{yyg} & 0\\ 0 & I_{\omega\omega g}\end{bmatrix}\begin{Bmatrix}\bar{\theta}'_{y3b}\\ \bar{\theta}''_{zb}\end{Bmatrix}dz$$

$$\bar{\bar{U}}_{es3}=G_3\int_0^L\left\langle \bar{u}'_{3b}\quad \bar{\theta}_{y3b}\quad \bar{\theta}'_{zb}\right\rangle\begin{bmatrix} A_3 & -A_3 & 0\\ -A_3 & A_3 & 0\\ 0 & 0 & J_3\end{bmatrix}\begin{Bmatrix}\bar{u}'_{3b}\\ \bar{\theta}_{y3b}\\ \bar{\theta}'_{zb}\end{Bmatrix}dz \tag{41}a-b$$

in which the section properties $I_{yyg}=t_gb^3/12,\ I_{\omega\omega g}=t_g^3b^3/144,\ A_3=bt_g$ and $J_3=bt_g^3/3$ are defined and $\bar{\bar{U}}_{ezn2},\bar{\bar{U}}_{esn2}$ and $\bar{\bar{U}}_{esz2}$ are the second variations of the internal strain energies within the adhesive layer (Appendix A) and are expressed as

$$\bar{\bar{U}}_{ezn2} = G_2 I_{yya} \int_0^L \left\langle \bar{\theta}_{y1b} \quad \bar{\theta}_{y3b} \quad \bar{\theta}'_{zb} \quad \bar{\psi}_{1b} \right\rangle \times$$

$$\begin{bmatrix} c_5^2 & -c_5^2 & -c_5(1+c_6) & c_5^2 c_7 \\ -c_5^2 & c_5^2 & c_5(1+c_6) & -c_5^2 c_7 \\ -c_5(1+c_6) & c_5(1+c_6) & (1+c_6)^2 & -c_5 c_7 (1+c_6) \\ c_5^2 c_7 & -c_5^2 c_7 & -c_5 c_7 (1+c_6) & c_5^2 c_7^2 \end{bmatrix} \begin{Bmatrix} \bar{\theta}_{y1b} \\ \bar{\theta}_{y3b} \\ \bar{\theta}'_{zb} \\ \bar{\psi}_{1b} \end{Bmatrix} dz$$

$$\bar{\bar{U}}_{esn2} = G_2 A_a \int_0^L \left\langle \bar{u}_{1b} \quad \bar{u}_{3b} \quad \bar{\theta}_{zb} \right\rangle \times$$

$$\begin{bmatrix} c_5^2 & -c_5^2 & c_5(1+c_6+c_5c_7) \\ -c_5^2 & c_5^2 & -c_5(1+c_6+c_5c_7) \\ c_5(1+c_6+c_5c_7) & -c_5(1+c_6+c_5c_7) & (1+c_6+c_5c_7)^2 \end{bmatrix} \begin{Bmatrix} \bar{u}_{1b} \\ \bar{u}_{3b} \\ \bar{\theta}_{zb} \end{Bmatrix} dz$$

$$\bar{\bar{U}}_{esz2} = \frac{1}{12} G_2 A_a \int_0^L \left\langle \bar{u}'_{1b} \quad \bar{\theta}_{y1b} \quad \bar{u}'_{3b} \quad \bar{\theta}_{y3b} \quad \bar{\theta}'_{zb} \quad \bar{\psi}_{1b} \right\rangle \times \qquad (42)\text{a-c}$$

$$\begin{bmatrix} 4 & -4 & 2 & -2 & 2c_8 & -4c_7 \\ -4 & 4 & -2 & 2 & -2c_8 & 4c_7 \\ 2 & -2 & 4 & -4 & c_9 & -2c_7 \\ -2 & 2 & -4 & 4 & -c_9 & 2c_7 \\ 2c_8 & -2c_8 & c_9 & -c_9 & c_{10} & -2c_7 c_8 \\ -4c_7 & 4c_7 & -2c_7 & 2c_7 & -2c_7 c_8 & 4c_7^2 \end{bmatrix} \begin{Bmatrix} \bar{u}'_{1b} \\ \bar{\theta}_{y1b} \\ \bar{u}'_{3b} \\ \bar{\theta}_{y3b} \\ \bar{\theta}'_{zb} \\ \bar{\psi}_{1b} \end{Bmatrix} dz$$

in which $I_{yya} = \int_{A_2} x^2(s)\, dA_2 = t_a b^3/12$; $c_5 = 1/t_a$; $c_6 = \left(t + t_g\right)/2t_a$; $c_7 = h_b/2$; $c_5 c_7 = h_b/2t_a$;

$c_6 + c_5 c_7 = \left(h + t_g\right)/2t_a$; $c_8 = h + t - t_g$; $c_9 = h + t - 4t_g$; $c_{10} = h^2 + t^2 + 4{t_g}^2 + 2ht - 2ht_g - 2tt_g$.

Also, $\bar{\bar{V}}_{gN_1}$ is the second variation of the load potential energy contributed by pre-buckling axial force $\lambda N_{1p}(z)$ (Appendix A) and takes the form

$$\bar{\bar{V}}_{gN_1} = \lambda \int_0^L N_{1p}(z) \left[\left(\bar{u}'_{1b}\right)^2 + \frac{\left(I_{xxs} + I_{yys}\right)}{A_s} \left(\bar{\theta}'_{zb}\right)^2 \right] dz \qquad (43)$$

in which $I_{xxs} = h_b^2 bt/2 + t_w h_w^3/12 + 2bt^3/12$; $I_{yys} = 2tb^3/12 + h_w t_w^3/12$; $\bar{\bar{V}}_{gM_x}$ is the second variation of the geometric potential energies contributed by pre-buckling bending moment M_{xp} of the steel beam (Appendix A) and can be evaluated as

$$\bar{\bar{V}}_{gM_x} = 2\lambda\int_0^L M_{xp}(z)\bar{u}'_{1b}\bar{\theta}'_{zb}dz \tag{44}$$

$\bar{\bar{V}}_{gM_s}$ is the second variation of the geometric potential energies contributed by pre-buckling bending moment M_{sp} of the steel beam (Appendix A) and can be evaluated as

$$\bar{\bar{V}}_{gM_s} = 2\frac{2I_{ssf}}{\bar{I}_{xx}}\lambda\int_0^L M_{sp}(z)\bar{u}'_{1b}\bar{\theta}'_{zb}dz + 2\frac{I_{ssg}}{\bar{I}_{xx}}\lambda\int_0^L M_{sp}(z)\bar{u}'_{3b}\delta\bar{\theta}'_{zb}dz \tag{45}$$

where $I_{ssf} = bt^3/12;\quad I_{ssg} = bt_g^3/12$. Also, the second variation of the pre-buckling shear force potential energy $\bar{\bar{V}}_{gQ_1}$ within the steel beam (Appendix A) can be evaluated as

$$\bar{\bar{V}}_{gQ_1} = -2\lambda\int_0^L Q_{1p}(z)\left(\bar{u}'_{1b}\bar{\theta}_{zb} + \frac{I_{yyw}}{A_w}\bar{u}''_{1b}\bar{\theta}'_{zb}\right)dz \tag{46}$$

in which $I_{yyw} = h_w t_w^3/12$ is defined. For the GFRP plate, the second variation of the potential energies contributed by axial force $\lambda N_{3p}(z)$ (Appendix A) can be evaluated as

$$\bar{\bar{V}}_{gN_3} = \lambda\int_0^L N_{3p}(z)\left[\left(\bar{u}'_{3b}\right)^2 + \frac{I_{xxg}+I_{yyg}}{A_g}\left(\bar{\theta}'_{zb}\right)^2\right]dz \tag{47}$$

in which $I_{xxg} = bt_g^3/12$, $I_{yyg} = t_g b^3/12$ are defined. Also, the second variation of the potential energy contributed by shear force $\lambda Q_{2p}(z)$ (Appendix A) can be evaluated as

$$\bar{\bar{V}}_{gQ2} = \lambda\int_0^L Q_{2p}(z)\left\{\left\langle \bar{u}_{1b} \;\middle|\; \bar{\theta}_{y1b} \;\middle|\; \bar{u}_{3b} \;\middle|\; \bar{\theta}_{y3b} \;\middle|\; \bar{\theta}_{zb} \;\middle|\; \bar{\theta}'_{zb} \;\middle|\; \bar{\psi}_{1b}\right\rangle\right.$$

$$\times\begin{bmatrix} -c_5 & 0 & -c_5 & 0 & -c_5c_{12} & 0 & 0 \\ 0 & -c_5\alpha_a & 0 & -c_5\alpha_a & 0 & c_5c_{11}\alpha_a & -c_5c_7\alpha_a \\ c_5 & 0 & c_5 & 0 & c_5c_{12} & 0 & 0 \\ 0 & c_5\alpha_a & 0 & c_5\alpha_a & 0 & -c_5c_{11}\alpha_a & c_5c_7\alpha_a \\ -(c_6+c_5c_7) & 0 & -(c_6+c_5c_7) & 0 & -(c_6+c_5c_7)c_{12} & 0 & 0 \\ 0 & c_6\alpha_a & 0 & c_6\alpha_a & 0 & -c_6c_{11}\alpha_a & c_6c_7\alpha_a \\ 0 & -c_5c_7\alpha_a & 0 & -c_5c_7\alpha_a & 0 & c_5c_7c_{11}\alpha_a & -c_5c_7^2\alpha_a \end{bmatrix}\left.\begin{Bmatrix} \bar{u}'_{1b} \\ \bar{\theta}'_{y1b} \\ \bar{u}'_{3b} \\ \bar{\theta}'_{y3b} \\ \bar{\theta}'_{zb} \\ \bar{\theta}''_{zb} \\ \bar{\psi}'_{1b} \end{Bmatrix}\right\}dz \tag{48}$$

in which $c_{11} = (t-t_g)/2;\quad c_{12} = (h-t_g)/2;\quad I_{yya} = \alpha_a A_a$ are defined.

12. Finite Element Formulation

12.1. Interpolation of pre-buckling stress resultants

The pre-buckling stress resultants $N_{1p}(z), Q_{1p}(z), M_{1p}(z), N_{3p}(z), M_{3p}(z)$ and $Q_{2p}(z)$ are related to nodal stress resultants obtained from the pre-buckling analysis by adopting linear interpolation functions $\langle \mathbf{L}(\mathbf{z})\rangle_{1\times 2}^{\mathbf{T}} = \langle L_1(z) \quad L_2(z)\rangle$ with $L_1(z) = 1 - z/L$ and $L_2(z) = z/L$:

$$
\begin{aligned}
&N_{1p}(z)=\left\langle \mathbf{L}(\mathbf{z})\right\rangle_{1\times 2}^{\mathbf{T}}\left\{\mathbf{N_{1p}}\right\}_{2\times 1},\quad \left\langle \mathbf{N_{1p}}\right\rangle_{1\times 2}^{\mathbf{T}}=\left\langle N_{1p}(0)\ \middle|\ -N_{1p}(L)\right\rangle\\
&Q_{1p}(z)=\left\langle \mathbf{L}(\mathbf{z})\right\rangle_{1\times 2}^{\mathbf{T}}\left\{\mathbf{Q_{1p}}\right\}_{2\times 1},\quad \left\langle \mathbf{Q_{1p}}\right\rangle_{1\times 2}^{\mathbf{T}}=\left\langle Q_{1p}(0)\ \middle|\ -Q_{1p}(L)\right\rangle\\
&M_{sp}(z)=\left\langle \mathbf{L}(\mathbf{z})\right\rangle_{1\times 2}^{\mathbf{T}}\left\{\mathbf{M}_{s\mathbf{p}}\right\}_{2\times 1},\ \left\langle \mathbf{M}_{s\mathbf{p}}\right\rangle_{1\times 2}^{\mathbf{T}}=\left\langle M_{sp}(0)\ \middle|\ -M_{sp}(L)\right\rangle\\
&M_{xp}(z)=\left\langle \mathbf{L}(\mathbf{z})\right\rangle_{1\times 2}^{\mathbf{T}}\left\{\mathbf{M}_{x\mathbf{p}}\right\}_{2\times 1},\ \left\langle \mathbf{M}_{x\mathbf{p}}\right\rangle_{1\times 2}^{\mathbf{T}}=\left\langle M_{xp}(0)\ \middle|\ -M_{xp}(L)\right\rangle\\
&N_{3p}(z)=\left\langle \mathbf{L}(\mathbf{z})\right\rangle_{1\times 2}^{\mathbf{T}}\left\{\mathbf{N_{3p}}\right\}_{2\times 1},\quad \left\langle \mathbf{N_{3p}}\right\rangle_{1\times 2}^{\mathbf{T}}=\left\langle N_{3p}(0)\ \middle|\ -N_{3p}(L)\right\rangle\\
&Q_{2p}(z)=\left\langle \mathbf{L}(\mathbf{z})\right\rangle_{1\times 2}^{\mathbf{T}}\left\{\mathbf{Q_{2p}}\right\}_{2\times 1},\quad \left\langle \mathbf{Q_{2p}}\right\rangle_{1\times 2}^{\mathbf{T}}=\left\langle Q_{2p}(0)\ \middle|\ -Q_{2p}(L)\right\rangle
\end{aligned}
\tag{49}
$$

12.2. Displacement Interpolation

Two finite elements are developed for the problem, a two-node element and a three-node element. The relevant nodal degrees of freedom are depicted in Fig. 4. When interpolating the displacement fields $\overline{u}_{1b}(z)$ and $\overline{\theta}_{zb}(z)$, cubic Hermitian shape functions are adopted in the case of the two-node element and quadratic Lagrange interpolation functions are used in the case of the three-node element. For the remaining displacement fields $\overline{\theta}_{y1b}(z),\overline{u}_{3b}(z),\overline{\theta}_{y3b}(z)$ and $\overline{\psi}_{1b}(z)$, linear interpolation is adopted in both elements. The two-node element possesses 16 degrees of freedom (DOFs), while the three-node has 14 DOFs.

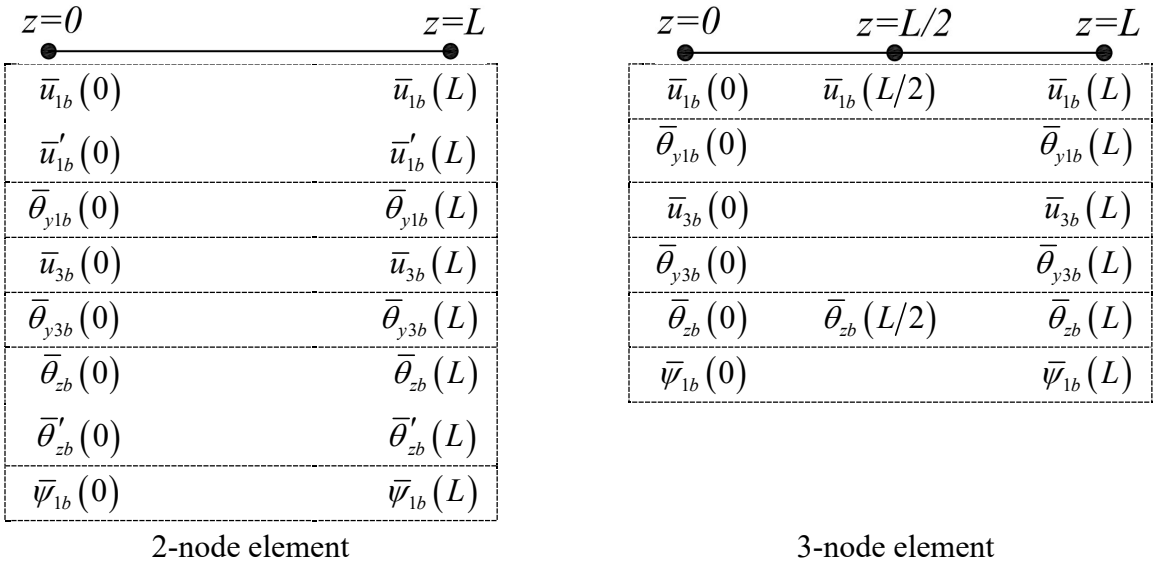

Figure 4. DOFs for Two and Three-node elements

12.2.1. Two-node element

The displacement fields $\overline{u}_{1b}(z),\overline{\theta}_{y1b}(z),\overline{u}_{3b}(z),\overline{\theta}_{y3b}(z),\overline{\theta}_{zb}(z),\overline{\psi}_{1b}(z)$ are related to the nodal displacement vector $\left\langle\overline{\mathbf{\Delta}}\right\rangle_{1\times 16}^{\mathbf{T}}=\left\langle\overline{\mathbf{d}}(0)_{1\times 8}^{\mathbf{T}}\ \middle|\ \overline{\mathbf{d}}(L)_{1\times 8}^{\mathbf{T}}\right\rangle$ where

$$\overline{\mathbf{d}}\left(z_i\right)_{1\times 8}^{\mathbf{T}}=\left\langle \overline{u}_{1b}\left(z_i\right) \quad \overline{u}'_{1b}\left(z_i\right) \mid \overline{\theta}_{y1b}\left(z_i\right) \mid \overline{u}_{3b}\left(z_i\right) \mid \overline{\theta}_{y3b}\left(z_i\right) \mid \overline{\theta}_{zb}\left(z_i\right) \quad \overline{\theta}'_{zb}\left(z_i\right) \mid \overline{\psi}_{1b}\left(z_i\right)\right\rangle, \text{and}$$

$z_i=0$ or L through

$$\begin{aligned}&\left\langle \overline{u}_{1b}\left(z\right),\overline{\theta}_{y1b}\left(z\right),\overline{u}_{3b}\left(z\right),\overline{\theta}_{y3b}\left(z\right),\overline{\theta}_{zb}\left(z\right),\overline{\psi}_{1b}\left(z\right)\right\rangle^{T}\\&\quad=\left\langle \overline{\mathbf{\Delta}}\right\rangle_{1\times 16}^{T}\left(\left\{\mathbf{S}_{\mathbf{u1}}\right\}_{16\times 1},\left\{\mathbf{S}_{\theta\mathbf{1}}\right\}_{16\times 1},\left\{\mathbf{S}_{\mathbf{u}3}\right\}_{16\times 1},\left\{\mathbf{S}_{\theta 3}\right\}_{16\times 1},\left\{\mathbf{S}_{\theta z}\right\}_{16\times 1},\left\{\mathbf{S}_{\psi\mathbf{1}}\right\}_{16\times 1}\right)\end{aligned} \tag{50}$$

in which the shape function vectors are defined as

$$\begin{aligned}\left\langle \mathbf{S}_{\mathbf{u1}}\right\rangle_{1\times 16}&=\left\langle H_1\left(z\right) \quad H_2\left(z\right) \quad 0 \quad 0 \quad 0 \quad 0 \quad 0 \quad 0 \mid H_3\left(z\right) \quad H_4\left(z\right) \quad 0 \quad 0 \quad 0 \quad 0 \quad 0 \quad 0\right\rangle\\
\left\langle \mathbf{S}_{\theta\mathbf{1}}\right\rangle_{1\times 16}&=\left\langle 0 \quad 0 \quad L_1\left(z\right) \quad 0 \quad 0 \quad 0 \quad 0 \quad 0 \mid 0 \quad 0 \quad L_2\left(z\right) \quad 0 \quad 0 \quad 0 \quad 0 \quad 0\right\rangle\\
\left\langle \mathbf{S}_{\mathbf{u}3}\right\rangle_{1\times 16}&=\left\langle 0 \quad 0 \quad 0 \quad L_1\left(z\right) \quad 0 \quad 0 \quad 0 \quad 0 \mid 0 \quad 0 \quad 0 \quad L_2\left(z\right) \quad 0 \quad 0 \quad 0 \quad 0\right\rangle\\
\left\langle \mathbf{S}_{\theta 3}\right\rangle_{1\times 16}&=\left\langle 0 \quad 0 \quad 0 \quad 0 \quad L_1\left(z\right) \quad 0 \quad 0 \quad 0 \mid 0 \quad 0 \quad 0 \quad 0 \quad L_2\left(z\right) \quad 0 \quad 0 \quad 0\right\rangle\\
\left\langle \mathbf{S}_{\theta z}\right\rangle_{1\times 16}&=\left\langle 0 \quad 0 \quad 0 \quad 0 \quad 0 \quad H_1\left(z\right) \quad H_2\left(z\right) \quad 0 \mid 0 \quad 0 \quad 0 \quad 0 \quad 0 \quad H_3\left(z\right) \quad H_4\left(z\right) \quad 0\right\rangle\\
\left\langle \mathbf{S}_{\psi\mathbf{1}}\right\rangle_{1\times 16}&=\left\langle 0 \quad 0 \quad 0 \quad 0 \quad 0 \quad 0 \quad 0 \quad L_1\left(z\right) \mid 0 \quad 0 \quad 0 \quad 0 \quad 0 \quad 0 \quad 0 \quad L_2\left(z\right)\right\rangle\end{aligned} \tag{51}$$

and $H_1\left(z\right)=1-3\left(z/L\right)^2+2\left(z/L\right)^3$, $H_2\left(z\right)=z-2\left(z^2/L\right)+\left(z^3/L^2\right)$, $H_3\left(z\right)=3\left(z/L\right)^2-2\left(z/L\right)^3$, $H_4\left(z\right)=z^3/L^2-z^2/L$. From Eqs.(50), by substituting into Eqs. (39) through (42)a-c, and from Eqs. (49) and (50) by substituting into Eqs. (43)-(48) and (34), the second variation of the total potential energy in Eq. (38) is obtained as

$$\delta\frac{1}{2}\overline{\overline{\pi}}=\delta\frac{1}{2}\left\langle \overline{\mathbf{\Delta}}\right\rangle_{1\times 16}^{\mathbf{T}}\left(\left[\mathbf{K}_{\mathbf{e}}\right]_{16\times 16}+\lambda\left[\mathbf{K}_{\mathbf{g}}\right]_{16\times 16}\right)\left\{\overline{\mathbf{\Delta}}\right\}_{16\times 1}=0 \tag{52}$$

in which $\left[\mathbf{K}_{\mathbf{e}}\right]_{16\times 16}$ and $\left[\mathbf{K}_{\mathbf{g}}\right]_{16\times 16}$ are elastic and geometric stiffness matrices, respectively as defined in Appendix B. A non-trivial solution of Eq. (52) leads to the eigenvalue solution $\left\{\left[\mathbf{K}_{\mathbf{e}}\right]_{16\times 16}+\lambda\left[\mathbf{K}_{\mathbf{g}}\right]_{16\times 16}\right\}\left\{\overline{\mathbf{\Delta}}\right\}_{16\times 1}=\left\{\mathbf{0}\right\}_{16\times 1}$ which is solved for the critical load multiplier λ and the corresponding buckling mode $\left\{\overline{\mathbf{\Delta}}\right\}_{16\times 1}$.

12.2.2. Three-node element

The displacement fields $\overline{u}_{1b}\left(z\right),\overline{\theta}_{y1b}\left(z\right),\overline{u}_{3b}\left(z\right),\overline{\theta}_{y3b}\left(z\right),\overline{\theta}_{zb}\left(z\right),\overline{\psi}_{1b}\left(z\right)$ are related to the nodal displacement vector $\left\langle \hat{\mathbf{\Delta}}\right\rangle_{1\times 14}^{\mathbf{T}}=\left\langle \hat{\mathbf{d}}\left(0\right)_{1\times 6}^{\mathbf{T}} \mid \hat{\hat{\mathbf{d}}}\left(L/2\right)_{1\times 2}^{\mathbf{T}} \mid \hat{\mathbf{d}}\left(L\right)_{1\times 6}^{\mathbf{T}}\right\rangle$ where

$$\hat{\mathbf{d}}(z_i)^{\mathbf{T}}_{1\times 6} = \left\langle \overline{u}_{1b}(z_i) \quad \overline{\theta}_{y1b}(z_i) \mid \overline{u}_{3b}(z_i) \quad \overline{\theta}_{y3b}(z_i) \mid \overline{\theta}_{zb}(z_i) \quad \overline{\psi}_{1b}(z_i) \right\rangle, \quad \text{and} \quad z_i = 0 \text{ or } L \quad \text{and}$$

$$\hat{\hat{\mathbf{d}}}(L/2)^{\mathbf{T}}_{1\times 2} = \left\langle \overline{u}_{1b}(L/2) \quad \overline{\theta}_{zb}(L/2) \right\rangle \text{ through}$$

$$\begin{aligned} &\left\langle \overline{u}_{1b}(z), \overline{\theta}_{y1b}(z), \overline{u}_{3b}(z), \overline{\theta}_{y3b}(z), \overline{\theta}_{zb}(z), \overline{\psi}_{1b}(z) \right\rangle^T \\ &\quad = \left\langle \hat{\mathbf{\Delta}} \right\rangle^T_{1\times 14} \left(\left\{ \hat{\mathbf{S}}_{\mathbf{u1}} \right\}_{14\times 1}, \left\{ \hat{\mathbf{S}}_{\theta \mathbf{1}} \right\}_{14\times 1}, \left\{ \hat{\mathbf{S}}_{\mathbf{u}3} \right\}_{14\times 1}, \left\{ \hat{\mathbf{S}}_{\theta 3} \right\}_{14\times 1}, \left\{ \hat{\mathbf{S}}_{\theta z} \right\}_{14\times 1}, \left\{ \hat{\mathbf{S}}_{\psi \mathbf{1}} \right\}_{14\times 1} \right) \end{aligned} \tag{53}$$

in which the shape function vectors are defined as

$$\begin{aligned}
\left\langle \hat{\mathbf{S}}_{\mathbf{u1}} \right\rangle_{1\times 14} &= \left\langle R_1(z) \;\; 0 \;\; 0 \;\; 0 \;\; 0 \;\; 0 \mid R_2(z) \;\; 0 \mid R_3(z) \;\; 0 \;\; 0 \;\; 0 \;\; 0 \;\; 0 \right\rangle \\
\left\langle \hat{\mathbf{S}}_{\theta \mathbf{1}} \right\rangle_{1\times 14} &= \left\langle 0 \;\; L_1(z) \;\; 0 \;\; 0 \;\; 0 \;\; 0 \mid 0 \;\; 0 \mid 0 \;\; L_2(z) \;\; 0 \;\; 0 \;\; 0 \;\; 0 \right\rangle \\
\left\langle \hat{\mathbf{S}}_{\mathbf{u}3} \right\rangle_{1\times 14} &= \left\langle 0 \;\; 0 \;\; L_1(z) \;\; 0 \;\; 0 \;\; 0 \mid 0 \;\; 0 \mid 0 \;\; 0 \;\; L_2(z) \;\; 0 \;\; 0 \;\; 0 \right\rangle \\
\left\langle \hat{\mathbf{S}}_{\theta 3} \right\rangle_{1\times 14} &= \left\langle 0 \;\; 0 \;\; 0 \;\; L_1(z) \;\; 0 \;\; 0 \mid 0 \;\; 0 \mid 0 \;\; 0 \;\; 0 \;\; L_2(z) \;\; 0 \;\; 0 \right\rangle \\
\left\langle \hat{\mathbf{S}}_{\theta z} \right\rangle_{1\times 14} &= \left\langle 0 \;\; 0 \;\; 0 \;\; 0 \;\; R_1(z) \;\; 0 \mid 0 \;\; R_2(z) \mid 0 \;\; 0 \;\; 0 \;\; 0 \;\; R_3(z) \;\; 0 \right\rangle \\
\left\langle \hat{\mathbf{S}}_{\psi \mathbf{1}} \right\rangle_{1\times 14} &= \left\langle 0 \;\; 0 \;\; 0 \;\; 0 \;\; 0 \;\; L_1(z) \mid 0 \;\; 0 \mid 0 \;\; 0 \;\; 0 \;\; 0 \;\; 0 \;\; L_2(z) \right\rangle
\end{aligned} \tag{54}$$

with $R_1(z) = (z/L-1)(2z/L-1)$, $R_2(z) = (4z/L)(1-z/L)$, and $R_3(z) = (z/L)(2z/L-1)$. From Eqs. (53), by substituting into Eqs. (39) through (42)a-c, and from Eqs. (49) and (53) by substituting into Eqs. (43)-(48) and (34), the second variation of the total potential energy in Eq. (38) is obtained as

$$\delta \frac{1}{2} \overline{\overline{\pi}} = \delta \frac{1}{2} \left\langle \hat{\mathbf{\Delta}} \right\rangle^{\mathbf{T}}_{1\times 14} \left(\left[\hat{\mathbf{K}}_{\mathbf{e}} \right]_{14\times 14} + \lambda \left[\hat{\mathbf{K}}_{\mathbf{g}} \right]_{14\times 14} \right) \left\{ \hat{\mathbf{\Delta}} \right\}_{14\times 1} = 0 \tag{55}$$

in which $\left[\hat{\mathbf{K}}_{\mathbf{e}} \right]_{14\times 14}$ and $\left[\hat{\mathbf{K}}_{\mathbf{g}} \right]_{14\times 14}$ are elastic and geometric stiffness matrices, respectively as defined in Appendix C. A non-trivial solution of Eq. (55) leads to the eigenvalue solution $\left\{ \left[\hat{\mathbf{K}}_{\mathbf{e}} \right]_{14\times 14} + \lambda \left[\hat{\mathbf{K}}_{\mathbf{g}} \right]_{14\times 14} \right\} \left\{ \hat{\mathbf{\Delta}} \right\}_{14\times 1} = \{\mathbf{0}\}_{14\times 1}$.

13. Validation and Examples

The elements developed in the present study are adopted to predict the buckling capacities of beams and columns and validated through comparisons with 3-dimentional finite element analyses (3D FEA) under ABAQUS software (and classical solutions for the degenerate case of no GFRP). Although these formulations are developed to apply for GFRP-strengthened beams, they can be also applied for steel beams alone by setting to zero the mechanical properties and/or dimensions of GFRP and adhesive materials.

13.1. Example 1 – Simply supported composite beam under a mid-span point load

A simply supported steel beam is subjected to a point load P applied at mid-span (Fig. 5a). The beam cross-section is W250x45 with the dimensions shown in Fig. 5b. One flange (i.e., compression flange or tension flange) is bonded to a 19mm-thick GFRP plate through a 1-mm thick layer of adhesive. Three span are considered; 4.0, 6.0 and 8.0m. Elasticity modulus of steel is 200GPa, that of GFRP is 17.2 GPa [10] and that of adhesive are 3.18 GPa [4]. Poisson's ratio for all materials is taken as 0.3 and the yield strength of steel is selected as 350 MPa. The buckling load P_{cr} and corresponding mode shapes for both the strengthened beam and the bare steel beam are determined from the present model and comparisons are made to 3D FEA results based on ABAQUS and standard equations based on the Eurocode Guide moment gradient factor [33].

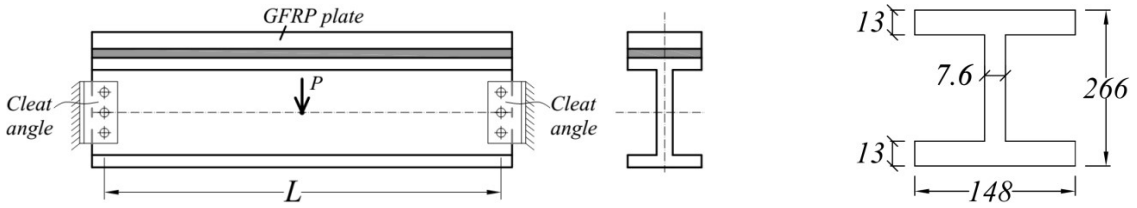

(a) (b)

Figure 5. Simply supported beams under a point load (a) beam profile and cross-section and (b) dimensions of W250x45 section

Based the given yield strength, the bare beam is found to meet Class 1 requirements of CAN-CSA S16 [34]. The corresponding plastic moment is $M_p = Z_x F_y = 210.7kNm$. Also, the nominal elastic buckling moment is $M_u = \left(C_b \pi / L\right)\sqrt{GJEI_{yy} + I_{yy} I_{\omega\omega} \left(\pi E / L\right)^2}$ where the moment gradient C_b depends on the standards adopted and ranges from 1.265 in CAN-CSA S16 [34] to 1.388 in Australian code AS4100 [35] and takes the value of 1.365 in the Eurocode guide [33] which is closest to FEA predictions [36]. In CAN-CSA S16 [34], when $M_u \le 0.67 M_p$, the elastic LTB resistance is deemed to govern the resistance and the nominal resistance is $M_n = M_u$ while when $M_u > 0.67 M_p$ the inelastic LTB capacity is $M_{in} = 1.15 M_p \left(1 - 0.28 M_p / M_u\right)$ and is deemed to govern the design $M_n = M_{in}$ when $M_{in} < M_p$. Otherwise, the plastic resistance is concluded to govern the design and the beam nominal resistance is governed by its plastic resistance, i.e., $M_n = M_p$. For the present section, the plastic resistance is found to govern the resistance of the beam when $L \le 2580mm$, the elastic LTB capacity to govern the resistance when $L > 5490mm$, while the inelastic LTB buckling governs the resistance when $2580 \le L \le 5490mm$. For the present

example, three spans are selected; L=4.0, 6.0, and 8.0m so that the smaller value lies in the inelastic LTB range, while the other two spans correspond to the elastic LTB failure mode.

Mesh study for present element: A mesh study is conducted by modeling the 6m span beam using both elements developed in the present study. Meshes consisting of 16, 32, 40, 80, 160 and 320 elements were considered (Fig. 6). For the three-node element, when adopting coarser meshes involving 16-40 elements, the critical loads predicted are found to decrease with the number of elements, afterward the solution stabilizes as meshes with 80- 320 elements provide identical buckling load predictions of 127.0 kN, suggesting that convergence is achieved when 80 elements are taken. The buckling load of 127.0 kN is taken as a reference value for comparison with solutions based on the two-node element. For the two-node element, the buckling loads based on 16, 32, 40, 80, 160, and 320 elements of the two-node elements are 409, 159, 142, 129, 127.9 and 127.5 kN, respectively and the corresponding differences from the reference critical load are 222%, 159%, 11.6%, 1.7%, 0.7% and 0.4%. The results suggest that the convergence rate is somewhat slower than that of the three-node element and hence the three-node element will be adopted in subsequent analyses.

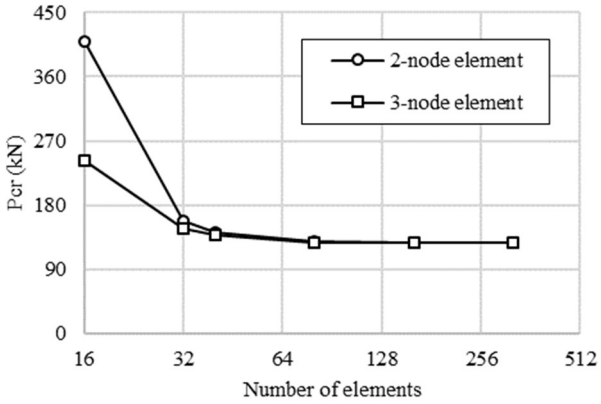

Figure 6. Mesh study of the present finite element formulation

Mesh study for the 3D FEA: The 3D FEA is conducted as a benchmark solution against which the results of the present theory are compared. The 8-node brick element C3D8R is selected from the ABAQUS library. The element has 8 nodes with three translations at each node, totaling 24 DOFs. The element uses reduced integration to avoid volumetric locking, and thus has a single integration point located at the centroid. A mesh study is performed to determine the mesh beyond which no improvement is attained in the solution. The mesh is fully characterized by seven parameters $n_1,...,n_7$ as shown in Fig. 7. For the 6m span, the study showed that convergence is attained when a mesh with $n_1 = 12, n_2 = n_4 = n_5 = n_6/2 = 4; n_3 = 60; n_7 = 600$ is taken, corresponding to 1,682,199

DOFs. Initially, the 3D FEA model exhibited web distortion and hence under-predicted the critical moments. To control distortional effects, transverse stiffeners were added to the model. Three stiffening arrangements were considered; (a) two stiffeners at both ends of the beam, (b) three stiffeners (two at the ends and one at mid-span), and (c) five stiffeners along the span L (at 0, L/4, L/2, 3L/4, and L). A comparison of the buckling loads for spans L=4.0, 6.0 and 8.0m are shown in Table 1. The addition of more web stiffeners is found to increase the buckling loads, and make the 3D FEA solutions approach the predictions of the present model. The beam with five-stiffener arrangement is found to yield the closest predictions to those of the present study.

The three-stiffener arrangement is adopted in subsequent runs.

Table 1. Comparison of buckling load (kN) for different stiffener arrangements

Span (m)	Number of stiffeners adopted:			Present study (*d*)	(*d*) / (*a*)	(*d*) / (*b*)	(*d*) / (*c*)
	2 (*a*)	3 (*b*)	5 (*c*)				
4	271	296	305	314	1.16	1.06	1.03
6	117	121	125.2	127	1.09	1.05	1.01
8	65.3	65.4	67.6	68.5	1.05	1.05	1.01

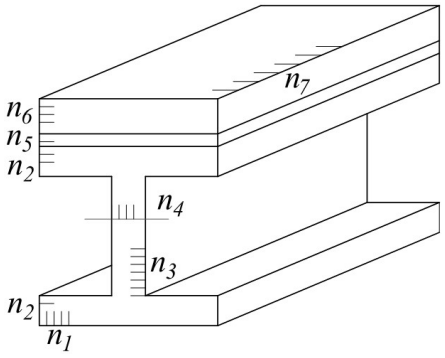

Figure 7. Number of elements defining the 3D FEA mesh

Verification of buckling loads: Table presents the buckling loads as predicted by the present model, the 3D FEA, and the critical moment based on the Eurocode guide moment gradient factor. For the bare steel beam, the present model respectively predicts buckling loads of 227, 89.0 and 47.8 kN, for the 4, 6 and 8m spans. These values compare to 3D FEA predictions of 223, 87.1 and 46.7 kN which correspond to 2.0%, 2.1 % and 2.3% differences. In comparison, the solution based on the critical moment gradient based on the Eurocode moment gradient factor overestimates the buckling loads by 4.1%, 3.5% and 2.9%.

For the case where the compression flange is strengthened, the buckling loads based on the present solution are 314, 127 and 68.5 kN for 4, 6, and 8m spans, respectively, while those based on the

3D FEA predictions are 296, 121 and 65.4 kN, corresponding to 5.9%, 4.9% and 4.5% differences (Table 2). For the case where the tension flange is strengthened, the buckling loads predicted by the present solution are 291, 121 and 66.0 kN for 4, 6, and 8m spans, respectively while those predicted by the 3D FEA solution are 274, 114, 62.6 kN, corresponding to 6.1%, 5.5% and 5.2% differences. The difference between the predictions of both models is attributed to minor web distortions between the stiffeners, which are captured in the 3D FEA solution but not in the present model. The differences between the non-distortional solution in the present model and the 3D FEA solution based on the Abaqus model is slightly larger than the bare beam results. The observation is qualitatively consistent with past research on bare steel beams sections (e.g., [36]) which suggest that webs for sections with thicker flanges exhibit more pronounced distortional effects. In this respect, the GFRP plate can be conceived to "thicken" the compression flange.

For the 6m span beam with the compression flange strengthened, when the load is moved to the top flange, the present model was found to predict a buckling load of 102 kN, which compares to 96.8 kN as predicted by the 3D FEA model, a 5.1% difference. Also, when the load is moved to the bottom flange, the present model predicted a buckling load of 154 kN which compares to150 kN as predicted by the 3D FEA, a 2.7% difference.

Table 2. Buckling loads P_{cr} (kN) for bare and strengthened W250x45 simply supported beam

Span	Bare steel beam					Compression Flange Strengthened			Tension Flange Strengthened		
(m)	PS (1)	E^{+} (2)	3D FEA (3)	(1)/ (3)	(2)/ (3)	PS (4)	3D FEA (5)	(4)/ (5)	PS (6)	3D FEA (7)	(6)/ (7)
4	227	232	223	1.02	1.04	314	296	1.06	291	274	1.06
6	89	90.3	87.1	1.02	1.04	127	121	1.05	121	114	1.06
8	47.8	48.1	46.7	1.02	1.03	68.5	65.4	1.05	66.0	62.6	1.05

* PS=Present study, $^{+}$E= classical solution based on moment gradient factor of Eurocode Guide [33]

Verification of buckling mode: The buckling configuration for the 6m span beam as predicted by the present solution are found to nearly overlap on that predicted by the 3D FEA in Figs. 8a-f which depicts the buckling displacements $u_{1b}, u_{3b}, \theta_{zb}, \theta_{y1b}, \theta_{y3b}$ and ψ_{1b}. In a strict sense, owing to cross-sectional distortion, the angle of twist θ_{zb} in the 3D FEA would slightly vary within a given cross-section z. Thus, a representative angle of twist was computed based on the lateral displacements extracted from the buckled configuration of the 3D FEA model at the web-to-flange junctions. In a similar manner, an estimate of the weak axis rotation θ_{y3b} for GFRP is computed

from the longitudinal displacements at the plate ends, as extracted from the buckled FEA configuration.

Also, at a given section z, in order to characterize the weak axis rotation θ_{y1b}, and warping deformation, ψ_{1b} as predicted by the 3D FEA model, the longitudinal displacements are extracted at four sampling points within the cross-section and the procedure introduced in [28,37] was adopted to estimate the weak axis rotation, warping deformation, (along with the longitudinal displacement at the section centroid, and strong axis as a by-product). Again, the predicted values would slightly vary within a cross-section depending on selection of the sampling points. In the present study, the four sampling points were selected at the tips of the flanges and the details are provided in (Pham 2018 [38]).

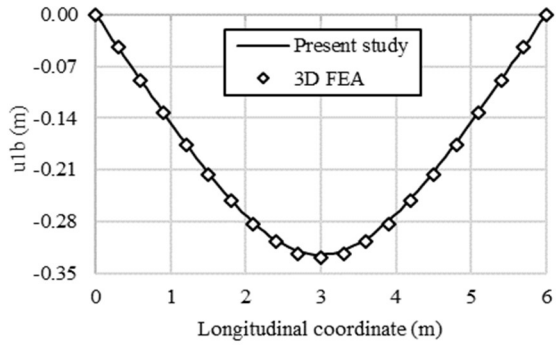

(a) $u_{1b}(z)$

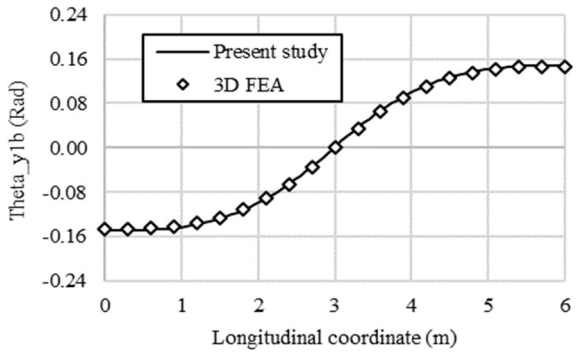

(b) $\theta_{y1b}(z)$

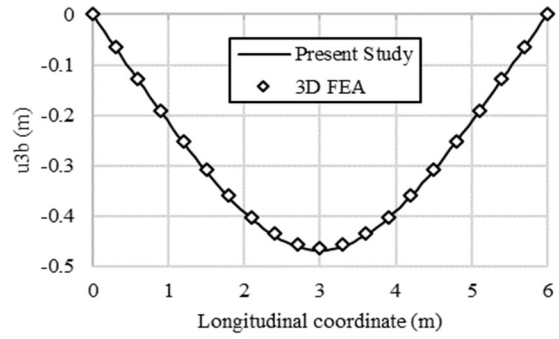

(c) $u_{3b}(z)$

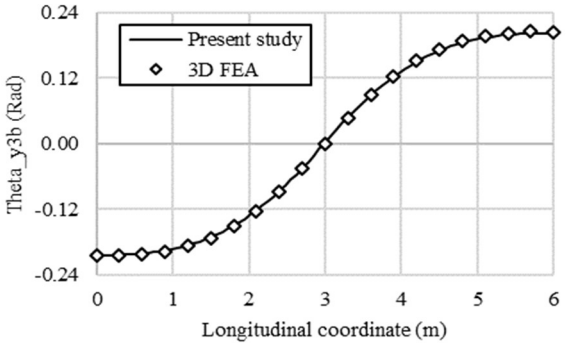

(d) $\theta_{y3b}(z)$

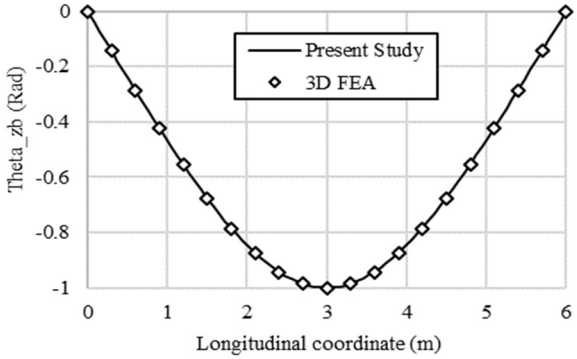

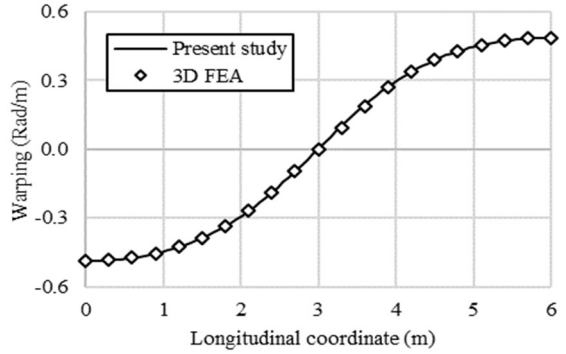

(e) $\theta_{zb}(z)$ (f) $\psi_{1b}(z)$

Figure 8. Comparison of mode shape for span L=6m between present study and 3D FEA solutions

Effectiveness of strengthening: When the compression flange of the present problem is strengthened, the present model predicts respective increases in the elastic critical loads of 38.4%, 42.8%, and 43.3%, for the 4, 6, and 8m spans, above the corresponding elastic critical loads of the bare beams. As expected, strengthening the tension flange leads to less gains in the elastic critical load of 28.2%, 36% and 38.1%, respectively.

Investigating the possibility of material failure prior to buckling: A common concern in beams strengthened with GFRP plates is the possible delamination induced by peeling and/or shear stresses near bond ends. For the 4, 6 and 8m spans investigated, the 3D FEA solution predicts peak peeling stresses near beam ends of 1.3, 0.52, and 0.24 MPa and peak shear stresses of 1.6, 0.67, and 0.37 MPa, respectively. These stresses are significantly smaller than typical adhesive and shear strengths of 33 MPa and 15 MPa, respectively [4]. Also, the peak longitudinal compressive stresses within the GFRP plates occur at mid-span and take the values 57.6, 34.8, and 24.4 MPa for 4, 6 and 8m spans. These values are much smaller than typical GFRP longitudinal strengths of 207 MPa [10]. The analysis suggests that material failure of GFRP and adhesive do not govern the capacity of the beams in a manner consistent with assumption (ix).

Effect of the load position: Table 3 shows the predicted critical loads when the load position is moved to the top and bottom flanges of the 6m and 8m span beams. The percentage gains/reductions due to the effect of load position are compared to the case of shear center loading for each span and each strengthening arrangement (i.e., bare beam, strengthened beams). When applying the load at the top flange of the 6m span bare beam, the buckling load is 75.4% of that of the shear center loading. For the beam strengthened at the compression flange, the buckling load for top flange loading is 80.3% of that of shear center loading. A comparable fraction of 80.4% is attained for tension flange strengthening. When applying the load at the bottom flange of the bare beam, the buckling load was found to increase to 132% of that of the shear center loading. For the strengthened beams, the buckling load increases to 123% for top flange strengthening, and 124% for bottom flange strengthening. Similar results are observed for the 8m span beam.

The limited set of results investigated herein suggests that adopting the load height reduction factors for top flange loading of the bare beam consistently yield conservative buckling strength predictions in the case of strengthened beams. Conversely, adopting load height gain factors for

bottom flange loading for the bare beam would consistently lead to un-conservative buckling load predictions.

Table 3. Effect of load height and Load height factors for W250x45 beams

Span (m)	Load position	Bare steel beam		Compression Flange Strengthened		Tension Flange Strengthened	
		Critical load (kN)	Load height factor*	Critical load (kN)	Load height factor	Critical load (kN)	Load height factor
6	Top	67.1	75.4%	102	80.3%	97.3	80.4%
	Shear center	89.0	100%	127	100%	121	100%
	Bottom	117	132%	157	123%	150	124%
8	Top	37.2	77.8%	57.5	83.9%	55.3	83.8%
	Shear center	47.8	100%	68.5	100%	66.0	100%
	Bottom	59.4	124%	80.5	118%	77.7	118%

*: Load height factor =buckling load for the given load position/ buckling load for shear center loading for the specified span and strengthening arrangement as applicable

Effect of GFRP and adhesive thicknesses on buckling strength: The 6m-span steel beam with the compression flange strengthened is considered under the effect of a mid-span point load acting at the shear center. The thickness of the GFRP plate first is varied from 0.0 to 30mm while keeping the adhesive layer thickness as 1.0mm and then thickness of the adhesive is varied from 0.5 to 4.0mm while keeping the GFRP plate thickness as 19mm. As observed in Fig. 9a, the buckling load increases in a nonlinear fashion with the GFRP thickness. While the buckling load for the bare beam is 89 kN, that corresponding to a 30mm thick plate is significantly increased to 173 kN, a 94.4% difference. In contrast, Fig. 9b shows that the buckling load increases only marginally with the thickness of the adhesive. The increase is attributed to the slightly deeper overall cross-section in the case of a thicker adhesive. While the buckling load for the 0.5mm thick adhesive is 126.9 kN, that corresponding to 4.0mm is marginally increased to 133 kN, a 4.6% difference.

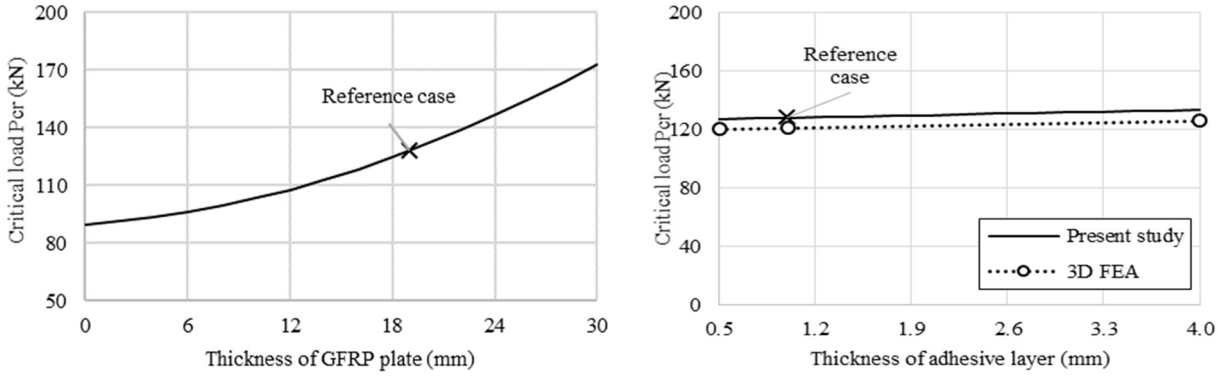

Figure 9. Critical loads P_{cr} (kN) against (a) GFRP plate thickness and (b) adhesive layer thickness

Effect of the steel section dimensions on buckling strength: The steel beam with the compression flange strengthening considered in Example 1 is re-considered while keeping all geometric parameters, material properties, boundary conditions, and loading unchanged. The W250x45 cross-section with dimensions (h_r, b_r, t_r, w_r) is taken as a reference case. Only one of the cross-sectional parameters (h, b, t, w) is varied one at a time in the ranges $0.5 \le R_h = (h/h_r) \le 1.5$; $0.5 \le R_b = (b/b_r) \le 1.5$; $0.5 \le R_w = (w/w_r) \le 1.5$; and $0.5 \le R_t = (t/t_r) \le 1.5$, while keeping the three remaining parameters unchanged from the reference values. The critical loads were extracted for all the cases (Fig. 10). It is observed that the flange width b is the most influential on the predicted critical load. The buckling load corresponding to $R_b = 0.5$ is 30 kN while that corresponding to $R_b = 1.5$ is 314 kN, a tenfold increase. The flange thickness is also observed to have a significant influence on the critical load while the section depth and the web thickness are found are less influencial. This finding is consistent with the CAN-CSA S16 solution [34] for steel sections in which the critical load is largely dependent on the moment of inertial I_{yy} about the weak axis and the warping constant $I_{\omega\omega}$.

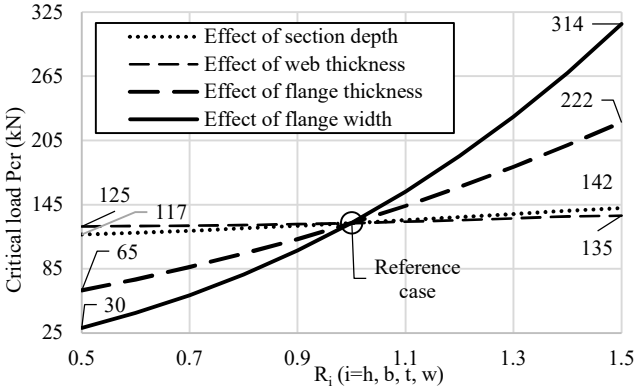

Figure 10. Critical loads P_{cr} (kN) against the changed dimensions of the reference section W250x45

13.2. Example 2 – Simply supported beam under linear bending moments

The steel beam with top flange strengthening in Example 1 is re-visited here under the action of strong axis linear bending moments induced by two end moments $M_x, \kappa M_x$ with $-1 \le \kappa \le 1$, where $\kappa = -1$ indicates uniform moments and $\kappa = 1$ denotes full reversed moments (Table 4). Span is taken as 5m. The end moments were applied as two equal and opposite axial unit forces acting at the flange-web junctions.

Critical moments: Table 4 provides the buckling loads for loading cases $\kappa = -1.0, -0.5, 0.0, 0.5, \text{and } 1.0$. For the bare beam, differences within 0.6% are observed between predictions of the present model and the 3D FEA solutions. For the strengthened beam, the differences between both solutions are found to lie within 5.7%. As discussed in previous examples, the difference is attributed to web distortion. A comparison between the critical moments (Table 4) for the bare and strengthened beams shows an effectiveness of strengthening of 38.9%, 36.5%, 38.2%, 35.7% and 35.5%, for loading Cases 1 through 5, respectively.

Moment gradient effect: For a given loading case κ, the moment gradient factor C_b evaluated from a buckling analysis can be obtained by dividing the predicted critical moment $M_{cr}(\kappa)$ by the critical uniform moment $M_{cr}(-1)$. Adopting this definition, one can obtain the moment gradient factors based on either the 3D FEA analysis, the present model, or the beam buckling element of Barsoum and Gallagher [39] and comparisons are made against moment gradient expressions provided in various standards. The relevant equations are $C_b(CAN) = 4M_{\max} \Big/ \sqrt{M_{\max}^2 + 4M_a^2 + 7M_b^2 + 4M_c^2} \le 2.5$ based on the Canadian Standards CAN CSA S16 [34], $C_b(AISC) = 12.5M_{\max} \Big/ (2.5M_{\max} + 3M_a + 4M_b + 3M_c)$ based on American standards AISC [40], and $C_b(AUS) = 1.7M_{\max} \Big/ \sqrt{M_a^2 + M_b^2 + M_c^2} \le 2.5$ based on the Australian standards AS4100 [35], and those based on Eurocode Guide [33] (Table 4).

The 3D FEA results are taken as a benchmark solution against which other solutions are compared. As observed in Fig. 11a, the present solution is in excellent agreement with the predictions of the 3D FEA model with the differences between both solutions within 0.6%. The Barsoum and Gallagher [39] and Eurocode Guide solutions slightly overestimate the moment gradient factors, while the CSA, AISC and AS solutions under-predict the results. For instance of the case of fully reversed moments $\kappa = 1$, the BG and EG solutions overestimate the moment gradients by 1.7% and 2.8%, while the CSA, AISC and AS underestimate the moment gradients by 14%, 15% and 9.1%, respectively. For the strengthened beam (Table 4 and Fig. 11b), the moment gradient factors are provided based on the present study and 3D FEA. As observed, the present study and the 3D FEA solutions are in close agreement. The maximum difference between the two solutions is 2.4% for the case of fully reversed moments $\kappa = 1$. Also shown on Fig. 11b is a comparison of the moment gradient factor for the strengthened beam overlaid on that of the bare beam. The moment gradients for the bare beam are observed to be marginally lower than those of the strengthened

beam in the case double curvature. Otherwise, the moment gradients of both beams nearly coincide for single curvature. The results suggest that moment gradients for bare beams can safely be applied to the design of strengthened beams.

Table 4. Comparison of buckling moments and moment gradient factors for beam W250x45

Cross-section	Loading Case		Buckling moment (kNm)			C_b of	Ratio of Moment Gradient Factor					
			PS	3D FEA	% Diff.	3DFEA	PS / 3DFEA	BG / 3DFEA	CSA / 3DFEA	EG / 3DFEA	AISC / 3DFEA	AS / 3DFEA
Bare beam	1	M_x $-M_x$	126	126	0.00	1.000	1.000	1.000	1.000	1.000	1.000	0.982
	2	M_x $-0.5M_x$	167	166	0.60	1.318	1.006	1.007	0.981	1.004	0.948	0.984
	3	M_x 0	228	227	0.44	1.802	1.004	1.029	0.969	1.043	0.925	1.009
	4	M_x $0.5M_x$	317	316	0.32	2.508	1.003	1.019	0.912	1.078	0.867	0.990
	5	M_x M_x	338	337	0.30	2.675	1.003	1.017	0.863	1.028	0.850	0.899
GFRP-strengthened beam	1	M_x $-M_x$	175	169	3.4	1.000	1.000					
	2	M_x $-0.5M_x$	228	221	3.1	1.308	1.000					
	3	M_x 0	315	303	3.8	1.793	1.004			N/A		
	4	M_x $0.5M_x$	430	411	4.4	2.432	1.010					
	5	M_x M_x	457	431	5.7	2.550	1.024					

PS=Present study, BG= Barsoum and Gallagher, CSA=Canadian code, EG=Eurocode guide, AISC=American code, AS=Australian code.

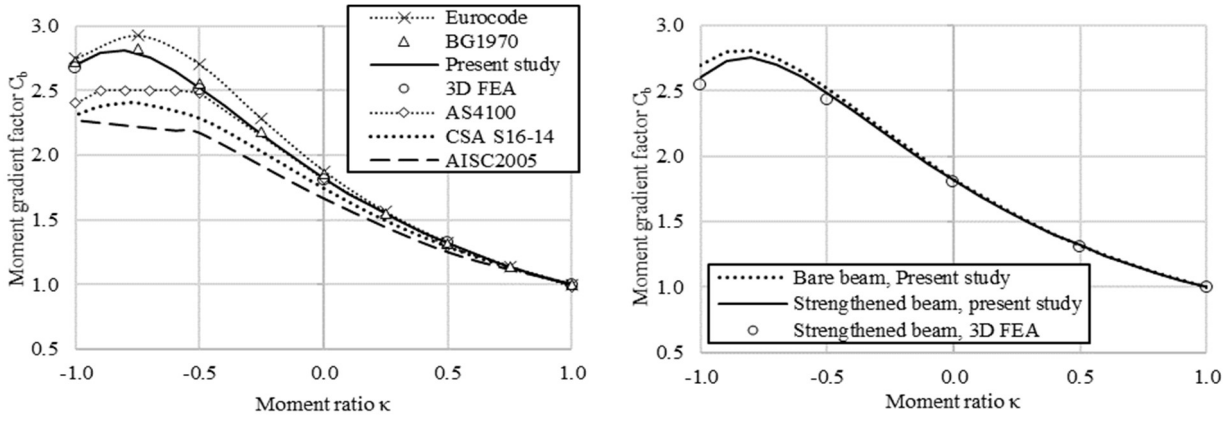

(a) (b)

Figure 11. Moment gradient factor against moment ratio κ for (a) bare steel beam and (b) strengthened steel beam with comparison to bare beam results

13.3. Example 3 – Fixed-free column

A fixed-free column is subjected to a compression force P acting at the steel section centroid. The column cross-section and the specifics of the strengthening GFRP and adhesive are identical to those in Example 1. The span is taken as 3m and 5m.

Table 5 presents the buckling loads for the bare columns and strengthened columns based on the present solution, the 3D FEA and the classical solution. The buckling load predictions for the bare column by the present solution are in nearly perfect agreement with the classical solution $P_{cr} = \pi^2 EI/4L^2$ and 3D FEA solution. Also, excellent agreement is obtained between the present solution and the 3D FEA solution for the strengthened column. Small differences (i.e., less than 0.7%) between two solutions are observed, showing the validity of the solution and correctness of implementation. A comparison of the critical loads of the bare and strengthened columns shows a minor increase in buckling strength of 6.8% for the 3m span and 6.5% for the 5m span. The strengthening effectiveness for the present column is significantly lower than that attained for beams in Examples 1 and 2.

Table 5. Comparison of critical buckling load P_{cr} for columns

Span (m)	Bare steel column					GFRP-strengthened column		
	Buckling load (kN)			Buckling load ratio		Buckling load (kN)		Buckling load ratio
	PS (1)	CS (2)	3D FEA (3)	(1)/ (3)	(2)/ (3)	PS (4)	3D FEA (5)	(4)/ (5)
3	385	386	384	1.003	1.005	411	408	1.007
5	139	139	139	1.000	1.000	148	147	1.007

* PS=Present study, CS=Classical Solution

13.4. Example 4 – Simply supported beam-column

The W250x58 4m span steel beam-column in Wu and Mohareb [17] is re-visited. In the present paper, in addition to the steel section, one of the flanges is bonded to a 19mm-thick GFRP plate through a 1-mm thick adhesive layer. Two scenarios are considered, where the strengthening is provided to the top flange (Fig. 12a) and to the bottom flange (Fig. 12b). The member is subjected to a compressive force P and a uniform strong axis bending moment M. Material properties for steel, GFRP, and adhesive are identical to those of Example 1.

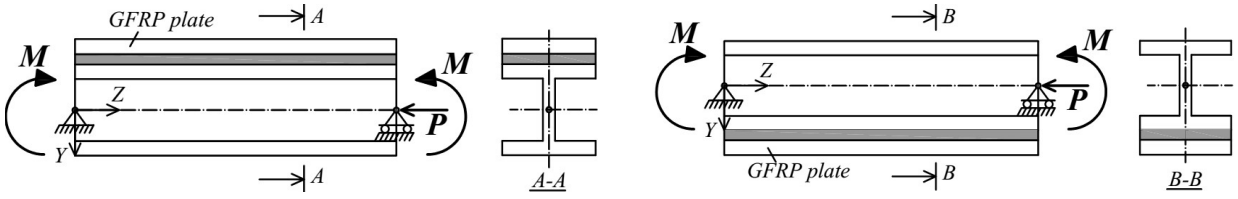

(a) (b)

Figure 12. Simply supported beam column (a) top flange strengthened (b) bottom flange strengthened

Table 6 presents the critical force P_0 in the absence of bending moments M and the critical moment M_0 in the absence of axial force P as predicted by Wu and Mohareb [17] (subsequently referenced as WM2011b), 3D FEA and by present study. The critical loads for the bare beams as predicted by the present solution are nearly identical to those of WM2011b solution. For the strengthened beams, the critical load P_0 as predicted by the present solution nearly coincides with the 3D FEA prediction while the critical moment M_0 predictions differ by about 3%.

Table 6. Critical buckling loads P_0 (kN) and M_0 (kNm) for the beam-column in Example 5

Critical buckling load	Bare steel beam			Top Flange Strengthened with GFRP			Bottom Flange Strengthened with GFRP		
	WM2011b (1)	PS (2)	(1)/ (2)	3D FEA (3)	PS (4)	(3)/ (4)	3D FEA (5)	PS (6)	(5)/ (6)
P_0 (kN)	2311	2321	1.00	2440	2475	0.99	2440	2475	0.99
M_0 (kNm)	378	377	1.00	477	486	0.98	448	460	0.97

* PS=Present study, WM2011b=Wu and Mohareb [17]

The critical load combinations $\lambda(P, M)$ were sought for different eccentricities M / P to generate the interaction diagrams. The results for the bare and strengthened beams were then normalized by dividing the obtained compressive force λP and moments λM respectively by P_0 and M_0 of the bare beam (Fig. 13). For the bare beam, the normalized interaction diagram obtained from the WM2011b solution essentially coincides with that based on the present study. For the strengthened beams (with top or bottom flange strengthening), the interaction diagrams based on the present study are found nearly identical to those based on 3D FEA solution. As expected, strengthening of the compressive flange is observed to be more effective in increasing the lateral torsional buckling strength than does the strengthening the tension flange. For instance, at a compressive force ratio of 0.557, the critical moment ratio predicted by present study is 0.557 while that predicted for the case of compression flange strengthening is 0.801, a 43.8% increase. This compares to a ratio of 0.719 when the tension flange is strengthened, a 29.1% increase.

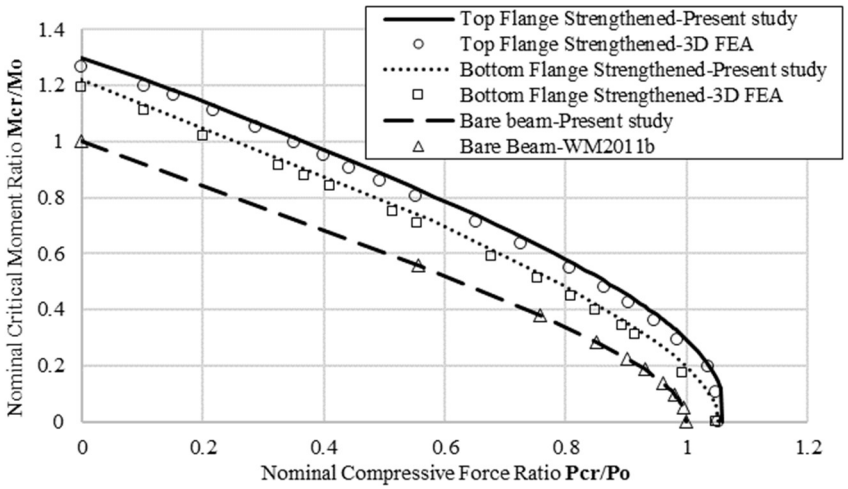

Figure 13. Normalized interaction diagram of a beam-column

14. Summary and Conclusions

The present study has successfully developed a shear deformable beam theory for the buckling analysis of GFRP-strengthened beam-columns. The principle of total stationary buckling energy was adopted to formulate a two-node finite element based on Hermitian shape functions and a three-node element based on Lagrangian shape functions. The three-node element is more favorable regarding shear-locking effects and possesses fewer degrees of freedom than the two-node elements. It is found to converge faster to the solution while involving less computational effort than the two-node element.

The following conclusions can be drawn from the examples investigated.

(1) The present study is able to reliably predict the buckling loads of GFRP-strengthened beam/column subjected to general load/boundary conditions, load height effects, moment gradient predictions and it accurately predicts mode shapes. Also, the buckling strength predictions of the present model for bare beams were shown to be consistent with other established solutions and equations in various standards ([33], [34], [35], [39] and [40]).

(2) Examples 1 and 2 suggest that GFRP strengthening is most effective in increasing the LTB strength of a beam when applied to strength compression flanges of laterally unsupported flexural members and moderately effective when strengthening their tension flange. For W250x45 beams strengthened with a 19-mm thick GFRP plate in Examples 1-2, the buckling loads were found to increase by 35.5%-43.3% when the compression flange was strengthened and by 28.2%-38.1% when the tension flange was strengthened. In contrast, the effectiveness

for a strengthened column, as evidenced in Example 3, is found small (i.e., 6.8%) as the gain in the flexural stiffness about weak axis is negligible.

(3) Example 1 suggests that the effectiveness of strengthening on lateral torsional buckling strength significantly depends on the GFRP plate thickness but is nearly independent of the adhesive thickness. The findings apply only to combinations of thicknesses and material properties of the adhesive investigated in this example and do not necessarily apply to other thicknesses and material properties.

(4) Example 1 suggests that load height factors for bare beams consistently yield conservative buckling strength predictions for strengthened beams. Conversely, adopting load height factors of bare beams to cases of bottom flange loading for the bare beam would consistently overestimate buckling load predictions. The observations are valid both for compression or tension flange strengthening.

(5) Example 2 suggests the possibility of adopting moment gradient factors for bare beams when designing strengthened beams subjected to linear moment gradients.

(6) The present solution is capable to generate moment-axial force interaction diagrams for beam-columns that account for beam and column stability effects. Example 4 shows that the interaction diagrams are non-linear. The size of the interaction diagrams was found to grow beyond that of the bare beam when the steel beam is strengthened by GFRP at the tension flange and to further grow when GFRP strengthening is applied at the compression flange.

(7) The computational effort involved in the present solution is orders of magnitudes less than that of 3D FEA analysis, particularly for the analysis of GFRP-strengthened beams. The present solutions, implemented in non-compiled MATLAB script files, typically took 40 seconds per run for examples 1-4 on a computer with two Intel(R) Xeon(R) CPU E5-24300 processors at 2.20 GHz speed, and 64.0 GB memory RAM. In comparison, the 3D FEA under ABAQUS took about 1.2 - 3.9 hours per run on the same computer. The present solution also involves less effort in modelling and post-processing compared to the 3D FEA solutions.

15. Acknowledgement

The authors gratefully acknowledge scholarship support from the University of Ottawa and Ontario Graduate scholarship (OGS) to the first author and research funding from the Natural Sciences and Engineering Research Council (NSERC) of Canada to the second and third authors.

Appendix A: Second variations of total potential energy expressed in Eq. 38

The elastic strain energies are defined as

$$\bar{\bar{U}}_{en1}=\int_0^L\int_{A_1}E_1\left[-n_1\sin\alpha\left(s_1\right)\bar{u}''_{1b}-x_1\left(s_1\right)\bar{\theta}'_{y1b}+n_1q\left(s_1\right)\bar{\theta}''_{zb}-\omega\left(s_1\right)\bar{\psi}'_{1b}\right]^2dA_1dz$$

$$\bar{\bar{U}}_{es1}=\int_0^L\int_{A_1}G_1\left[\cos\alpha\left(s_1\right)\bar{u}'_{1b}-\cos\alpha\left(s_1\right)\bar{\theta}_{y1b}+\left\{r\left(s_1\right)+2n_1\right\}\bar{\theta}'_{zb}-r\left(s_1\right)\bar{\psi}_{1b}\right]^2dA_1dz$$

$$\bar{\bar{U}}_{en3}=\int_0^L\int_{A_3}E_3\left[-x_2\left(s_2\right)\bar{\theta}'_{y3b}+n_3x_2\left(s_2\right)\bar{\theta}''_{zb}\right]^2dA_3dz$$

$$\bar{\bar{U}}_{es3}=\int_0^L\int_{A_3}G_3\left(\bar{u}'_{3b}-\bar{\theta}_{y3b}+2n_3\bar{\theta}'_{zb}\right)^2dA_3dz$$

$$\bar{\bar{U}}_{ezn2}=\int_0^L\int_{A_2}G_2\left[c_5x\left(s\right)\bar{\theta}_{y1b}-c_5x\left(s\right)\bar{\theta}_{y3b}-\left(1+c_6\right)x\left(s\right)\bar{\theta}'_{zb}+c_5c_7x\left(s\right)\bar{\psi}_{1b}\right]^2dA_2dz$$

$$\bar{\bar{U}}_{esn2}=\int_0^L\int_{A_2}G_2\left[-c_5\bar{u}_{1b}+c_5\bar{u}_{3b}-\left(1+c_6+c_5c_7\right)\bar{\theta}_{zb}\right]^2dA_2dz+$$

$$\bar{\bar{U}}_{esz2}=\int_0^L\int_{A_2}G_2\left[c_1\left(n_2\right)\bar{u}'_{1b}-c_1\left(n_2\right)\bar{\theta}_{y1b}+c_2\left(n_2\right)\bar{u}'_{3b}-c_2\left(n_2\right)\bar{\theta}_{y3b}+\right.$$

$$\left.+\left[c_3\left(n_2\right)+c_4\left(n_2\right)\right]\bar{\theta}'_{zb}-c_7c_1\left(n_2\right)\bar{\psi}_{1b}\right]^2dA_2dz$$

Also, the geometric potential energies are defined as

$$\bar{\bar{V}}_{gN_1}=\lambda\int_0^L\int_{A_1}\frac{N_{1p}\left(z\right)}{A_s}\left\{\left(\bar{u}'_{1b}\right)^2+2\left[n_1\cos\alpha\left(s_1\right)-y_1\left(s_1\right)\right]\bar{u}'_{1b}\bar{\theta}'_{zb}+\left[q^2+r^2+2rn_1+n_1^2\right]\left(\bar{\theta}'_{zb}\right)^2\right\}dA_1dz;$$

$$\bar{\bar{V}}_{gM_s}=\lambda\int_0^L\int_{A_1}\left[\frac{n_1\cos\alpha\left(s_1\right)}{I_{ss}}M_{sp}\left(z\right)\right]\left\{\left(\bar{u}'_{1b}\right)^2+2\left[n_1\cos\alpha\left(s_1\right)-y_1\left(s_1\right)\right]\bar{u}'_{1b}\bar{\theta}'_{zb}+\left(q^2+r^2+2rn_1+n_1^2\right)\left(\bar{\theta}'_{zb}\right)^2\right\}dA_1dz+$$

$$+\lambda\int_0^L\int_{A_3}\left[\frac{n_3}{I_{xxg}}M_{sp}\left(z\right)\right]\left\{\left(\bar{u}'_{3b}\right)^2+2n_3\bar{u}'_{3b}\bar{\theta}'_{zb}+\left[n_3^2+x_3^2\left(s_3\right)\right]\left(\bar{\theta}'_{zb}\right)^2\right\}dA_3dz;$$

$$\bar{\bar{V}}_{gM_x}=\lambda\int_0^L\int_{A_1}\left[-\frac{y_1\left(s_1\right)}{I_{xx}}M_{xp}\left(z\right)\right]\left\{\left(\bar{u}'_{1b}\right)^2+2\left[n_1\cos\alpha\left(s_1\right)-y_1\left(s_1\right)\right]\bar{u}'_{1b}\bar{\theta}'_{zb}+\left(q^2+r^2+2rn_1+n_1^2\right)\left(\bar{\theta}'_{zb}\right)^2\right\}dA_1dz;$$

$$\bar{\bar{V}}_{gQ_1}=\lambda\int_0^L\int_{A_1}\frac{Q_{1p}}{A_s}\sin\alpha\left(s_1\right)\left\{-2\sin\alpha\left(s_1\right)\bar{u}'_{1b}\bar{\theta}_{zb}-2n_1^2\sin\alpha\left(s_1\right)\bar{u}''_{1b}\bar{\theta}'_{zb}+2n_1r\left(s_1\right)\sin\alpha\left(s_1\right)\bar{u}''_{1b}\bar{\psi}_{1b}+\right.$$

$$+2x\left(s_1\right)\cos\alpha\left(s_1\right)\bar{\theta}_{y1b}\bar{\theta}'_{y1b}-2n_1q\left(s_1\right)\cos\alpha\left(s_1\right)\bar{\theta}_{y1b}\bar{\theta}''_{zb}+2\omega\left(s_1\right)\cos\alpha\left(s_1\right)\bar{\theta}_{y1b}\bar{\psi}'_{1b}+2q\left(s_1\right)\bar{\theta}_{zb}\bar{\theta}'_{zb}+$$

$$-2x\left(s_1\right)n_1\bar{\theta}'_{y1b}\bar{\theta}'_{zb}+2x\left(s_1\right)r\left(s_1\right)\bar{\theta}'_{y1b}\bar{\psi}_{1b}+2n_1^2q\left(s_1\right)\bar{\theta}'_{zb}\bar{\theta}''_{zb}-2\omega\left(s_1\right)n_1\bar{\theta}'_{zb}\bar{\psi}'_{1b}-2r\left(s_1\right)n_1q\left(s_1\right)\bar{\theta}''_{zb}\bar{\psi}_{1b}+$$

$$\left.+2\omega\left(s_1\right)r\left(s_1\right)\bar{\psi}'_{1b}\bar{\psi}_{1b}\right\}dA_1dz;$$

$$\bar{\bar{V}}_{gN_3}=\lambda\int_0^L\int_{A_3}\frac{N_{3p}\left(z\right)}{A_g}\left\{\left(\bar{u}'_{3b}\right)^2+2n_3\bar{u}'_{3b}\bar{\theta}'_{zb}+\left[n_3^2+x_3^2\left(s_3\right)\right]\left(\bar{\theta}'_{zb}\right)^2\right\}dA_3dz;$$

$$\begin{aligned}\bar{\bar{V}}_{gQ2}=\lambda\int_0^L\int_{A_2}\frac{Q_{2p}(z)}{A_a}\Big\{&-2c_5c_1(n_2)x^2(s)\bar{\theta}'_{y1b}\bar{\theta}_{y1b}-2c_5c_2(n_2)x^2(s)\bar{\theta}_{y1b}\bar{\theta}'_{y3b}+2c_5c_3(n_2)x^2(s)\bar{\theta}''_{zb}\bar{\theta}_{y1b}+\\&-2c_5c_7c_1(n_2)x^2(s)\bar{\psi}'_{1b}\bar{\theta}_{y1b}+2c_5c_1(n_2)x^2(s)\bar{\theta}'_{y1b}\bar{\theta}_{y3b}+2c_5c_2(n_2)x^2(s)\bar{\theta}'_{y3b}\theta'_{y3b}+\\&-2c_5c_3(n_2)x^2(s)\bar{\theta}''_{zb}\bar{\theta}_{y3b}+2c_5c_7c_1(n_2)x^2(s)\bar{\psi}'_{1b}\bar{\theta}_{y3b}+2c_6c_1(n_2)x^2(s)\bar{\theta}'_{y1b}\bar{\theta}'_{zb}+\\&+2c_6c_2(n_2)x^2(s)\bar{\theta}'_{y3b}\bar{\theta}'_{zb}-2c_6c_3(n_2)x^2(s)\bar{\theta}''_{zb}\bar{\theta}'_{zb}+2c_6c_7c_1(n_2)x^2\bar{\psi}'_{1b}\bar{\theta}'_{zb}+\\&-2c_5c_7c_1(n_2)x^2(s)\bar{\theta}'_{y1b}\bar{\psi}_{1b}-2c_5c_7c_2(n_2)x^2(s)\bar{\theta}'_{y3b}\bar{\psi}_{1b}+2c_5c_7c_3(n_2)x^2(s)\bar{\theta}''_{zb}\bar{\psi}_{1b}+\\&-2c_5c_7^2c_1(n_2)x^2(s)\bar{\psi}'_{1b}\bar{\psi}_{1b}-2c_5c_1(n_2)\bar{u}_{1b}\bar{u}'_{1b}-2c_5c_2(n_2)\bar{u}_{1b}\bar{u}'_{3b}-2c_5c_4(n_2)\bar{u}_{1b}\bar{\theta}'_{zb}+\\&+2c_5c_1(n_2)\bar{u}'_{1b}\bar{u}_{3b}+2c_5c_2(n_2)\bar{u}_{3b}\bar{u}'_{3b}+2c_5c_4(n_2)\bar{u}_{3b}\bar{\theta}'_{zb}-2(c_6+c_5c_7)c_1(n_2)\bar{u}'_{1b}\bar{\theta}_{zb}+\\&-2(c_6+c_5c_7)c_2(n_2)\bar{u}'_{3b}\bar{\theta}_{zb}-2(c_6+c_5c_7)c_4(n_2)\bar{\theta}_{zb}\bar{\theta}'_{zb}\Big\}dA_2dz;\end{aligned}$$

$$\bar{\bar{V}}_{gqy}=-\frac{1}{2}\lambda\int_0^L q_y(z)y_{q_y}(z)\left(\bar{\theta}_{zb}\right)^2dz;\qquad \bar{\bar{V}}_{gqz}=-\frac{1}{2}\lambda\int_0^L q_z(z)y_{q_z}(z)\bar{\theta}_{zb}\bar{\theta}_{y1b}dz;$$

$$\bar{\bar{V}}_{gP_{yi}}=-\frac{1}{2}\lambda\sum_{z_i=0,L}P_{yi}y_{Pyi}(z)\left[\bar{\theta}_{zb}(z_i)\right]^2;\qquad \bar{\bar{V}}_{gP_{zi}}=-\frac{1}{2}\lambda\sum_{z_i=0,L}P_{zi}y_{Pzi}(z)\bar{\theta}_{zb}(z_i)\bar{\theta}_{y1b}(z_i);$$

Appendix B: Elastic and geometric stiffness matrices of the two-node element

The elastic and geometric stiffness matrices are defined as

$$\left[\mathbf{K_e}\right]_{16\times16}=\left[\mathbf{K_{en1}}+\mathbf{K_{es1}}+\mathbf{K_{en3}}+\mathbf{K_{es3}}+\mathbf{K_{ezn2}}+\mathbf{K_{esn2}}+\mathbf{K_{esz2}}\right]_{16\times16}$$

$$\left[\mathbf{K_g}\right]_{16\times16}=\left[\mathbf{K_{gN_1}}+\mathbf{K_{gM_x}}+\mathbf{K_{gM_s}}+\mathbf{K_{gQ_1}}+\mathbf{K_{gN_3}}+\mathbf{K_{gQ_2}}-\mathbf{K}_{gqy}-\mathbf{K}_{gqz}-\mathbf{K}_{gP_{yi}}-\mathbf{K}_{gP_{zi}}\right]_{16\times16}$$

in which elastic matrices are

$$\left[\mathbf{K_{en1}}\right]_{16\times16}=E_1\int_0^L\left[\left\{\mathbf{S''_{u1}}\right\}^{\mathbf{T}}_{16\times1}\quad\left\{\mathbf{S'_{\theta1}}\right\}^{\mathbf{T}}_{16\times1}\quad\left\{\mathbf{S''_{\theta z}}\right\}^{\mathbf{T}}_{16\times1}\quad\left\{\mathbf{S'_{\psi1}}\right\}^{\mathbf{T}}_{16\times1}\right]\begin{bmatrix}I_{yyw}&0&0&0\\0&2I_{yyf}&0&0\\0&0&I_{\omega\omega l}&0\\0&0&0&I_{\omega\omega gs}\end{bmatrix}\begin{bmatrix}\left\langle\mathbf{S''_{u1}}\right\rangle_{1\times16}\\\left\langle\mathbf{S'_{\theta1}}\right\rangle_{1\times16}\\\left\langle\mathbf{S''_{\theta z}}\right\rangle_{1\times16}\\\left\langle\mathbf{S'_{\psi1}}\right\rangle_{1\times16}\end{bmatrix}dz$$

$$\left[\mathbf{K_{es1}}\right]_{16\times16}$$

$$=G_1\int_0^L\left[\left\{\mathbf{S'_{u1}}\right\}^{\mathbf{T}}_{16\times1}\quad\left\{\mathbf{S}_{\theta1}\right\}^{\mathbf{T}}_{16\times1}\quad\left\{\mathbf{S'_{\theta z}}\right\}^{\mathbf{T}}_{16\times1}\quad\left\{\mathbf{S}_{\psi1}\right\}^{\mathbf{T}}_{16\times1}\right]\begin{bmatrix}2A_f&-2A_f&0&0\\-2A_f&2A_f&0&0\\0&0&J_1&-h_b^2A_f/2\\0&0&-h_b^2A_f/2&h_b^2A_f/2\end{bmatrix}\begin{bmatrix}\left\langle\mathbf{S'_{u1}}\right\rangle_{1\times16}\\\left\langle\mathbf{S}_{\theta1}\right\rangle_{1\times16}\\\left\langle\mathbf{S'_{\theta z}}\right\rangle_{1\times16}\\\left\langle\mathbf{S}_{\psi1}\right\rangle_{1\times16}\end{bmatrix}dz$$

$$\left[\mathbf{K_{en3}}\right]_{16\times16}=E_3\int_0^L\left[\left\{\mathbf{S'_{\theta3}}\right\}^{\mathbf{T}}_{16\times1}\quad\left\{\mathbf{S''_{\theta z}}\right\}^{\mathbf{T}}_{16\times1}\right]\begin{bmatrix}I_{yyg}&0\\0&I_{\omega\omega g}\end{bmatrix}\begin{bmatrix}\left\langle\mathbf{S'_{\theta3}}\right\rangle_{1\times16}\\\left\langle\mathbf{S''_{\theta z}}\right\rangle_{1\times16}\end{bmatrix}dz$$

$$\left[\mathbf{K_{es3}}\right]_{16\times16}=G_3\int_0^L\left\langle\left\{\mathbf{S'_{u3}}\right\}^{\mathbf{T}}_{16\times1}\quad\left\{\mathbf{S}_{\theta3}\right\}^{\mathbf{T}}_{16\times1}\quad\left\{\mathbf{S'_{\theta z}}\right\}^{\mathbf{T}}_{16\times1}\right\rangle\begin{bmatrix}A_3&-A_3&0\\-A_3&A_3&0\\0&0&J_3\end{bmatrix}\begin{bmatrix}\left\langle\mathbf{S'_{u3}}\right\rangle_{1\times16}\\\left\langle\mathbf{S}_{\theta3}\right\rangle_{1\times16}\\\left\langle\mathbf{S'_{\theta z}}\right\rangle_{1\times16}\end{bmatrix}dz$$

$$\left[\mathbf{K_{ezn2}}\right]_{16\times16}=G_2I_{yya}\int_0^L\left[\left\{\mathbf{S}_{\theta\mathbf{1}}\right\}_{16\times1}\quad\left\{\mathbf{S}_{\theta3}\right\}_{16\times1}\quad\left\{\mathbf{S}'_{\theta z}\right\}_{16\times1}\quad\left\{\mathbf{S}_{\psi\mathbf{1}}\right\}_{16\times1}\right]\times$$

$$\times\begin{bmatrix}c_5^2 & -c_5^2 & -c_5\left(1+c_6\right) & c_5^2c_7\\ -c_5^2 & c_5^2 & c_5\left(1+c_6\right) & -c_5^2c_7\\ -c_5\left(1+c_6\right) & c_5\left(1+c_6\right) & \left(1+c_6\right)^2 & -c_5c_7\left(1+c_6\right)\\ c_5^2c_7 & -c_5^2c_7 & -c_5c_7\left(1+c_6\right) & c_5^2c_7^2\end{bmatrix}\begin{bmatrix}\left\langle\mathbf{S}_{\theta\mathbf{1}}\right\rangle_{1\times16}\\ \left\langle\mathbf{S}_{\theta3}\right\rangle_{1\times16}\\ \left\langle\mathbf{S}'_{\theta z}\right\rangle_{1\times16}\\ \left\langle\mathbf{S}_{\psi\mathbf{1}}\right\rangle_{1\times16}\end{bmatrix}dz$$

$$\left[\mathbf{K_{esn2}}\right]_{16\times16}=G_2A_a\int_0^L\left[\left\{\mathbf{S_{u1}}\right\}_{16\times1}^{\mathbf{T}}\quad\left\{\mathbf{S_{u}}3\right\}_{16\times1}^{\mathbf{T}}\quad\left\{\mathbf{S}_{\theta z}\right\}_{16\times1}^{\mathbf{T}}\right]\times$$

$$\times\begin{bmatrix}c_5^2 & -c_5^2 & c_5\left(1+c_6+c_5c_7\right)\\ -c_5^2 & c_5^2 & -c_5\left(1+c_6+c_5c_7\right)\\ c_5\left(1+c_6+c_5c_7\right) & -c_5\left(1+c_6+c_5c_7\right) & \left(1+c_6+c_5c_7\right)^2\end{bmatrix}\begin{bmatrix}\left\langle\mathbf{S_{u1}}\right\rangle_{1\times16}\\ \left\langle\mathbf{S_{u}}3\right\rangle_{1\times16}\\ \left\langle\mathbf{S}_{\theta z}\right\rangle_{1\times16}\end{bmatrix}dz$$

$$\left[\mathbf{K_{esz2}}\right]_{16\times16}=\frac{G_2A_a}{12}\int_0^L\left[\left\{\mathbf{S'_{u1}}\right\}_{16\times1}^{\mathbf{T}}\quad\left\{\mathbf{S}_{\theta\mathbf{1}}\right\}_{16\times1}^{\mathbf{T}}\quad\left\{\mathbf{S'_{u}}3\right\}_{16\times1}^{\mathbf{T}}\quad\left\{\mathbf{S}_{\theta3}\right\}_{16\times1}^{\mathbf{T}}\quad\left\{\mathbf{S}'_{\theta z}\right\}_{16\times1}^{\mathbf{T}}\quad\left\{\mathbf{S}_{\psi\mathbf{1}}\right\}_{16\times1}^{\mathbf{T}}\right]\times$$

$$\times\begin{bmatrix}4 & -4 & 2 & -2 & 2c_8 & -4c_7\\ -4 & 4 & -2 & 2 & -2c_8 & 4c_7\\ 2 & -2 & 4 & -4 & c_9 & -2c_7\\ -2 & 2 & -4 & 4 & -c_9 & 2c_7\\ 2c_8 & -2c_8 & c_9 & -c_9 & c_{10} & -2c_7c_8\\ -4c_7 & 4c_7 & -2c_7 & 2c_7 & -2c_7c_8 & 4c_7^2\end{bmatrix}\begin{bmatrix}\left\langle\mathbf{S'_{u1}}\right\rangle_{1\times16}\\ \left\langle\mathbf{S}_{\theta\mathbf{1}}\right\rangle_{1\times16}\\ \left\langle\mathbf{S'_{u}}3\right\rangle_{1\times16}\\ \left\langle\mathbf{S}_{\theta3}\right\rangle_{1\times16}\\ \left\langle\mathbf{S}'_{\theta z}\right\rangle_{1\times16}\\ \left\langle\mathbf{S}_{\psi\mathbf{1}}\right\rangle_{1\times16}\end{bmatrix}dz$$

and geometric matrices are

$$\left[\mathbf{K_{gN_1}}\right]_{16\times16}=\int_0^L\left\langle\mathbf{L(z)}\right\rangle_{1\times2}^{\mathbf{T}}\left\{\mathbf{N_{1p}}\right\}_{2\times1}\left[\left\{\mathbf{S'_{u1}}\right\}_{16\times1}^{\mathbf{T}}\left\langle\mathbf{S'_{u1}}\right\rangle_{1\times16}+\frac{\left(I_{xxs}+I_{yys}\right)}{A_s}\left\{\mathbf{S}'_{\theta z}\right\}_{16\times1}^{\mathbf{T}}\left\langle\mathbf{S}'_{\theta z}\right\rangle_{1\times16}\right]dz$$

$$\left[\mathbf{K_{gM}}_x\right]_{16\times16}=\int_0^L\left\langle\mathbf{L(z)}\right\rangle_{1\times2}^{\mathbf{T}}\left\{\mathbf{M}_{x\mathbf{p}}\right\}_{2\times1}\left[\left\langle\mathbf{S'_{u1}}\right\rangle_{16\times1}^{\mathbf{T}}\left\langle\mathbf{S}'_{\theta z}\right\rangle_{1\times16}+\left\langle\mathbf{S}'_{\theta z}\right\rangle_{16\times1}^{\mathbf{T}}\left\langle\mathbf{S'_{u1}}\right\rangle_{1\times16}\right]dz$$

$$\left[\mathbf{K_{gM}}_s\right]_{16\times16}=\frac{2I_{ssf}}{I_{ss}}\int_0^L\left\langle\mathbf{L(z)}\right\rangle_{1\times2}^{\mathbf{T}}\left\{\mathbf{M}_{s\mathbf{p}}\right\}_{2\times1}\left[\left\langle\mathbf{S'_{u1}}\right\rangle_{16\times1}^{\mathbf{T}}\left\langle\mathbf{S}'_{\theta z}\right\rangle_{1\times16}+\left\langle\mathbf{S}'_{\theta z}\right\rangle_{16\times1}^{\mathbf{T}}\left\langle\mathbf{S'_{u1}}\right\rangle_{1\times16}\right]dz$$

$$+\frac{I_{ssg}}{I_{xxg}}\int_0^L\left\langle\mathbf{L(z)}\right\rangle_{1\times2}^{\mathbf{T}}\left\{\mathbf{M}_{s\mathbf{p}}\right\}_{2\times1}\left[\left\langle\mathbf{S'_{u}}3\right\rangle_{16\times1}^{\mathbf{T}}\left\langle\mathbf{S}'_{\theta z}\right\rangle_{1\times16}+\left\langle\mathbf{S}'_{\theta z}\right\rangle_{16\times1}^{\mathbf{T}}\left\langle\mathbf{S'_{u}}3\right\rangle_{1\times16}\right]dz$$

$$\left[\mathbf{K_{gQ_1}}\right]_{16\times16}=-\int_0^L\left\langle\mathbf{L(z)}\right\rangle_{1\times2}^{\mathbf{T}}\left\{\mathbf{Q_{1p}}\right\}_{2\times1}\left[\left\{\mathbf{S'_{u1}}\right\}_{16\times1}^{\mathbf{T}}\left\langle\mathbf{S}_{\theta z}\right\rangle_{1\times16}+\frac{I_{yyw}}{A_w}\left\{\mathbf{S''_{u1}}\right\}_{16\times1}^{\mathbf{T}}\left\langle\mathbf{S}'_{\theta z}\right\rangle_{1\times16}\right]dz$$

$$-\int_0^L\left\langle\mathbf{L(z)}\right\rangle_{1\times2}^{\mathbf{T}}\left\{\mathbf{Q_{1p}}\right\}_{2\times1}\left[\left\{\mathbf{S}_{\theta z}\right\}_{16\times1}^{\mathbf{T}}\left\langle\mathbf{S'_{u1}}\right\rangle_{1\times16}+\frac{I_{yyw}}{A_w}\left\{\mathbf{S}'_{\theta z}\right\}_{16\times1}^{\mathbf{T}}\left\langle\mathbf{S''_{u1}}\right\rangle_{1\times16}\right]dz$$

$$\left[\mathbf{K_{gN_3}}\right]_{16\times16}=\int_0^L\left\langle\mathbf{L(z)}\right\rangle_{1\times2}^{\mathbf{T}}\left\{\mathbf{N_{3p}}\right\}_{2\times1}\left[\left\{\mathbf{S'_{u}}3\right\}_{16\times1}^{\mathbf{T}}\left\langle\mathbf{S'_{u}}3\right\rangle_{1\times16}+\frac{I_{xxg}+I_{yyg}}{A_g}\left\{\mathbf{S}'_{\theta z}\right\}_{16\times1}^{\mathbf{T}}\left\langle\mathbf{S}'_{\theta z}\right\rangle_{1\times16}\right]dz$$

$$\left[\mathbf{K}_{\mathbf{gQ_2}}\right]_{16\times16}=\frac{\lambda}{2}\int_0^L\left\langle\mathbf{L(z)}\right\rangle_{1\times2}^{\mathbf{T}}\left\{\mathbf{Q_{2p}}\right\}_{2\times1}\left\{\left[\left\{\mathbf{S_{u1}}\right\}_{16\times1}^{\mathbf{T}}\;\middle|\;\left\{\mathbf{S}_{\theta\mathbf{1}}\right\}_{16\times1}^{\mathbf{T}}\;\middle|\;\left\{\mathbf{S_{u3}}\right\}_{16\times1}^{\mathbf{T}}\;\middle|\;\left\{\mathbf{S}_{\theta3}\right\}_{16\times1}^{\mathbf{T}}\;\middle|\;\left\{\mathbf{S}_{\theta z}\right\}_{16\times1}^{\mathbf{T}}\;\middle|\;\left\{\mathbf{S}'_{\theta z}\right\}_{16\times1}^{\mathbf{T}}\;\middle|\;\left\{\mathbf{S}_{\psi\mathbf{1}}\right\}_{16\times1}^{\mathbf{T}}\right]\times\right.$$

$$\times\begin{bmatrix}-c_5&0&-c_5&0&-c_5c_{12}&0&0\\0&-c_5\alpha_a&0&-c_5\alpha_a&0&c_5c_{11}\alpha_a&-c_5c_7\alpha_a\\c_5&0&c_5&0&c_5c_{12}&0&0\\0&c_5\alpha_a&0&c_5\alpha_a&0&-c_5c_{11}\alpha_a&c_5c_7\alpha_a\\-\left(c_6+c_5c_7\right)&0&-\left(c_6+c_5c_7\right)&0&-\left(c_6+c_5c_7\right)c_{12}&0&0\\0&c_6\alpha_a&0&c_6\alpha_a&0&-c_6c_{11}\alpha_a&c_6c_7\alpha_a\\0&-c_5c_7\alpha_a&0&-c_5c_7\alpha_a&0&c_5c_7c_{11}\alpha_a&-c_5c_7^2\alpha_a\end{bmatrix}\begin{bmatrix}\left\langle\mathbf{S'_{u1}}\right\rangle_{1\times16}\\\left\langle\mathbf{S}'_{\theta\mathbf{1}}\right\rangle_{1\times16}\\\left\langle\mathbf{S'_{u3}}\right\rangle_{1\times16}\\\left\langle\mathbf{S}'_{\theta3}\right\rangle_{1\times16}\\\left\langle\mathbf{S}'_{\theta z}\right\rangle_{1\times16}\\\left\langle\mathbf{S}''_{\theta z}\right\rangle_{1\times16}\\\left\langle\mathbf{S}'_{\psi\mathbf{1}}\right\rangle_{1\times16}\end{bmatrix}+$$

$$\left.+\left\langle\mathbf{L(z)}\right\rangle_{1\times2}^{\mathbf{T}}\left\{\mathbf{Q_{2p}}\right\}_{2\times1}\left\{\left[\left\{\mathbf{S'_{u1}}\right\}_{16\times1}^{\mathbf{T}}\;\middle|\;\left\{\mathbf{S}'_{\theta\mathbf{1}}\right\}_{16\times1}^{\mathbf{T}}\;\middle|\;\left\{\mathbf{S'_{u3}}\right\}_{16\times1}^{\mathbf{T}}\;\middle|\;\left\{\mathbf{S}'_{\theta3}\right\}_{16\times1}^{\mathbf{T}}\;\middle|\;\left\{\mathbf{S}'_{\theta z}\right\}_{16\times1}^{\mathbf{T}}\;\middle|\;\left\{\mathbf{S}''_{\theta z}\right\}_{16\times1}^{\mathbf{T}}\;\middle|\;\left\{\mathbf{S}'_{\psi\mathbf{1}}\right\}_{16\times1}^{\mathbf{T}}\right]\times\right.$$

$$\times\begin{bmatrix}-c_5&0&c_5&0&-\left(c_6+c_5c_7\right)&0&0\\0&-c_5\alpha_a&0&c_5\alpha_a&0&c_6\alpha_a&-c_5c_7\alpha_a\\-c_5&0&c_5&0&-\left(c_6+c_5c_7\right)&0&0\\0&-c_5\alpha_a&0&c_5\alpha_a&0&c_6\alpha_a&-c_5c_7\alpha_a\\-c_5c_{12}&0&c_5c_{12}&0&-\left(c_6+c_5c_7\right)c_{12}&0&0\\0&c_5c_{11}\alpha_a&0&-c_5c_{11}\alpha_a&0&-c_6c_{11}\alpha_a&c_5c_7c_{11}\alpha_a\\0&-c_5c_7\alpha_a&0&c_5c_7\alpha_a&0&c_6c_7\alpha_a&-c_5c_7^2\alpha_a\end{bmatrix}\begin{bmatrix}\left\langle\mathbf{S_{u1}}\right\rangle_{1\times16}\\\left\langle\mathbf{S}_{\theta\mathbf{1}}\right\rangle_{1\times16}\\\left\langle\mathbf{S_{u3}}\right\rangle_{1\times16}\\\left\langle\mathbf{S}_{\theta3}\right\rangle_{1\times16}\\\left\langle\mathbf{S}_{\theta z}\right\rangle_{1\times16}\\\left\langle\mathbf{S}'_{\theta z}\right\rangle_{1\times16}\\\left\langle\mathbf{S}_{\psi\mathbf{1}}\right\rangle_{1\times16}\end{bmatrix}dz$$

$$\left[\mathbf{K}_{gqy}\right]_{16\times16}=\frac{1}{2}\int_0^L q_y(z)\,y_{q_y}(z)\left\{\mathbf{S}_{\theta z}\right\}_{16\times1}^{\mathbf{T}}\left\langle\mathbf{S}_{\theta z}\right\rangle_{1\times16}dz;\left[\mathbf{K}_{gP_{yi}}\right]_{16\times16}=\frac{1}{2}\sum_{z_i=0,L}P_{yi}y_i(z_i)\left\{\mathbf{S}_{\theta z}(z_i)\right\}_{16\times1}^{\mathbf{T}}\left\langle\mathbf{S}_{\theta z}(z_i)\right\rangle_{1\times16};$$

$$\left[\mathbf{K}_{gqz}\right]_{16\times16}=\frac{1}{4}\int_0^L q_z(z)\,y_{q_z}(z)\left\{\mathbf{S}_{\theta z}\right\}_{16\times1}^{\mathbf{T}}\left\langle\mathbf{S}_{\theta1}\right\rangle_{1\times16}dz+\frac{1}{4}\int_0^L q_z(z)\,y_{q_z}(z)\left\{\mathbf{S}_{\theta1}\right\}_{16\times1}^{\mathbf{T}}\left\langle\mathbf{S}_{\theta z}\right\rangle_{1\times16}dz;$$

and

$$\left[\mathbf{K}_{gP_{zi}}\right]_{16\times16}=\frac{1}{4}\sum_{z_i=0,L}P_{zi}y_i(z_i)\left\{\mathbf{S}_{\theta z}(z_i)\right\}_{16\times1}^{\mathbf{T}}\left\langle\mathbf{S}_{\theta1}(z_i)\right\rangle_{1\times16}+\frac{1}{4}\sum_{z_i=0,L}P_{zi}y_i(z_i)\left\{\mathbf{S}_{\theta1}(z_i)\right\}_{16\times1}^{\mathbf{T}}\left\langle\mathbf{S}_{\theta z}(z_i)\right\rangle_{1\times16};$$

Appendix C: Elastic and geometric stiffness matrices of the three-node element

The elastic and geometric stiffness matrices are given by

$$\left[\hat{\mathbf{K}}_{\mathbf{e}}\right]_{14\times14}=\left[\hat{\mathbf{K}}_{\mathbf{en1}}+\hat{\mathbf{K}}_{\mathbf{es1}}+\hat{\mathbf{K}}_{\mathbf{en3}}+\hat{\mathbf{K}}_{\mathbf{es3}}+\hat{\mathbf{K}}_{\mathbf{ezn2}}+\hat{\mathbf{K}}_{\mathbf{esn2}}+\hat{\mathbf{K}}_{\mathbf{esz2}}\right]_{14\times14}$$

$$\left[\hat{\mathbf{K}}_{\mathbf{g}}\right]_{14\times14}=\left[\hat{\mathbf{K}}_{\mathbf{gN_1}}+\hat{\mathbf{K}}_{\mathbf{gM}_x}+\hat{\mathbf{K}}_{\mathbf{gM}_s}+\hat{\mathbf{K}}_{\mathbf{gQ_1}}+\hat{\mathbf{K}}_{\mathbf{gN_3}}+\hat{\mathbf{K}}_{\mathbf{gQ_2}}-\hat{\mathbf{K}}_{gqy}-\hat{\mathbf{K}}_{gqz}-\hat{\mathbf{K}}_{gP_{yi}}-\hat{\mathbf{K}}_{gP_{zi}}\right]_{14\times14}$$

in which the elastic stiffness matrices are

$$\left[\hat{\mathbf{K}}_{\mathbf{en1}}\right]=E_1\int_0^L\left[\left\{\hat{\mathbf{S}}''_{\mathbf{u1}}\right\}_{14\times1}^{\mathbf{T}}\quad\left\{\hat{\mathbf{S}}'_{\theta\mathbf{1}}\right\}_{14\times1}^{\mathbf{T}}\quad\left\{\hat{\mathbf{S}}''_{\theta z}\right\}_{14\times1}^{\mathbf{T}}\quad\left\{\hat{\mathbf{S}}'_{\psi\mathbf{1}}\right\}_{14\times1}^{\mathbf{T}}\right]\begin{bmatrix}I_{yyw}&0&0&0\\0&2I_{yyf}&0&0\\0&0&I_{\omega\omega l}&0\\0&0&0&I_{\omega\omega gs}\end{bmatrix}\begin{bmatrix}\left\langle\hat{\mathbf{S}}''_{\mathbf{u1}}\right\rangle_{1\times14}\\\left\langle\hat{\mathbf{S}}'_{\theta\mathbf{1}}\right\rangle_{1\times14}\\\left\langle\hat{\mathbf{S}}''_{\theta z}\right\rangle_{1\times14}\\\left\langle\hat{\mathbf{S}}'_{\psi\mathbf{1}}\right\rangle_{1\times14}\end{bmatrix}dz$$

$$\left[\hat{\mathbf{K}}_{\mathbf{es1}}\right]=G_1\int_0^L\left[\left\{\hat{\mathbf{S}}'_{\mathbf{u1}}\right\}_{14\times1}^{\mathbf{T}}\quad\left\{\hat{\mathbf{S}}_{\theta\mathbf{1}}\right\}_{14\times1}^{\mathbf{T}}\quad\left\{\hat{\mathbf{S}}'_{\theta z}\right\}_{14\times1}^{\mathbf{T}}\quad\left\{\hat{\mathbf{S}}_{\psi\mathbf{1}}\right\}_{14\times1}^{\mathbf{T}}\right]\begin{bmatrix}2A_f&-2A_f&0&0\\-2A_f&2A_f&0&0\\0&0&J_1&-h_b^2A_f/2\\0&0&-h_b^2A_f/2&h_b^2A_f/2\end{bmatrix}\begin{bmatrix}\left\langle\hat{\mathbf{S}}'_{\mathbf{u1}}\right\rangle_{1\times14}\\\left\langle\hat{\mathbf{S}}_{\theta\mathbf{1}}\right\rangle_{1\times14}\\\left\langle\hat{\mathbf{S}}'_{\theta z}\right\rangle_{1\times14}\\\left\langle\hat{\mathbf{S}}_{\psi\mathbf{1}}\right\rangle_{1\times14}\end{bmatrix}dz$$

$$\left[\hat{\mathbf{K}}_{\mathbf{en3}}\right]=E_3\int_0^L\left[\left\{\hat{\mathbf{S}}'_{\theta3}\right\}_{14\times1}^{\mathbf{T}}\quad\left\{\hat{\mathbf{S}}''_{\theta z}\right\}_{14\times1}^{\mathbf{T}}\right]\begin{bmatrix}I_{yyg}&0\\0&I_{\omega\omega g}\end{bmatrix}\begin{bmatrix}\left\langle\hat{\mathbf{S}}'_{\theta3}\right\rangle_{1\times14}\\\left\langle\hat{\mathbf{S}}''_{\theta z}\right\rangle_{1\times14}\end{bmatrix}dz$$

$$\left[\hat{\mathbf{K}}_{\mathbf{es3}}\right]=G_3\int_0^L\left\langle\left\{\hat{\mathbf{S}}'_{\mathbf{u}3}\right\}_{14\times1}^{\mathbf{T}}\quad\left\{\hat{\mathbf{S}}_{\theta3}\right\}_{14\times1}^{\mathbf{T}}\quad\left\{\hat{\mathbf{S}}'_{\theta z}\right\}_{14\times1}^{\mathbf{T}}\right\rangle\begin{bmatrix}A_3&-A_3&0\\-A_3&A_3&0\\0&0&J_3\end{bmatrix}\begin{bmatrix}\left\langle\hat{\mathbf{S}}'_{\mathbf{u}3}\right\rangle_{1\times14}\\\left\langle\hat{\mathbf{S}}_{\theta3}\right\rangle_{1\times14}\\\left\langle\hat{\mathbf{S}}'_{\theta z}\right\rangle_{1\times14}\end{bmatrix}dz$$

$$\left[\hat{\mathbf{K}}_{\mathbf{ezn2}}\right]=G_2I_{yya}\int_0^L\left[\left\{\hat{\mathbf{S}}_{\theta\mathbf{1}}\right\}_{14\times1}\quad\left\{\hat{\mathbf{S}}_{\theta3}\right\}_{14\times1}\quad\left\{\hat{\mathbf{S}}'_{\theta z}\right\}_{14\times1}\quad\left\{\hat{\mathbf{S}}_{\psi\mathbf{1}}\right\}_{14\times1}\right]$$
$$\times\begin{bmatrix}c_5^2&-c_5^2&-c_5(1+c_6)&c_5^2c_7\\-c_5^2&c_5^2&c_5(1+c_6)&-c_5^2c_7\\-c_5(1+c_6)&c_5(1+c_6)&(1+c_6)^2&-c_5c_7(1+c_6)\\c_5^2c_7&-c_5^2c_7&-c_5c_7(1+c_6)&c_5^2c_7^2\end{bmatrix}\begin{bmatrix}\left\langle\hat{\mathbf{S}}_{\theta\mathbf{1}}\right\rangle_{1\times14}\\\left\langle\hat{\mathbf{S}}_{\theta3}\right\rangle_{1\times14}\\\left\langle\hat{\mathbf{S}}'_{\theta z}\right\rangle_{1\times14}\\\left\langle\hat{\mathbf{S}}_{\psi\mathbf{1}}\right\rangle_{1\times14}\end{bmatrix}dz$$

$$\left[\hat{\mathbf{K}}_{\mathbf{esn2}}\right]=G_2A_a\int_0^L\left[\left\{\hat{\mathbf{S}}_{\mathbf{u1}}\right\}_{14\times1}^{\mathbf{T}}\quad\left\{\hat{\mathbf{S}}_{\mathbf{u}3}\right\}_{14\times1}^{\mathbf{T}}\quad\left\{\hat{\mathbf{S}}_{\theta z}\right\}_{14\times1}^{\mathbf{T}}\right]$$
$$\times\begin{bmatrix}c_5^2&-c_5^2&c_5(1+c_6+c_5c_7)\\-c_5^2&c_5^2&-c_5(1+c_6+c_5c_7)\\c_5(1+c_6+c_5c_7)&-c_5(1+c_6+c_5c_7)&(1+c_6+c_5c_7)^2\end{bmatrix}\begin{bmatrix}\left\langle\hat{\mathbf{S}}_{\mathbf{u1}}\right\rangle_{1\times14}\\\left\langle\hat{\mathbf{S}}_{\mathbf{u}3}\right\rangle_{1\times14}\\\left\langle\hat{\mathbf{S}}_{\theta z}\right\rangle_{1\times14}\end{bmatrix}dz$$

$$\left[\hat{\mathbf{K}}_{\mathbf{esz2}}\right]=\frac{G_2A_a}{12}\int_0^L\left[\left\{\hat{\mathbf{S}}'_{\mathbf{u1}}\right\}_{14\times1}^{\mathbf{T}}\quad\left\{\hat{\mathbf{S}}_{\theta\mathbf{1}}\right\}_{14\times1}^{\mathbf{T}}\quad\left\{\hat{\mathbf{S}}'_{\mathbf{u}3}\right\}_{14\times1}^{\mathbf{T}}\quad\left\{\hat{\mathbf{S}}_{\theta3}\right\}_{14\times1}^{\mathbf{T}}\quad\left\{\hat{\mathbf{S}}'_{\theta z}\right\}_{14\times1}^{\mathbf{T}}\quad\left\{\hat{\mathbf{S}}_{\psi\mathbf{1}}\right\}_{14\times1}^{\mathbf{T}}\right]$$
$$\times\begin{bmatrix}4&-4&2&-2&2c_8&-4c_7\\-4&4&-2&2&-2c_8&4c_7\\2&-2&4&-4&c_9&-2c_7\\-2&2&-4&4&-c_9&2c_7\\2c_8&-2c_8&c_9&-c_9&c_{10}&-2c_7c_8\\-4c_7&4c_7&-2c_7&2c_7&-2c_7c_8&4c_7^2\end{bmatrix}\begin{bmatrix}\left\langle\hat{\mathbf{S}}'_{\mathbf{u1}}\right\rangle_{1\times14}\\\left\langle\hat{\mathbf{S}}_{\theta\mathbf{1}}\right\rangle_{1\times14}\\\left\langle\hat{\mathbf{S}}'_{\mathbf{u}3}\right\rangle_{1\times14}\\\left\langle\hat{\mathbf{S}}_{\theta3}\right\rangle_{1\times14}\\\left\langle\hat{\mathbf{S}}'_{\theta z}\right\rangle_{1\times14}\\\left\langle\hat{\mathbf{S}}_{\psi\mathbf{1}}\right\rangle_{1\times14}\end{bmatrix}dz$$

and the geometric stiffness matrices include

$$\left[\hat{\mathbf{K}}_{\mathbf{gN_1}}\right]=\int_0^L\left\langle\mathbf{L}(\mathbf{z})\right\rangle_{1\times2}^{\mathbf{T}}\left\{\mathbf{N_{1p}}\right\}_{2\times1}\left[\left\{\hat{\mathbf{S}}'_{\mathbf{u1}}\right\}_{14\times1}^{\mathbf{T}}\left\langle\hat{\mathbf{S}}'_{\mathbf{u1}}\right\rangle_{1\times14}+\frac{\left(I_{xxs}+I_{yys}\right)}{A_s}\left\{\hat{\mathbf{S}}'_{\theta z}\right\}_{14\times1}^{\mathbf{T}}\left\langle\hat{\mathbf{S}}'_{\theta z}\right\rangle_{1\times14}\right]dz$$

$$\left[\hat{\mathbf{K}}_{\mathbf{gQ_2}}\right]=\frac{\lambda}{2}\int_0^L\left\langle\mathbf{L}(\mathbf{z})\right\rangle_{1\times2}^{\mathbf{T}}\left\{\mathbf{Q_{2p}}\right\}_{2\times1}\left\{\left[\left\{\hat{\mathbf{S}}_{\mathbf{u1}}\right\}_{14\times1}^{\mathbf{T}}\middle|\left\{\hat{\mathbf{S}}_{\theta\mathbf{1}}\right\}_{14\times1}^{\mathbf{T}}\middle|\left\{\hat{\mathbf{S}}_{\mathbf{u3}}\right\}_{14\times1}^{\mathbf{T}}\middle|\left\{\hat{\mathbf{S}}_{\theta3}\right\}_{14\times1}^{\mathbf{T}}\middle|\left\{\mathbf{S}_{\theta z}\right\}_{14\times1}^{\mathbf{T}}\middle|\left\{\hat{\mathbf{S}}'_{\theta z}\right\}_{14\times1}^{\mathbf{T}}\middle|\left\{\hat{\mathbf{S}}_{\psi\mathbf{1}}\right\}_{14\times1}^{\mathbf{T}}\right]\times\right.$$

$$\times\begin{bmatrix}-c_5 & 0 & -c_5 & 0 & -c_5c_{12} & 0 & 0\\ 0 & -c_5\alpha_a & 0 & -c_5\alpha_a & 0 & c_5c_{11}\alpha_a & -c_5c_7\alpha_a\\ c_5 & 0 & c_5 & 0 & c_5c_{12} & 0 & 0\\ 0 & c_5\alpha_a & 0 & c_5\alpha_a & 0 & -c_5c_{11}\alpha_a & c_5c_7\alpha_a\\ -\left(c_6+c_5c_7\right) & 0 & -\left(c_6+c_5c_7\right) & 0 & -\left(c_6+c_5c_7\right)c_{12} & 0 & 0\\ 0 & c_6\alpha_a & 0 & c_6\alpha_a & 0 & -c_6c_{11}\alpha_a & c_6c_7\alpha_a\\ 0 & -c_5c_7\alpha_a & 0 & -c_5c_7\alpha_a & 0 & c_5c_7c_{11}\alpha_a & -c_5c_7^2\alpha_a\end{bmatrix}\begin{bmatrix}\left\langle\hat{\mathbf{S}}'_{\mathbf{u1}}\right\rangle_{1\times14}\\ \left\langle\hat{\mathbf{S}}'_{\theta\mathbf{1}}\right\rangle_{1\times14}\\ \left\langle\hat{\mathbf{S}}'_{\mathbf{u3}}\right\rangle_{1\times14}\\ \left\langle\hat{\mathbf{S}}'_{\theta3}\right\rangle_{1\times14}\\ \left\langle\hat{\mathbf{S}}'_{\theta z}\right\rangle_{1\times14}\\ \left\langle\hat{\mathbf{S}}''_{\theta z}\right\rangle_{1\times14}\\ \left\langle\hat{\mathbf{S}}'_{\psi\mathbf{1}}\right\rangle_{1\times14}\end{bmatrix}+$$

$$\left.+\left\langle\mathbf{L}(\mathbf{z})\right\rangle_{1\times2}^{\mathbf{T}}\left\{\mathbf{Q_{2p}}\right\}_{2\times1}\left\{\left[\left\{\hat{\mathbf{S}}'_{\mathbf{u1}}\right\}_{14\times1}^{\mathbf{T}}\middle|\left\{\hat{\mathbf{S}}'_{\theta\mathbf{1}}\right\}_{14\times1}^{\mathbf{T}}\middle|\left\{\hat{\mathbf{S}}'_{\mathbf{u3}}\right\}_{14\times1}^{\mathbf{T}}\middle|\left\{\hat{\mathbf{S}}'_{\theta3}\right\}_{14\times1}^{\mathbf{T}}\middle|\left\{\hat{\mathbf{S}}'_{\theta z}\right\}_{14\times1}^{\mathbf{T}}\middle|\left\{\hat{\mathbf{S}}''_{\theta z}\right\}_{14\times1}^{\mathbf{T}}\middle|\left\{\mathbf{S}'_{\psi\mathbf{1}}\right\}_{14\times1}^{\mathbf{T}}\right]\times\right.$$

$$\times\begin{bmatrix}-c_5 & 0 & c_5 & 0 & -\left(c_6+c_5c_7\right) & 0 & 0\\ 0 & -c_5\alpha_a & 0 & c_5\alpha_a & 0 & c_6\alpha_a & -c_5c_7\alpha_a\\ -c_5 & 0 & c_5 & 0 & -\left(c_6+c_5c_7\right) & 0 & 0\\ 0 & -c_5\alpha_a & 0 & c_5\alpha_a & 0 & c_6\alpha_a & -c_5c_7\alpha_a\\ -c_5c_{12} & 0 & c_5c_{12} & 0 & -\left(c_6+c_5c_7\right)c_{12} & 0 & 0\\ 0 & c_5c_{11}\alpha_a & 0 & -c_5c_{11}\alpha_a & 0 & -c_6c_{11}\alpha_a & c_5c_7c_{11}\alpha_a\\ 0 & -c_5c_7\alpha_a & 0 & c_5c_7\alpha_a & 0 & c_6c_7\alpha_a & -c_5c_7^2\alpha_a\end{bmatrix}\begin{bmatrix}\left\langle\hat{\mathbf{S}}_{\mathbf{u1}}\right\rangle_{1\times14}\\ \left\langle\hat{\mathbf{S}}_{\theta\mathbf{1}}\right\rangle_{1\times14}\\ \left\langle\hat{\mathbf{S}}_{\mathbf{u3}}\right\rangle_{1\times14}\\ \left\langle\hat{\mathbf{S}}_{\theta3}\right\rangle_{1\times14}\\ \left\langle\hat{\mathbf{S}}_{\theta z}\right\rangle_{1\times14}\\ \left\langle\hat{\mathbf{S}}'_{\theta z}\right\rangle_{1\times14}\\ \left\langle\hat{\mathbf{S}}_{\psi\mathbf{1}}\right\rangle_{1\times14}\end{bmatrix}dz$$

$$\left[\hat{\mathbf{K}}_{\mathbf{gM}_x}\right]=\int_0^L\left\langle\mathbf{L}(\mathbf{z})\right\rangle_{1\times2}^{\mathbf{T}}\left\{\mathbf{M}_{x\mathbf{p}}\right\}_{2\times1}\left[\left\langle\hat{\mathbf{S}}'_{\mathbf{u1}}\right\rangle_{14\times1}^{\mathbf{T}}\left\langle\hat{\mathbf{S}}'_{\theta z}\right\rangle_{1\times14}+\left\langle\hat{\mathbf{S}}'_{\theta z}\right\rangle_{14\times1}^{\mathbf{T}}\left\langle\hat{\mathbf{S}}'_{\mathbf{u1}}\right\rangle_{1\times14}\right]dz$$

$$\left[\hat{\mathbf{K}}_{\mathbf{gM}_s}\right]=\frac{2I_{ssf}}{I_{ss}}\int_0^L\left\langle\mathbf{L}(\mathbf{z})\right\rangle_{1\times2}^{\mathbf{T}}\left\{\mathbf{M}_{s\mathbf{p}}\right\}_{2\times1}\left[\left\langle\hat{\mathbf{S}}'_{\mathbf{u1}}\right\rangle_{14\times1}^{\mathbf{T}}\left\langle\hat{\mathbf{S}}'_{\theta z}\right\rangle_{1\times14}+\left\langle\hat{\mathbf{S}}'_{\theta z}\right\rangle_{14\times1}^{\mathbf{T}}\left\langle\hat{\mathbf{S}}'_{\mathbf{u1}}\right\rangle_{1\times14}\right]dz$$

$$+\frac{I_{ssg}}{I_{xxg}}\int_0^L\left\langle\mathbf{L}(\mathbf{z})\right\rangle_{1\times2}^{\mathbf{T}}\left\{\mathbf{M}_{s\mathbf{p}}\right\}_{2\times1}\left[\left\langle\hat{\mathbf{S}}'_{\mathbf{u3}}\right\rangle_{14\times1}^{\mathbf{T}}\left\langle\hat{\mathbf{S}}'_{\theta z}\right\rangle_{1\times14}+\left\langle\hat{\mathbf{S}}'_{\theta z}\right\rangle_{14\times1}^{\mathbf{T}}\left\langle\hat{\mathbf{S}}'_{\mathbf{u3}}\right\rangle_{1\times14}\right]dz$$

$$\left[\hat{\mathbf{K}}_{\mathbf{gQ_1}}\right]=-\int_0^L\left\langle\mathbf{L}(\mathbf{z})\right\rangle_{1\times2}^{\mathbf{T}}\left\{\mathbf{Q_{1p}}\right\}_{2\times1}\left[\left\{\hat{\mathbf{S}}'_{\mathbf{u1}}\right\}_{14\times1}^{\mathbf{T}}\left\langle\hat{\mathbf{S}}_{\theta z}\right\rangle_{1\times14}+\frac{I_{yyw}}{A_w}\left\{\hat{\mathbf{S}}''_{\mathbf{u1}}\right\}_{14\times1}^{\mathbf{T}}\left\langle\hat{\mathbf{S}}'_{\theta z}\right\rangle_{1\times14}\right]dz$$

$$-\int_0^L\left\langle\mathbf{L}(\mathbf{z})\right\rangle_{1\times2}^{\mathbf{T}}\left\{\mathbf{Q_{1p}}\right\}_{2\times1}\left[\left\{\hat{\mathbf{S}}_{\theta z}\right\}_{14\times1}^{\mathbf{T}}\left\langle\hat{\mathbf{S}}'_{\mathbf{u1}}\right\rangle_{1\times14}+\frac{I_{yyw}}{A_w}\left\{\hat{\mathbf{S}}'_{\theta z}\right\}_{14\times1}^{\mathbf{T}}\left\langle\hat{\mathbf{S}}''_{\mathbf{u1}}\right\rangle_{1\times14}\right]dz$$

$$\left[\hat{\mathbf{K}}_{\mathbf{gN_3}}\right]=\int_0^L\left\langle\mathbf{L}(\mathbf{z})\right\rangle_{1\times2}^{\mathbf{T}}\left\{\mathbf{N_{3p}}\right\}_{2\times1}\left[\left\{\hat{\mathbf{S}}'_{\mathbf{u3}}\right\}_{14\times1}^{\mathbf{T}}\left\langle\hat{\mathbf{S}}'_{\mathbf{u3}}\right\rangle_{1\times14}+\frac{I_{xxg}+I_{yyg}}{A_g}\left\{\hat{\mathbf{S}}'_{\theta z}\right\}_{14\times1}^{\mathbf{T}}\left\langle\hat{\mathbf{S}}'_{\theta z}\right\rangle_{1\times14}\right]dz$$

$$\left[\hat{\mathbf{K}}_{gqy}\right]=\frac{1}{2}\int_0^L q_y(z)\,y_{q_y}(z)\left\{\hat{\mathbf{S}}_{\theta z}\right\}_{14\times1}^{\mathbf{T}}\left\langle\hat{\mathbf{S}}_{\theta z}\right\rangle_{1\times14}dz;\left[\hat{\mathbf{K}}_{gP_{yi}}\right]_{16\times16}=\frac{1}{2}\sum_{z_i=0,L}P_{yi}y_i(z_i)\left\{\hat{\mathbf{S}}_{\theta z}(z_i)\right\}_{14\times1}^{\mathbf{T}}\left\langle\hat{\mathbf{S}}_{\theta z}(z_i)\right\rangle_{1\times14};$$

$$\left[\hat{\mathbf{K}}_{gqz}\right]=\frac{1}{4}\int_0^L q_z(z)\,y_{q_z}(z)\left\{\hat{\mathbf{S}}_{\theta z}\right\}_{14\times1}^{\mathbf{T}}\left\langle\hat{\mathbf{S}}_{\theta1}\right\rangle_{1\times14}dz+\frac{1}{4}\int_0^L q_z(z)\,y_{q_z}(z)\left\{\hat{\mathbf{S}}_{\theta1}\right\}_{14\times1}^{\mathbf{T}}\left\langle\hat{\mathbf{S}}_{\theta z}\right\rangle_{1\times14}dz;$$

and

$$\left[\hat{\mathbf{K}}_{gP_{zi}}\right]=\frac{1}{4}\sum_{z_i=0,L}P_{zi}y_i(z_i)\left\{\hat{\mathbf{S}}_{\theta z}(z_i)\right\}_{14\times1}^{\mathbf{T}}\left\langle\hat{\mathbf{S}}_{\theta1}(z_i)\right\rangle_{1\times14}+\frac{1}{4}\sum_{z_i=0,L}P_{zi}y_i(z_i)\left\{\hat{\mathbf{S}}_{\theta1}(z_i)\right\}_{14\times1}^{\mathbf{T}}\left\langle\hat{\mathbf{S}}_{\theta z}(z_i)\right\rangle_{1\times14};$$

References

[1] El Damatty, A., Abushagur, M. and Youssef, M. A., Experimental and analytical investigation of steel beams rehabilitated using GFRP sheets, J. Steel &Composite Structures 3 (2003) 421-438.

[2] Liu, Y. and Gannon, L., Finite element study of steel beam reinforced while under load, Engineering Structures, 31 (2009) 2630-2642.

[3] Miller, C.T., Chajes J.M. and Hastings N.J., Strengthening of a steel bridge girder using CFRP plates, Journal of Bridge Engineering 6 (2001) 514-522.

[4] Shaat, A., and Fam, A., Slender Steel Columns Strengthened Using High Modulus CFRP Plates for Buckling Control, Journal of Composites for Construction, 13 (2009) 2-12.

[5] Accord, E., and Earls, C.J., Use of fiber-reinforced polymer composite elements to enhance structural steel member ductility, J. of composites for construction ASCE, 10 (2006) 337-344.

[6] Aguilera, J. and Fam, A., Bonded FRP plates for strengthening rectangular hollow steel section T-joints against web buckling induced by transverse compression, Journal of composites for constructions ASCE, 17 (2013) 421-432.

[7] Youssef, M., Analytical Prediction of the Linear and Nonlinear Behaviour of Steel Beams Rehabilitated using FRP Sheets. Engineering Structures, 28 (2006) 903-911.

[8] Harries, K.A., Peck A.J., Abraham, E.J., Enhancing stability of structural steel sections using FRP, Thin-walled structures, 47 (2009) 2092-1101.

[9] Aydin E. and Aktas, M. Obtaining a permanent repair by using GFRP in steel plates reformed by heat-treatment, Thin-Walled Structures, 94 (2015) 13-22.

[10] Siddique, M.A.A. and El Damatty, A.A. Improvement of local buckling behaviour of steel beams through bonding GFRP plates, Composite Structures, 96 (2013) 44-56.

[11] Zaghian, S., Buckling analysis of steel plates reinforced with GFRP, Master of Science thesis, University of Ottawa (2015).

[12] Girhammar, U.A. and Pan, D.H., Exact static analysis of partially composite beams and beam-columns, International Journal of Mechanical Sciences, 49 (2007) 239-255.

[13] Xu, R., and Wu Y., Static, dynamic, and buckling analysis of partial interaction composite members using Timoshenko's beam theory, Int. J. of mechanical sciences, 49 (2007) 1139-1155.
[14]Challamel,N. and Girhammar,U.A., Lateral-torsional buckling of vertically layered composite beams with interlayer slip under uniform moment, Engineering Structures, 34 (2012) 505-513.
[15] Erkmen, R.E., and Mohareb, M., Buckling analysis of thin-walled open structures – A finite element formulation, Thin-walled structures, 46 (2008) 618-636.
[16] Wu, L., and Mohareb, M., Buckling of shear deformable thin-walled members —I. Variational principle and analytical solutions. Thin-walled Structures, 49 (2011) 197 –207.
[17] Wu, L., and Mohareb, M., Buckling formulation for shear deformable thin-walled members— II. Finite element formulation. Thin-walled Structures, 49 (2011) 208 –222.
[18] Sahraei, A., Wu, L., and Mohareb, M., Finite element formulation for lateral torsional buckling analysis of shear deformable mono-symmetric thin-walled members, Thin-walled structures, 89 (2015) 212-226.
[19] Sahraei, A., and Mohareb, M., Upper and lower bound solutions for lateral-torsional buckling of double symmetric members, Thin-walled structures, 102 (2016) 180-196.
[20] Pham, P.V and Mohareb, M., Nonshear Deformable Theory for Analysis of Steel Beams Reinforced with GFRP Plate Closed-Form Solution, Journal of Structural Engineering ASCE, 141 (2015) 04015063.
[21] Pham, P.V. and Mohareb, M., A shear deformable theory for the analysis of steel beams reinforced with GFRP plates, Thin-Walled Structures, 85 (2014) 165-182.
[22] Pham, P.V. and Mohareb, M., Finite-Element Formulations for the Spatial Static Response of Steel Beams Bonded to a GFRP Plate, J. of Engineering Mechanics ASCE, 141 (2015) 04014143.
[23] Pham, P.V., Mohareb, M., and Fam, A., Elastic analysis of steel beams strengthened with GFRP plates including pre-existing loading effects, Journal of Structural Engineering ASCE, 143 (2017) 04017163.
[24] Gara, F., Ranzi, G. and Leoni, G., Displacement-based formulations for composite beams with longitudinal slip and vertical uplift, Int. J. Numerical Method in Eng., 65 (2006) 1197-1220.
[25] Wenwei, W. and Guo, L., Experimental study and analysis of RC beams strengthened with CFRP laminates under sustaining load, Int. J. of solids and structures, 43 (2006) 1372-1387.
[26] Vlasov, V. Z., Thin-walled elastic beams, 2nd Ed., Israel Program for Scientific Translations, Jerusalem (1961).

[27] Gjelsvik A., The Theory of Thin Walled Bars, 1st Edition, New York, et al., John Wiley & Sons publishing Incorporation (1981).
[28] Xiao, Q., Doudak, G, and Mohareb, M., Lateral torsional buckling of wood beams: FEA-modelling and sensitivity analysis, World conference on Timber Engineering, Montreal, 2014.
[29] Du, Y., Mohareb, M., and Doudak, G., Nonsway model for lateral torsional buckling of wooden beams under wind uplift, J. Engineering Mechanics ASCE, 142 (2016) 04016104.
[30] Hu, Y., Mohareb, M., and Doudak, G., Lateral torsional buckling of wooden beams with midspan lateral bracing offset from section midheight, J. Eng. Mechanics, 143 (2017) 04017134.
[31] Trahair, N.S., Flexual torsional buckling of structures, CRC Press, USA (1993).
[32] Pham, V. P, Stress-deformation theories for the analysis of steel beams reinforced with GFRP plates, Master of Science thesis, Dept. of Civil Engineering, Univ. of Ottawa, Ottawa (2013).
[33] Gardner, L., and Nethercot, D. A., designers' guide to EUROCODE 3: Design of steel buildings, Imperial College London, UK (2011).
[34] CSA, Limit states design of steel structures, Standard CAN/CSA-S16-14, Canadian Standards Association, Mississauga, Ontario (2014).
[35] Standards Association of Australia (SAA), Steel Structures, AS4100-1998, SAA, Australian Institute of Steel Construction, Sydney, Australia (1998).
[36] Hassan, R. and Mohareb, M., Distortional lateral torsional buckling for simply supported beams with web cleats, Canadian journal of civil engineering, 42 (2015) 1091-1103.
[37] Hjaji, M.A. and Mohareb, M., Finite-element formulation for the linear steady-state response of asymmetric thin-walled members under harmonic forces, Journal of Engineering Mechanics ASCE, 141 (2015) 04014126.
[38] Pham, V. P., Analysis of steel beams strengthened with GFRP plates, Ph.D. thesis, Department of Civil Engineering, University of Ottawa, 2018.
[39] Barsoum, R. S., and Gallagher, R. H., Finite element analysis of torsional and torsional–flexural stability problems, Int. J. for Numerical Methods in Engineering, 2 (1970) 335-352.
[40] ANSI/AISC-360-16, ANSI/AISC 360-16, Specification for structural steel buildings, American Institute of Steel Construction (AISC), Chicago, IL (2016).